NASA CONTRACTOR REPORT

NASA CR-460

X-15 DATA DISPLAY SYSTEM

Prepared under Contract No. NAS 4-589 *by*
SPACELABS, INC.
Van Nuys, Calif.
for Flight Research Center

NATIONAL AERONAUTICS AND SPACE ADMINISTRATION - WASHINGTON, D. C. - MAY 1966

X-15 DATA DISPLAY SYSTEM

Prepared under Contract No. NAS 4-589 by
SPACELABS, INC.
Van Nuys, Calif.

for Flight Research Center

NATIONAL AERONAUTICS AND SPACE ADMINISTRATION

For sale by the Clearinghouse for Federal Scientific and Technical Information
Springfield, Virginia 22151 – Price $5.00

FOREWORD

The work discussed in this report was performed under Contract NAS 4-589 for the National Aeronautics and Space Administration, Flight Research Center. The data processing and digital simulation was performed under subcontract by the International Business Machines Corporation.

TABLE OF CONTENTS

TABLE OF CONTENTS (Continued)

LIST OF ILLUSTRATIONS

Section 1

INTRODUCTION

The purpose of this report is to summarize the Phase I study of the X-15 Data Display System under contract NAS4-589 for the National Aeronautics and Space Administration, Flight Research Center.

The objectives of this program are to develop signal enhancement and display techniques which present certain physiological and environmental parameters of interest to the medical monitor in a manner which is most readily comprehended by him. The usual methods of presenting this data (strip chart recorders, etc.) require constant monitoring if the observer is to detect significant changes in the parameters. In addition, the degradation of the data due to noise, motion artifact, and poor transducers makes the observer's task just that much more difficult. Methods of reliably extracting heart and respiration rates from noisy data, enhancing ECG waveforms for display and detecting changes in the ECG waveform were investigated in the Phase I study.

The data processing and digital simulation was performed under subcontract by the International Business Machines Corporation. This work was directed toward enhancement of information contained in four physiological signals: the electrocardiogram (ECG), Korotkow sound (KS), suit-helmet pressure differential (SHPD) and cuff pressure (CP). In particular, the initial effort was directed toward reliably measuring the heart rate and respiration rate from the electrocardiogram and suit-helmet pressure differential signals, respectively. As a firm ground work was established, the efforts proceeded toward enhancement of the ECG waveform and investigation of techniques for

improved reliability in the automatic readout of acoustic blood pressures obtained through appropriate combined processing of Korotkow sound and cuff pressure signals.

The techniques of bandpass filtering, autocorrelation, power spectral density and averaging were investigated. Bandpass filtering was applied to all signals with bandwidths controlled in accord with the signal bandwidth desired in the output. Autocorrelation and power spectral density techniques were applied to the ECG and SHPD signals in an attempt to enhance the desired rate information. The effect of averaging over many cycles to lessen the noise degredation was investigated to determine ways of providing the ECG complex in a cleaner form.

The investigations are presented as separate sections in this report. Each report section will discuss the general formulation of a technique and the results obtained through its specific applications. Section 2 discusses the physiological signals that were obtained from the NASA Flight Research Center at Edwards AFB, and their conversion for the purpose of our study. The autocorrelation function and the results of its application to ECG, SHPD and KS data are presented in section 3. In section 4, the autocorrelation function is transformed to the frequency domain in the form of the power spectral density function, which was computed for ECG, SHPD and KS signals. Section 5 contains a presentation of digital filtering and its applications in which the effect of reduced bandwidth was studied for the ECG, SHPD, and KS signals. The formulation, technique of application, and the results obtained through applying waveform averaging to the ECG signal are presented in section 6.

Section 7 presents the technique of zero crossing detection, the signal preconditioning required in its use and how it may be applied to the ECG and SHPD signal to obtain the fundamental rates. To

assist in a quantitative evaluation of technique failure and reliability estimation; ECG synthesis, and noise synthesis techniques and programs were developed and are discussed in section 8. Although the scope of the present effort did not permit completion of these last two investigations, the intent and preliminary results are indicated. Section 9 presents a discussion of the application of these studies to a pattern change subsystem for the ECG waveforms. And finally, the results of these investigations are summarized in section 10 along with an evaluation of their applicability to the Data Display System and recommendations on future courses of study. A report of the results of the Phase I extension investigations is included in Appendix II.

Section 2

X-15 PHYSIOLOGICAL SIGNALS

The physiological signals (electrocardiogram, suit-helmet pressure differential, Korotkow sound and cuff pressure) obtained from the pilots on the X-15 aircraft in flight were recorded on FM-FM modulated analog tape. Liaison was initiated with NASA personnel at the Flight Research Center to select typical segments of the signals for use as experimental data for testing and investigating digital simulation techniques. The signals selected represented varying degrees of degradation such that the investigations could proceed in a step-wise manner. The intelligence bandwidths of the signals were established, and analog-to-digital conversion (ADC) pre-filter selections and sampling rates were specified.

The general noise content of the signals ranged from little or no noise to the point where no signal identification could be made. The ECG signal was generally quite good but contained regions where the signal-to-noise ratio was significantly below the critical value required for a standard cardiotachometer or an averager, paced by attempted R-wave detections, to operate with desired performance. The respiration signal (S-HPD) had a high signal-to-noise power ratio but displayed a very erratic nature due to artifact. The low cyclic power-to-DC power ratio presented obvious problems with respect to applying thresholding techniques for respiration rate. The cuff pressure signal was essentially free from noise, and it was quite apparent that low-pass filtering would handle any degradation encountered. The Korotkow sound signal, which must be used in conjunction with the CP to predict acoustic blood pressures, was

essentially, totally corrupted by noise and artifact. In the data selection, no KS signal identification could be made for any of the flight records.

The A-to-D conversion process required close interaction with Air Force personnel at the Digital Data Processing Branch, Edwards AFB, to establish the ADC ground rules. Some signal pre-conditioning was required before the ADC could be initiated. A timing signal was dubbed onto the analog records, strip-charts produced with the appropriate signal bandwidths, the sampling rates selected and the modes of multiplexing identified. An extensive post-ADC effort was required to properly label the data, eliminate spurious output from the ADC gear, and to get the data into an IBM word compatible format. The total data obtained encompassed approximately 20 flight minutes of all four physiological channels. The ADC operation was checked by the production of digital plots and comparison with the strip charts.

Section 3

AUTOCORRELATION FUNCTION OF NOISE DEGRADED PERIODIC SIGNALS

The autocorrelation function showed promise in the enhancement of the rate information contained in noise degraded signals due to unique properties. The first of these is the fact that in construction of the autocorrelation function, all phase information is integrated out, thus leaving only the basic harmonic structure of the signal. A second important property is the action of autocorrelation on additive band-limited white noise, for which autocorrelation produces an exponentially decaying function of lag. The definition of the autocorrelation function, $\psi(\tau)$ of a time function, $x(t)$ is given by

$$\psi(\tau) = \lim_{T \to \infty} \frac{1}{T} \int_{-T/2}^{T/2} x(t)\, x(t+\tau)\, dt. \tag{1}$$

Let a degraded signal $x_d(t)$ be represented as the sum of a clean signal $x_c(t)$ and an independent bandlimited noise function $x_n(t)$

$$x_d(t) = x_c(t) + x_n(t). \tag{2}$$

Then the autocorrelation function of $x_d(t)$ is represented by

$$\psi_d(\tau) = \psi_c(\tau) + \psi_n(\tau). \tag{3}$$

The power spectrum of the noise function is assumed to be σ_n^2 from 0 to β cycles per second and drops rapidly to zero above β cps. When this power spectrum function is Fourier transformed into the time domain, thus producing the autocorrelation function, the result becomes

$$\psi_n(\tau) = \sigma_n^2 e^{-\beta\tau} \tag{4}$$

When the clean signal is a periodic function of time with H harmonics, it can be represented as the Fourier series

$$x_c(t) = \sum_{i=1}^{H} a_i \cos(i\,\omega_o\, t + \varphi_i), \tag{5}$$

where ω_o represents the base rate (1st harmonic or fundamental frequency) of the signal.

The autocorrelation function of $x_c(t)$ is

$$\psi_c(\tau) = \frac{1}{2} \sum_{i=1}^{H} a_i^2 \cos(i\,\omega_o \tau) \tag{6}$$

The clean signal power is given by the autocorrelation at zero lag

$$\psi_c(0) = \sigma_c^2 = \frac{1}{2} \sum_{i=1}^{H} a_i^2 . \tag{7}$$

If independent, additive, periodic noise components, $x_p(t)$, are present in the total signal, again the contribution to the autocorrelation function will be given by

$$\psi_p(\tau) = \sigma_p^2 \cos(\omega'_p \tau), \tag{8}$$

where σ_p^2 is the power and ω'_p is the angular frequency of $x_p(t)$.

With the above relations, we see that if the degraded signal $x_d(t)$ contains a clean periodic component $x_c(t)$ mixed with a random bandlimited noise component $x_n(t)$, then the autocorrelation function of the noisy

$x_d(t)$ becomes (from equations (3), (4), and (6)):

$$\psi_d(\tau) = \frac{1}{2} \sum_{i=1}^{H} a_i^2 \cos(i\,\omega_o\,\tau) + \sigma_n^2\, e^{-\beta\tau} \tag{9}$$

Now from (6) it is seen that $\psi_c(\tau)$, the autocorrelation of the clean periodic component $x_c(t)$, is a periodic function of lag (τ). The fundamental angular frequency of $\psi_c(\tau)$ is ω_o radians/sec. The fundamental cyclic frequency of $\psi_c(\tau)$ is

$$f_o = \omega_o / 2\,\pi \text{ cps} \tag{10}$$

The period of $\psi_c(\tau)$ is

$$\tau_o = 1/f_o = 2\,\pi/\omega_o \text{ seconds/cycle.} \tag{11}$$

Another important feature of $\psi_c(\tau)$ is that its maximum value occurs exactly once per cycle, and at a known constant phase which is independent of φ_i in (5). This peak amplitude occurs at $\tau = 0$, $\tau = \tau_o$, $\tau = 2\tau_o$, $\cdots$, and its value is given by (7) as σ_c^2.

Thus, we see that $\psi_d(\tau)$ contains a periodic component $\psi_c(\tau)$ with peak amplitude σ_c^2 and period τ_o, and an exponentially decaying component $\psi_n(\tau)$ with initial amplitude σ_n^2 and decay time constant τ_n, where τ_n is the reciprocal of the noise bandwidth.

$$\tau_n = \frac{1}{\beta} \text{ seconds.} \tag{12}$$

To determine the signal-to-noise power ratio of $x_d(t)$ from $\psi_d(\tau)$, we first compute the total power at zero lag

$$\psi_d(0) = \sigma_c^2 + \sigma_n^2 \tag{13}$$

We next take

$$\tau_1 = k\tau_o \tag{14}$$

i.e., we take τ_1 as some multiple of τ_o, such that

$$\tau_1 \geq 4.61\ \tau_n. \tag{15}$$

(For example, for a noise bandwidth of β = 10 cps and τ_n = 0.1 sec., $\tau_1 \geq .46$ seconds).

For each τ_1, we have $\psi_c(\tau)$ at a peak value (from (6), (11), and (14))

$$\psi_c(\tau_1) = \psi_c(k\tau_o) = \sigma_c^2 \tag{16}$$

and we have $\psi_n(\tau)$ decayed to a very small value

$$\psi_n(\tau_1) = \sigma_n^2 e^{-\beta\tau} \leq \sigma_n^2\, e^{-4.61\ \beta\tau_n} = \sigma_n^2 e^{-4.61} = .01\ \sigma_n^2 \tag{17}$$

Hence, to a good approximation, $\psi_d(\tau_1)$ becomes

$$\psi_d(\tau_1) = \psi_d(k\tau_o) = \sigma_c^2 \tag{18}$$

From (13) and (18) we can readily compute clean signal-to-noise and degraded signal-to-noise power ratios from degraded signal auto-correlation values at $\tau = 0$ and $\tau = \tau_1$.

$$Q = \frac{\sigma_c^2}{\sigma_n^2} = \psi_d(\tau_1)/(\psi_d(0) - \psi_d(\tau_1)) \tag{19}$$

$$\frac{\sigma_d^2}{\sigma_n^2} = \frac{\sigma_c^2 + \sigma_n^2}{\sigma_n^2} = \psi_d(0)/(\psi_d(0) - \psi_d(\tau_1)) = \Omega + 1 \qquad (20)$$

One thing we can conclude from the above analysis is that for a periodic signal degraded by random noise, computation of the autocorrelation of the degraded signal will enable us to determine both the frequency of the periodic signal as well as the signal-to-noise power ratio. For example, in applying autocorrelation to a degraded rythmic EGG signal, we would expect to be able to determine heart rate HR by computing the values of lag τ at which $\psi_d(\tau)$ peaks. The lag interval between any two such successive lag values should give us the heart period τ_o, from which we could compute HR from

$$HR = 60/\tau_o \text{ beats/minute} \qquad (21)$$

3.1 Normalized Autocorrelation Functions

To make the analysis and technique independent of gain variations and absolute power levels in the signal conditioning chain, it is best to introduce and work with the normalized autocorrelation function, $R(\tau)$. $R(\tau)$ is simply defined and calculated from $\psi(\tau)$ as follows:

$$R(\tau) = \psi(\tau)/\psi(0) \qquad (22)$$

from which we have a value of unity for the normalized autocorrelation at zero lag,

$$R(0) = 1 \qquad (23)$$

which means we are adjusting the relative power of the input signal to one unit (In physical terms $R(0) = 1$ watt).

Reformulation of previous relations in terms of normalized auto-correlation functions gives, for

$$x_d(t) = x_c(t) + x_n(t), \tag{24}$$

$$R_d(\tau) = \frac{Q}{Q+1} R_c(\tau) + \frac{1}{Q+1} R_n(\tau) \tag{25}$$

where:

$$R_c(\tau) = \frac{1}{2\sigma_c^2} \sum_{i=1}^{H} a_i^2 \cos(i\omega_o \tau) = \frac{\sum_{i=1}^{H} a_i^2 \cos(i\omega_o \tau)}{\sum_{i=1}^{H} a_i^2} \tag{26}$$

$$R_c(\tau) = \sum_{i=1}^{H} r_i \cos(i\omega_o \tau), \text{ with } r_i = \frac{a_i^2}{\sum_{j=1}^{H} a_j^2} \tag{27}$$

$$R_n(\tau) = e^{-\beta\tau} \tag{28}$$

$$Q = \frac{\sigma_s^2}{\sigma_n^2} \tag{29}$$

Equation (25) can be rewritten by defining

$$p_c = \frac{Q}{Q+1}, \quad p_n = \frac{1}{Q+1}; \tag{30}$$

giving

$$R_d(\tau) = p_c R_c(\tau) + p_n R_n(\tau) \tag{31}$$

Now we see that:

$$R_d(0) = p_c R_c(0) = p_c + p_n = \frac{Q+1}{Q+1} = 1 \qquad (32)$$

$$R_d(\tau_1) = p_c R_c(\tau_1) + p_n R_n(\tau_1) \qquad (33)$$

Since $R_c(\tau_1) = R_c(k\tau_o)$, we have $R_c(\tau_1) = R_c(0) = 1$.

Since $R_n(\tau_1) = e^{-\beta\tau_1} = e^{-\tau_1/\tau_n} \leq e^{-4.61}$, we have $R_n(\tau_1) \leq .01$

Thus, to a good approximation, (33) becomes:

$$R_d(\tau_1) = p_c = \frac{Q}{Q+1} \qquad (35)$$

The ability to discriminate the normalized degraded autocorrelation peaks in terms of signal-to-noise power ratio or quality, Q, is now easily studied with the aid of expression (35) which related Q to p_c, the peak amplitude R_d has after the noise component of R_d has decayed.

Consider the following chart which depicts corresponding values of Q, p_c, and p_n

Q	.01	.05	.10	.20	.25	.50	.75	1.0	2.00	4.0	8.00	19.00
p_c	.01	.05	.09	.17	.20	.33	.44	.5	.67	.8	.89	.95
p_n	.99	.95	.91	.83	.80	.67	.56	.5	.33	.2	.11	.05

We see that for small values of signal-to-noise ratio Q, p_c, is also small and approximately equal to Q, and the ability to discriminate the peak values of $R_d(\tau)$ is limited. For intermediate values of Q, Q = .5 to 1, p_c changes from .33 to .5, less than Q changes. In this

range, the ability to detect $R(\tau)$ peaks is good. For high quality signals, p_c approaches 1.

3.2 Applying Autocorrelation to Measure Periodicity

How well measurement of τ_o from $R_d(\tau)$ can be made also depends on other parameters of the autocorrelation process, such as: the harmonic structure of $x_c(t)$, both the bandwidth and shape of the spectrum of x_c, which affect the relative amplitudes of the subpeaks of $R_c(\tau)$; the relationship between τ_o and τ_n, the period of x_c and the time constant of x_n; the degree of aperiodicity of x_c and the integration time T for which $R_d(\tau)$ is computed; the variation, if any, in harmonic structure of $s_c(t)$, i.e., aberrant beats which give rise to waveform changes; and the resolution of any discrete process by which $R_d(\tau)$ might be computed, the measure of resolution being $\Delta\tau$.

To study the effects and to determine the control required of these and other parameters of the autocorrelation process in its ability to yield rate information about degraded input signals were major tasks of the investigation. In performing the investigation, an autocorrelation program was developed and tested. This program was applied to the degraded input data prepared by A-to-D conversion of X-15 flight tapes. Autocorrelation runs were made on all four (ECG, SHPD, KS, CP) signals. The most extensive set of runs were made on ECG signals.

For the purposes of digital simulation, the signal is represented by a series of signal amplitudes sampled every Δt seconds from the continuous signal; $x_i = x(i\,\Delta t)$, and the normalized autocorrelation function is computed by the approximation

$$R_j = R(j\,\Delta\tau) = \frac{\sum_{i=1}^{N/2} x_i\, x_{i+j}}{\sum_{i=1}^{N/2} x_i^2} \qquad (36)$$

Here N is the total number of points in the signal time series, and N/2 is the number of sampling intervals contained in the integration interval. The program to digitally compute the autocorrelation function based on equation (36) was written to operate on an IBM 7094, and to provide printer listings and printer plots as outputs.

3.3 ECG Autocorrelation Runs and Results

Five major sets of autocorrelation runs were made on X-15 flight ECG signals. The following chart depicts characteristics of these runs.

Run Set	Number Flight Segments	Integration Times T	Δt-Time Increments	Δt-Lag Increments	Number Cases In Run Set
Preliminary Unfiltered	8	2 to 3.5 sec	.5 ms	.2 to 3 ms	8
Preliminary High Pass	3	1 sec	.5 ms	.5 ms	3
Preliminary Band Pass	1	1 sec	2.5 to 20 ms	2.5 to 20 ms	4
Parametric High Pass	3	.4 to 1 sec	5 to 50 ms	5 to 50 ms	45
Parametric Band Pass	1	.4 to .65 sec	2.5 to 100 ms	2.5 to 200 ms	34

3.3.1 Preliminary Unfiltered Runs

The preliminary unfiltered runs were made on raw signals selected from eight different segments of ECG flight data to obtain an initial idea of what normalized autocorrelations of clean and degraded raw ECG signals look like. The heart rates in the segments used for these runs varied from about 120 to 150 bpm. For the integration times and maximum lags used in the autocorrelation runs, this meant that the data segments were about 10 heart cycles in duration, with about five beats or peaks in the autocorrelation function.

One of the preliminary unfiltered run cases was for one of the least noisy or highest quality ECG segments in the data. Figure 1 represents such a relatively clean ECG signal segment from X-15 Test 1-45. The pilot's heart rate at that time in flight is easily computed as 120 bpm. The normalized autocorrelation function of this signal was computed and plotted. A plot of normalized autocorrelation amplitude as a function of lag τ in seconds comprises Figure 2. (Manual interpolation between discrete computed points was made to provide a smooth continuous curve.) It is of interest to note several things from this plot.

First, it is clear that the four peaks of $R_d(\tau)$ are unmistakable: they occur at $\tau = 0$, .504, 1.006, 1.509, and 2.005 seconds of lag. The average heart period τ_o can be estimated either by computing any of the four peak-to-peak lag intervals (.504 or .502 or .503 or .496 sec.), or by dividing the lag at any peak by the number of cycles or beats covered by that lag value. The estimate in either case is very close to .5 seconds/beat, giving (from equation 21):

$$\overline{HR} = 60/.5 = 120 \text{ bpm} \tag{37}$$

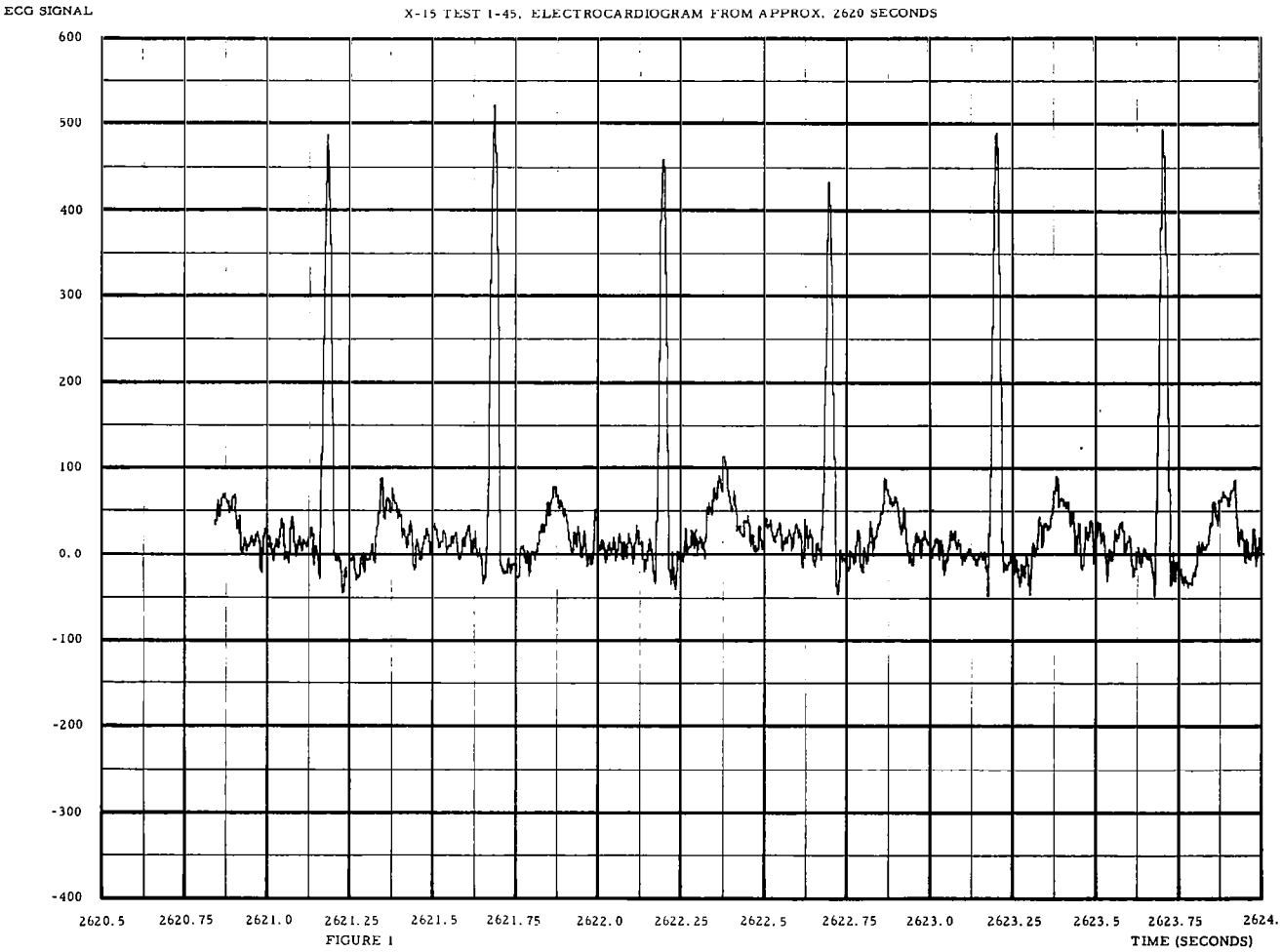
ECG SIGNAL
X-15 TEST 1-45, ELECTROCARDIOGRAM FROM APPROX. 2620 SECONDS
600
500
400
300
200
100
0.0
-100
-200
-300
-400
2620.5
2620.75
2621.0
2621.25
2621.5
2621.75
2622.0
2622.25
2622.5
2622.75
2623.0
2623.25
2623.5
2623.75
2624.
TIME (SECONDS)

FIGURE 1

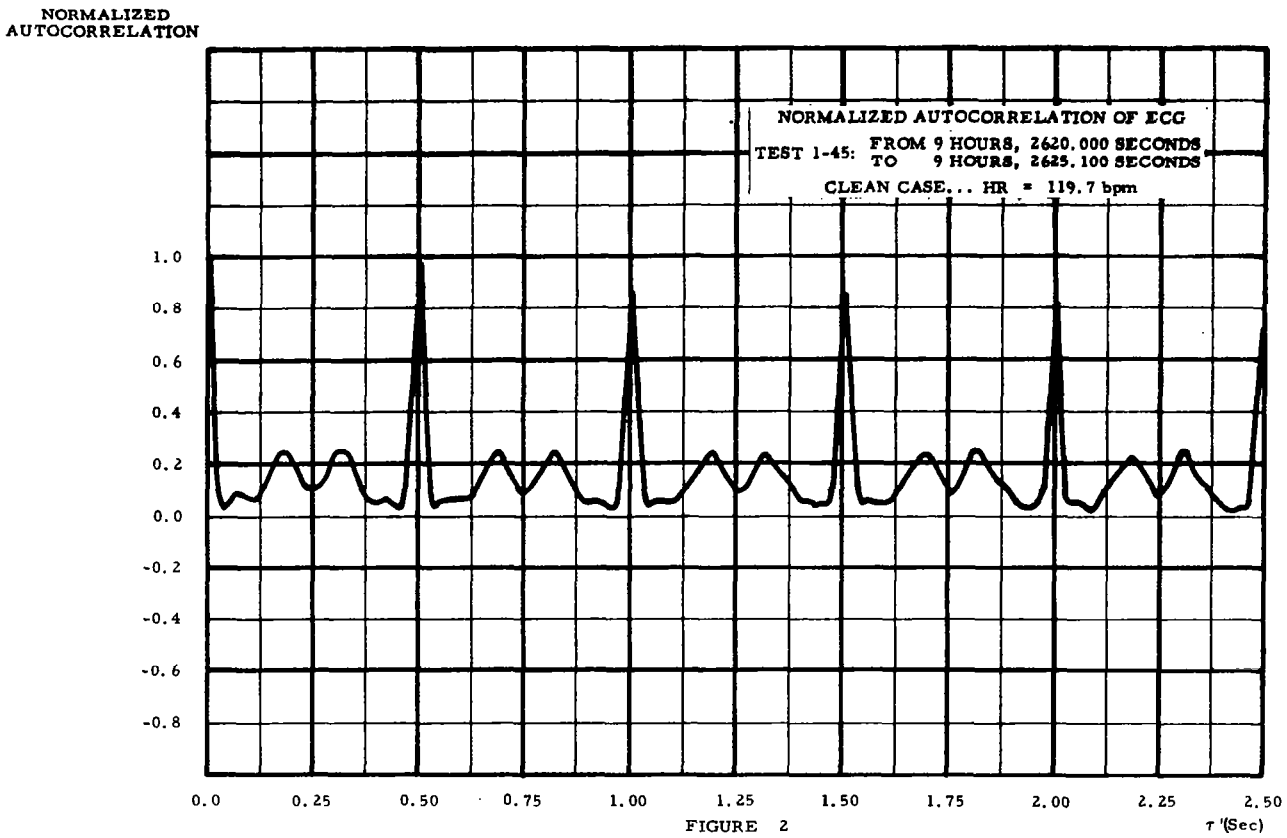
NORMALIZED AUTOCORRELATION
NORMALIZED AUTOCORRELATION OF ECG
TEST 1-45: FROM 9 HOURS, 2620.000 SECONDS
TO 9 HOURS, 2625.100 SECONDS
CLEAN CASE... HR = 119.7 bpm
1.0
0.8
0.6
0.4
0.2
0.0
-0.2
-0.4
-0.6
-0.8
0.0
0.25
0.50
0.75
1.00
1.25
1.50
1.75
2.00
2.25
2.50
τ (Sec)

FIGURE 2

The second subpeak appears to be due to the correlation of the T-Wave of a cycle with the R-Wave of the following cycle, and T-R peak lag value (.31 sec. in Figure 2) probably a measure of the time interval from T peak to following R peak. This interpretation checks the fact that the sum of the R-T interval and the T-R intervals as so defined and measured is equal to the R-R interval:

$$.19 + .31 = .5 \text{ sec.} = \overline{\tau_o} \tag{39}$$

This point bears further investigation, but it can be suggested here that it might well be feasible and economical to compute several of the ECG segment intervals using autocorrelation techniques on clean or averaged ECG signals.

To summarize conclusions for this clean signal case, it is clear that a very high discrimination factor for heart cycle detection and, hence rate determination is attainable through ECG autocorrelation. This is primarily due to the harmonic structure or spectra of the ECG signal which produces one well defined, high amplitude spike in the autocorrelation function for each heart period of lag. This sharp spike in the ECG autocorrelation has some of the appearance of the R wave in the ECG itself, but it should be remembered that all ECG segments (P, Q, R, S, and T) of the ECG signal contribute to the autocorrelation spike amplitude and shape.

Another preliminary unfiltered case was that of an ECG segment from X-15 Test 1-41 exhibiting considerable noise. The lower trace of Figure 3 is a plot of this degraded ECG segment. (The slanted straight lines on this trace are due to a digital plotting process artifact and can be ignored). A plot of the normalized autocorrelation of this degraded ECG appears in Figure 4.

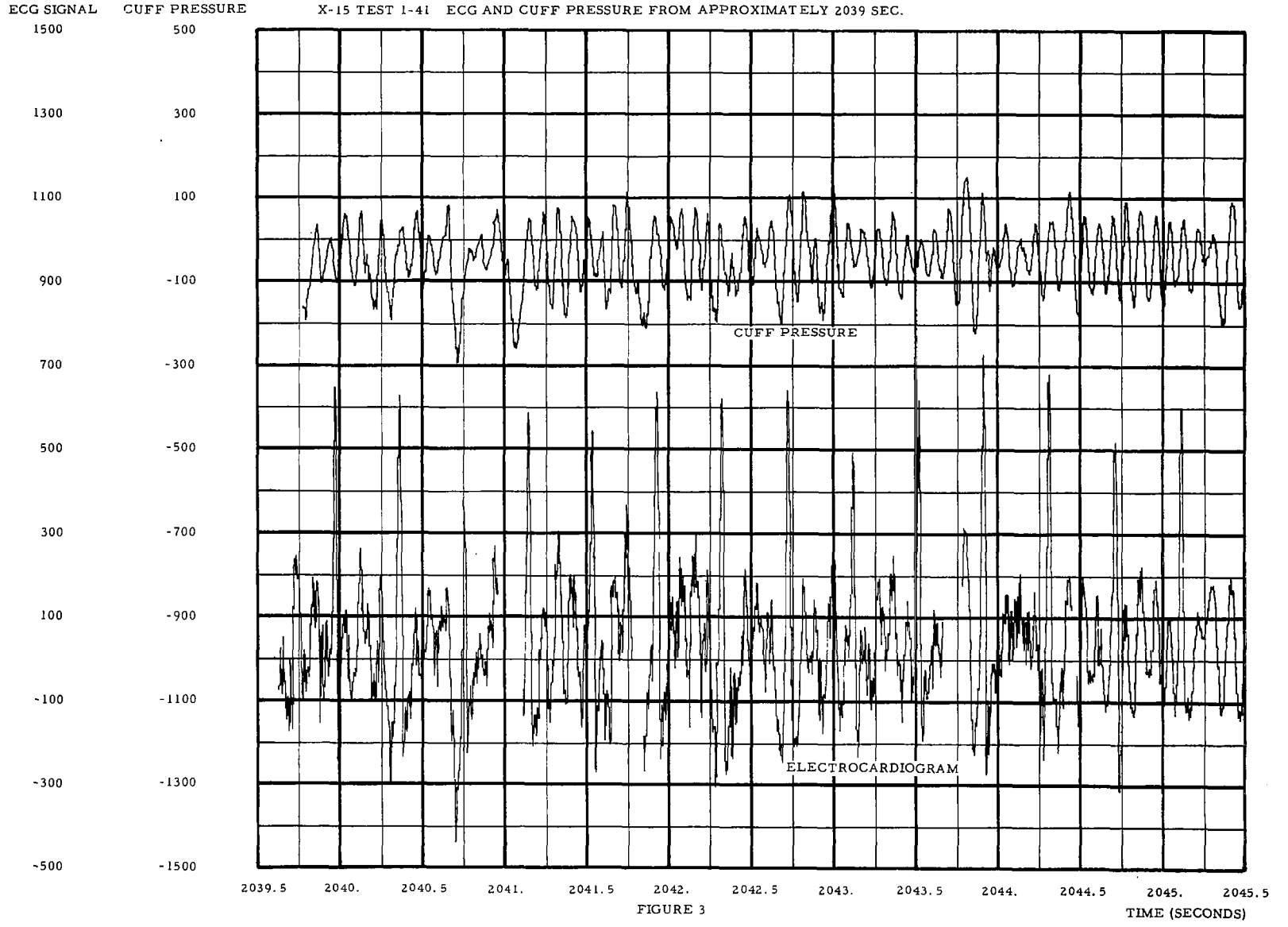
ECG SIGNAL
CUFF PRESSURE
X-15 TEST 1-41 ECG AND CUFF PRESSURE FROM APPROXIMATELY 2039 SEC.
1500
500
1300
300
1100
100
900
-100
700
-300
500
-500
300
-700
100
-900
-100
-1100
-300
-1300
-500
-1500
CUFF PRESSURE
ELECTROCARDIOGRAM
2039.5
2040.
2040.5
2041.
2041.5
2042.
2042.5
2043.
2043.5
2044.
2044.5
2045.
2045.5
TIME (SECONDS)

FIGURE 3

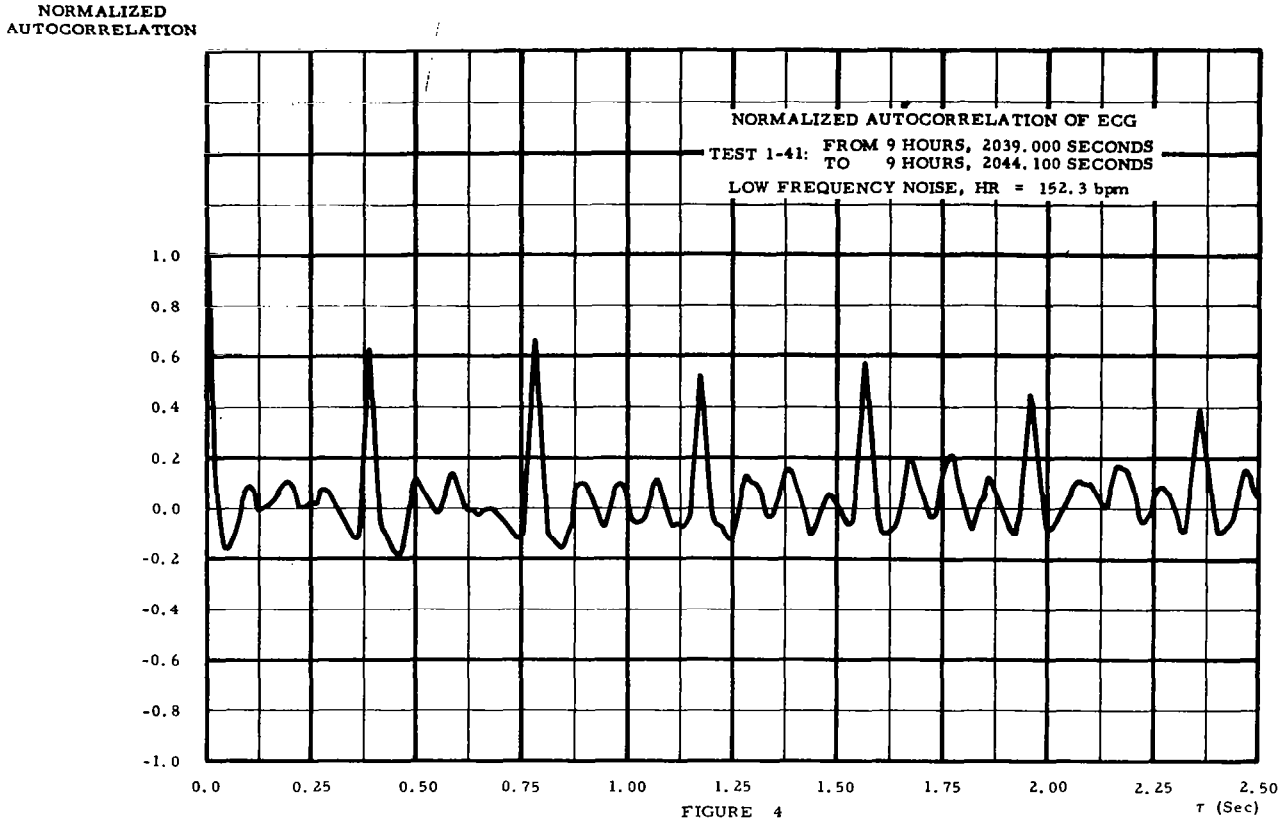
NORMALIZED AUTOCORRELATION
NORMALIZED AUTOCORRELATION OF ECG
TEST 1-41: FROM 9 HOURS, 2039.000 SECONDS
TO 9 HOURS, 2044.100 SECONDS
LOW FREQUENCY NOISE, HR = 152.3 bpm
1.0
0.8
0.6
0.4
0.2
0.0
-0.2
-0.4
-0.6
-0.8
-1.0
0.0
0.25
0.50
0.75
1.00
1.25
1.50
1.75
2.00
2.25
2.50
τ (Sec)

FIGURE 4

which agrees very well indeed with the rate computed from the ECG signal itself.

A second interesting feature of the $R_d(\tau)$ in Figure 2 is the relative amplitude and sharpness of the spikes. For such spikes, it is fair to assume the noise time constant τ_n to be 0.1 sec. or less (noise bandwidth $\beta \geq 10$ cps). With this assumption, $\tau_1 = .5$ seconds, and we can compute the signal-to-noise ratio Q as

$$Q = \frac{R_d(.5)}{R_d(0) - R_d(.5)} = \frac{.98}{1 - .98} = 49 \qquad (38)$$

A high signal-to-noise ratio is also confirmed by the relative symmetry and regularity of the normalized autocorrelation waveform.

Another point of interest about Figure 2 is that the mean value of $R_d(\tau)$ is not zero. A good estimate of $\overline{R_d(\tau)}$ is about .15 units of amplitude. This represents a non-cyclic or DC component in the autocorrelation function. We can verify the DC component present in the ECG signal from Figure 1. Such a DC component raises the amplitude of the subpeaks, reducing the spread between subpeak and peak amplitudes. To keep this spread as large as possible for ease and reliability of using autocorrelation for rate measurement, it is desirable to reduce or eliminate the DC component of the signal. This matter will be discussed more fully later.

A final point at this time is the matter of interpreting the subpeak amplitudes and the associated subpeak lag values. Preliminary study of this question seems to indicate that the first subpeak is due to R-T segment correlation within a cycle and the R-T peak lag value (about .19 seconds in Figure 2) is a measure of the time interval between the peak of the R-Wave and the peak of the T-Wave of the same cycle.

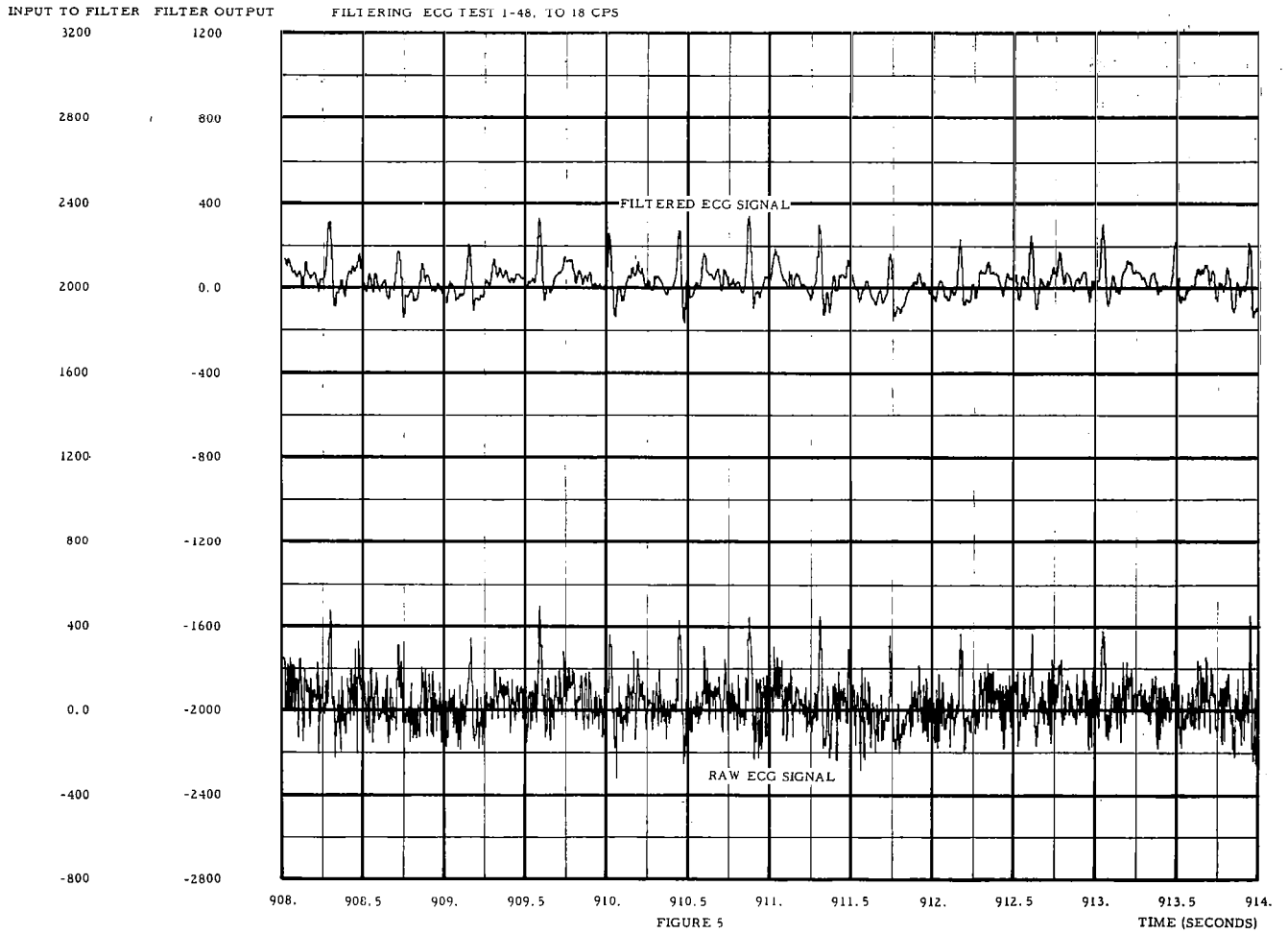
INPUT TO FILTER
FILTER OUTPUT
FILTERING ECG TEST 1-48, TO 18 CPS
3200
1200
2800
800
2400
400
2000
0.0
1600
-400
1200
-800
800
-1200
400
-1600
0.0
-2000
-400
-2400
-800
-2800
FILTERED ECG SIGNAL
RAW ECG SIGNAL
908.
908.5
909.
909.5
910.
910.5
911.
911.5
912.
912.5
913.
913.5
914.
TIME (SECONDS)

FIGURE 5

The almost zero average amplitude of the ECG is reflected in the small mean value of the autocorrelation. The effects of the noise are evident in $R_d(\tau)$ as both reduction of the amplitude of major peaks and as an increase in number and variety of subpeaks.

For this case, the seven peaks occur at lags of τ = 0, .390, .775, 1.175, 1.57, 1.96, and 2.36 seconds; and the peak-to-peak lag intervals are .390, .385, .400, .395, .390, and .400 second. An estimate of average period is $\overline{\tau}_o$ = .394 sec., from which the rate is readily computed as:

$$HR = 60/.394 = 152 \text{ bpm} \tag{40}$$

Based on previously stated assumptions, the quality or signal-to-noise ratio is

$$Q = 1.8$$

In spite of this low ECG quality, the spread in the peak and subpeak amplitudes in the first cycle is still .54, showing that the autocorrelation still gives a good discrimination ratio.

An ECG segment from X-15 Test 1-48 was selected as a preliminary unfiltered run case exhibiting very heavy degradation. The ECG plot is the lower trace of Figure 5; Figure 7 is the normalized autocorrelation plot for this case. Although a great deal of noise is present, particularly of high frequency which produces pseudo R-waves in the ECG, the one-per-cycle spikes of $R_d(\tau)$ are clearly discernible, demonstrating the ability of the autocorrelation technique to discriminate signal information reliably even with a signal-to-noise ratio of less than one. For this case:

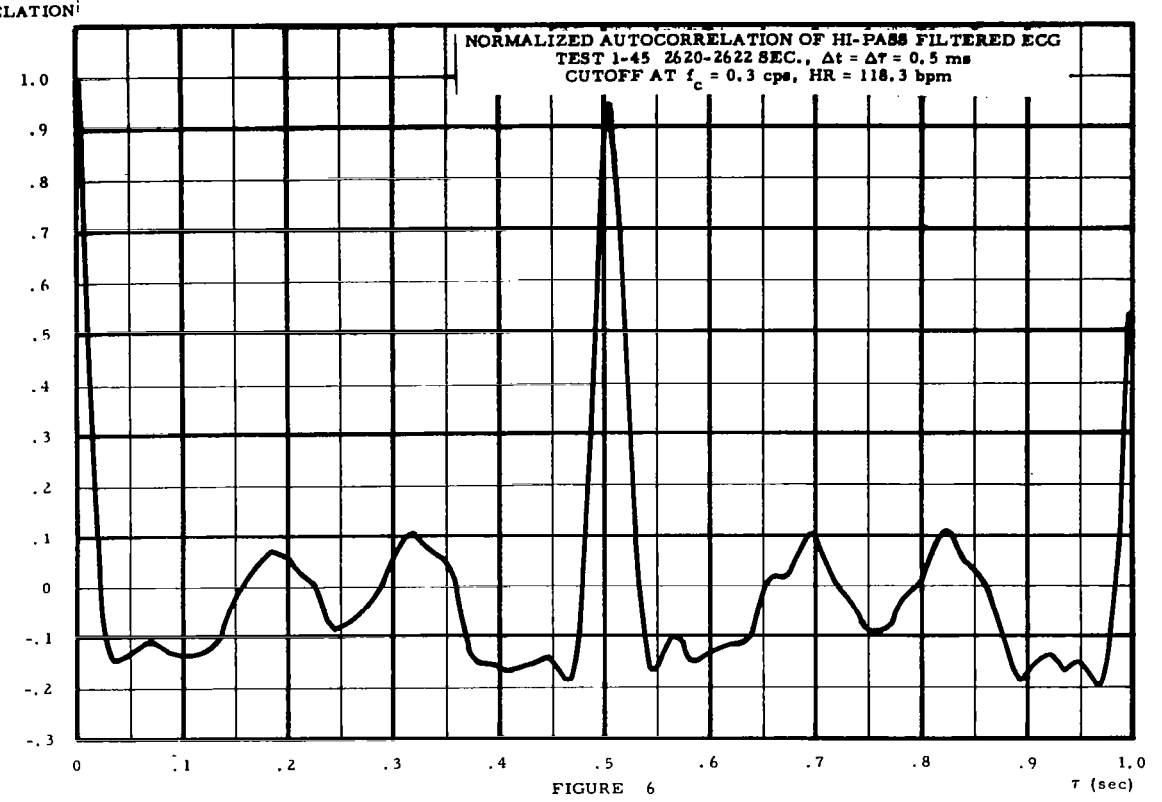

FIGURE 6

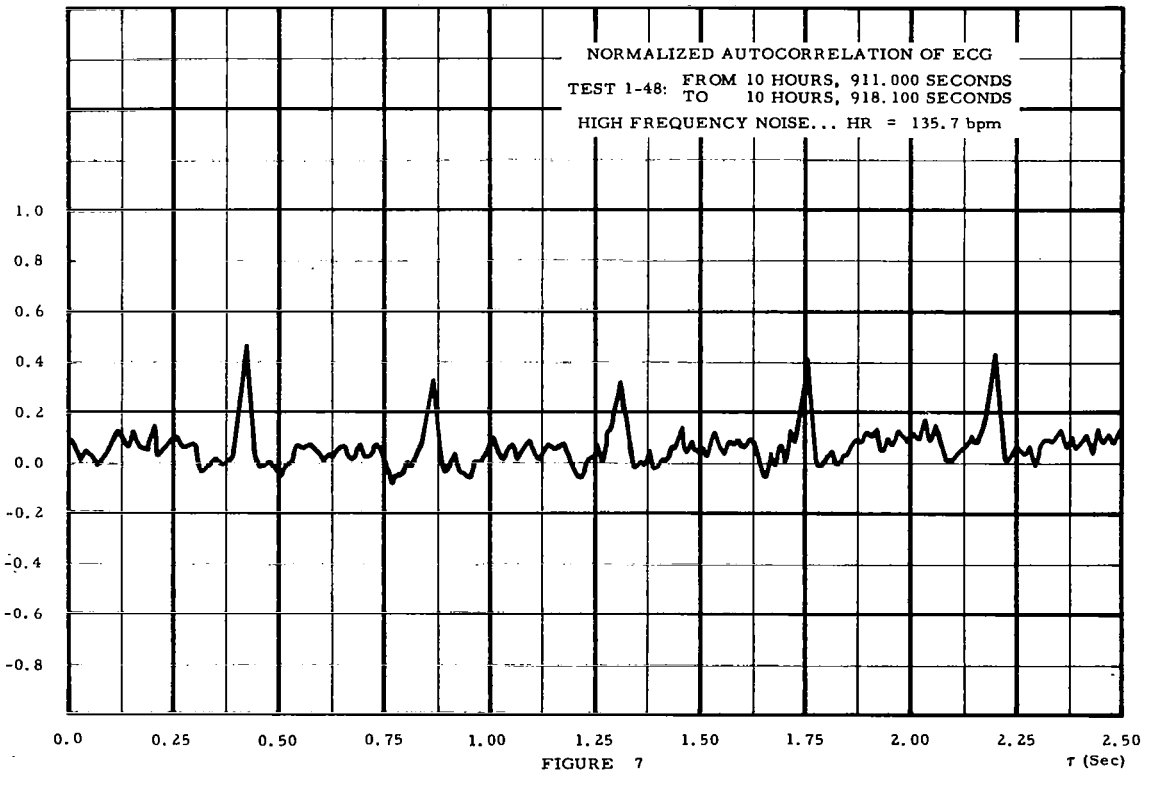

FIGURE 7

$R_d(\tau)$ peaks six times at τ = 0, .428, .875, 1.318, 1.76, and 2.21 sec.

Peak-to-peak lag intervals are: .428, .447, .443, .442, and .45 sec.

Average period is $\overline{\tau_o} = \frac{2.210}{5} = .442$ sec.

$HR = \frac{60}{.442} = 136$ bpm

$Q = .85$

The spread between peak and subpeak amplitudes in $R_d(\tau)$ in the first period of lag has dropped to .33 for this case. This somewhat low spread could be partly increased if the DC component were removed before autocorrelation with the same 2.5 second integration time.

3.3.2 Preliminary High Pass Runs

Following the study of the results of the preliminary unfiltered runs, various methods of improving the ability of rate extraction of autocorrelation processes as well as methods of reducing computation in such processes were sought. As a result, several changes in the process were formulated before specifying and conducting the second set of preliminary runs. These changes were: introduction of high pass ECG filtering; reduction of autocorrelation integration time; and reduction in maximum lag τ_m.

Consider two noise degraded periodic signals $x_{d1}(t)$ and $x_{d2}(t)$, and their normalized autocorrelation functions $R_{d1}(\tau)$ and $R_{d2}(\tau)$. Signal x_{d1} contains a DC component and x_{d2} does not; otherwise they are assumed identical. For such signals, if x_o represents the DC

amplitude, we have

$$x_{d1}(t) = x_c(t) + x_n + x_o \tag{42}$$

$$x_{d2}(t) = x_c(t) + x_n(t) \tag{43}$$

$$R_{d1}(\tau) = \left[\frac{1}{1 + x_o^2}\right] \left[p_c R_c(\tau) + p_n R_n(\tau) + x_o^2\right] \tag{44}$$

$$R_{d2}(\tau) = p_c R_c(\tau) + p_n R_n(\tau) \tag{45}$$

From these expressions, it can be determined that the spread ΔR_{d1} between peak and subpeak amplitudes of $R_{d1}(\tau)$ is less than the spread ΔR_{d2} of $R_{d2}(\tau)$ in the following ratio

$$\frac{\Delta R_{d1}}{\Delta R_{d2}} = \frac{1}{1 + x_o^2} \tag{46}$$

Thus, to make the spread ΔR_d as large as possible, it is desirable to filter out any DC component from $x_d(t)$ before computing its autocorrelation. The maximum possible spread is necessary to get the best discrimination ability for $R_d(\tau)$ spike discernment. For this reason, it was decided to filter the raw ECG signals with a high pass filter to remove DC components.

Another consideration arose in studying the results of the first set of preliminary runs. This was that the variation of the peak-to-peak lag intervals was small so that computation of any lag interval, such as the first, would yield a good estimate of average period. Furthermore, since decreasing the maximum lag reduced the extent of the

computation, choosing τ_m (maximum lag) to be just larger than the expected period seemed both workable and efficient. Moreover, if determination of individual beat-to-beat periods rather than multi-beat averages is to be made, it is necessary to reduce integration time to less than two periods (i.e., $T < 2\tau_o$).

To enable study of the effects of high pass filtering and reduced integration time, the second set of runs was made. In these runs, DC was "filtered" out of the raw ECG signals simply by computing and then subtracting out the mean. The high pass filtered data were then autocorrelated using a one-second integration time.

The segments used in these runs were the same segments discussed in the first run set, from X-15 Tests 1-45, 1-41, and 1-48. As noted previously, plots of the raw ECG signals appear in Figures 1, 3, and 5, respectively. The major effect of the high pass filtering on the plots would be a shift in the vertical scale values. The normalized autocorrelation functions for these three cases are plotted in Figures 6, 8, and 9.

To display the effect of the high pass filtering and the shorter integration time, various parameters of both the unfiltered and filtered runs computed from autocorrelation functions on each of the three segments are shown in the following table.

X-15 Test Number	Filtering	Heart Rate	Q	$R_d(\tau_o)$	ΔR_d	R_s
1-45	Unfiltered	119.7 bpm	49.00	.98	.72	.26
1-45	High Pass	118.3 bpm	19.00	.95	.84	.11
1-41	Unfiltered	152.3 bpm	1.80	.64	.52	.12
1-41	High Pass	153.0 bpm	1.80	.62	.42	.20
1-48	Unfiltered	135.7 bpm	.85	.48	.33	.15
1-48	High Pass	137.9 bpm	.92	.48	.31	.17

AUTOCORRELATION

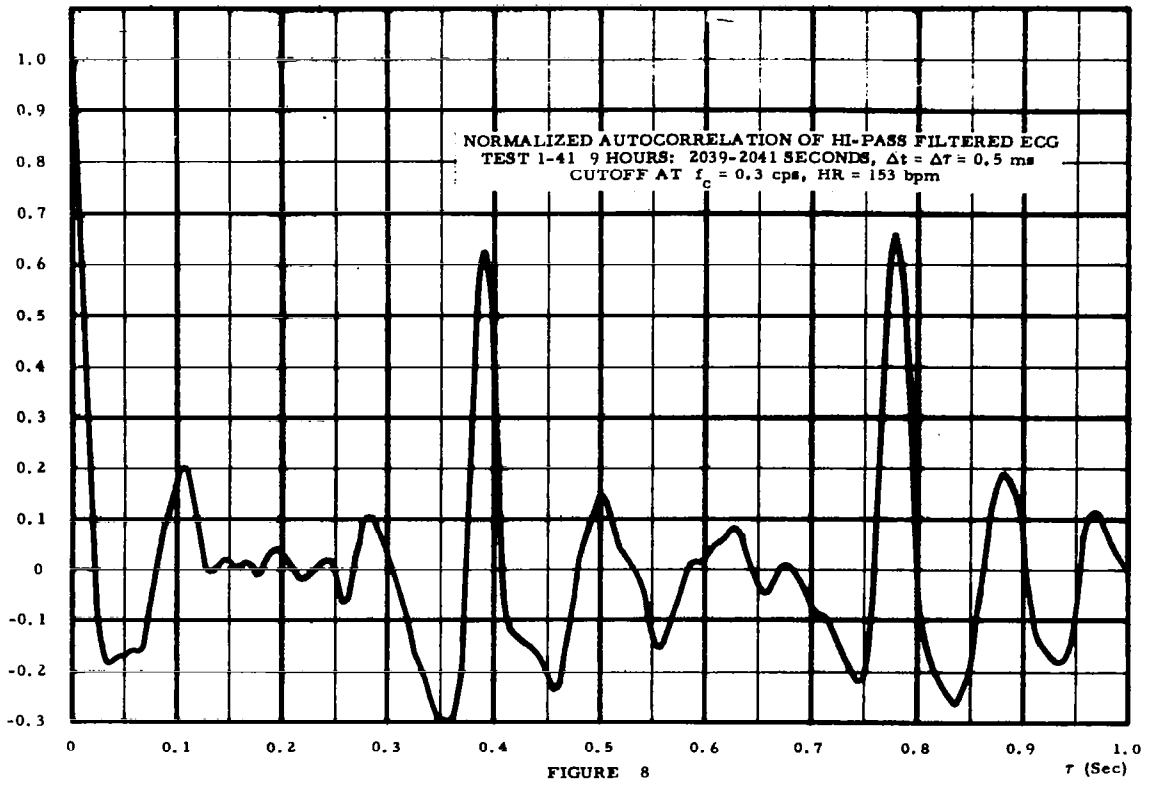

FIGURE 8

AUTOCORRELATION

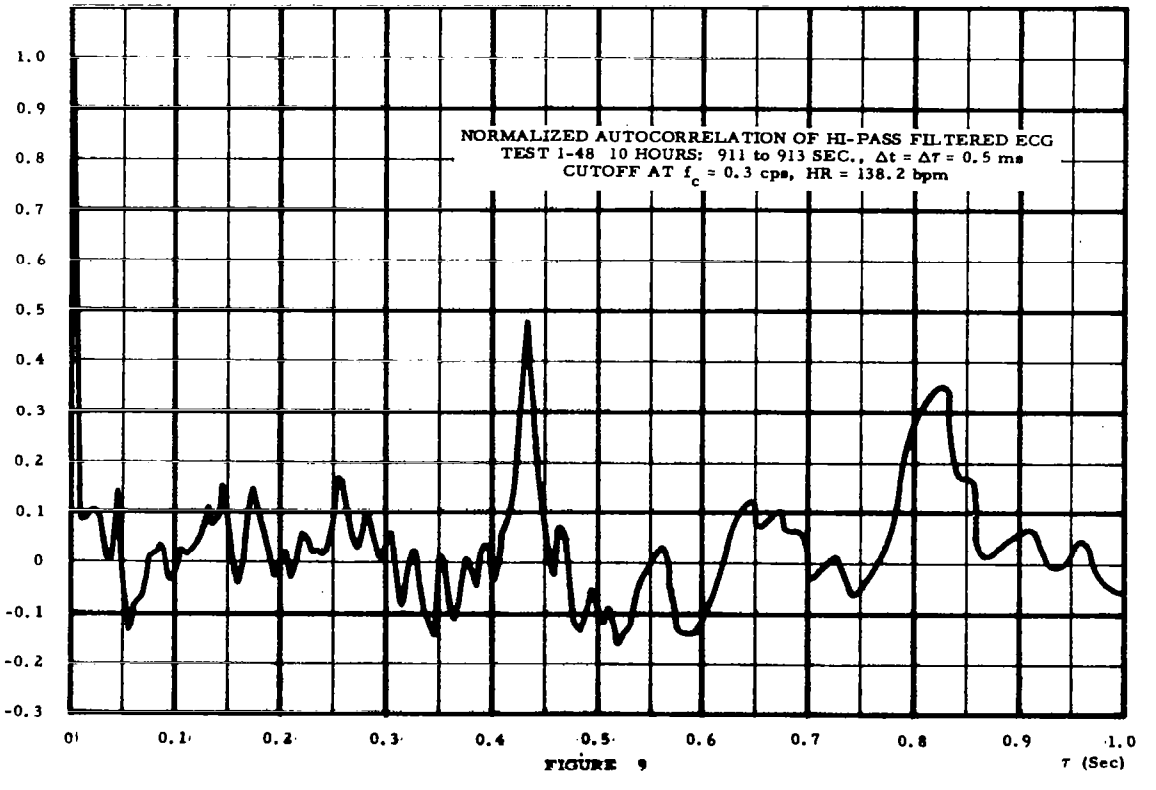

FIGURE 9

It can be seen from this table that the one or two cycle average agrees quite well with the five or six cycle average of heart rate, so that for rate computation, the shorter integration time is quite adequate. It might be noted here that the 70 percent shorter integration time effects about an 84 percent reduction in computation time. Thus, for these cases at least, the reduced integration time has no adverse effect on rate determination.

We also note from the table and from the plots that the spread ΔR_d between the peak and subpeak amplitudes is increased by filtering and T reduction for high Q (Test 1-45) data; in contract ΔR_d is reduced when the same process is applied for low Q (Test 1-41 and 1-48) data. This effect on ΔR_d can probably be explained as follows: For test 1-41, the DC component of $R_d(\tau)$ is large (See Figure 2) and hence the expected improvement in spread produced by mean extraction of high pass filtering which is predicted by expression (46) is appreciable. In addition, Q is high and so we have a small loss of noise cancellation effect together with the reduced averaging that occurs with shorter integration time. This reduced averaging could well permit any noise present to boost the subpeak amplitude more than peak amplitude, since more subpeaks than peaks occur in $R(\tau)$. So, reduced averaging is accompanied by reduced spread to a degree dependent on noise. Thus, the large spread increase due to filtering offsets any small spread decrease, since x_o (the DC component of x_d) is large and noise is small for the Test 1-45 ECG.

The reverse situation is true, however, for the ECG signals from Tests 1-41 and 1-48. For 1-41, x_o is close to zero and Q is less than 2. So, the ΔR_d spread is lost due to less averaging and none is gained by high pass filtering in this case. For the case of Test 1-41 data, the two opposite effects are both present in almost equal degrees and the change of spread is small. There is a slight spread loss, however, due to the very low signal-to-noise ratio.

The above results show that the improvement predicted by expression (46) are realized in practice by high pass filtering prior to autocorrelation. They also show that short integration time is workable, even though it can result in some spread reduction if Q is low.

3.3.3 Preliminary Bandpass Runs

It is clear that increasing Q will increase spread in autocorrelation amplitudes and thus the reliability of autocorrelation tachometry. From a study of both flight and synthetic ECG spectra, an understanding was gained of the general relationships between Δ R and ECG bandwidth. For clean ECG spectra it was found that Δ R would be small if less than the third harmonic of the ECG were fed into the autocorrelation. Increasing the bandwidth beyond the third harmonic in successive steps would give increases of spread, but these increases would become successively smaller and become negligible after inclusion of the 12th harmonic of the heart rate.

Parallel to this is consideration of noise spectra and their effect on Δ R when mixed with a clean ECG and the bandwidth of the degraded signal varied before autocorrelation. If the noise spectrum is flat, for example, bandwidth reduction would result in a proportional or linear reduction of noise power.

Combining these two factors, we would expect for white noise degradation, increase in spread Δ R with bandwidth reductions which would still pass some harmonics beyond the third but below the 13th and no frequencies below the fundamental. To test these ideas, a degraded flight ECG was bandpass filtered with four different upper frequency cutoffs, and the bandpassed signals were autocorrelated. The digital bandpass filtering is discussed later (Section 5). The four passbands used were:

.5 to 40 cps
.5 to 20 cps
.5 to 10 cps
.5 to 5 cps

The filtered ECG segments are plotted in Figures 71, 72, 73, and 74. Autocorrelation of these bandpassed ECG's constituted the third set of preliminary runs. The normalized autocorrelation functions are plotted in Figures 10, 11, 12, and 13.

Elimination of high frequency noise is observed by noting the smoothing of autocorrelation waveform with a lowering of the high frequency cutoff. The effect of elimination of the higher ECG harmonics is to widen the spikes centered at $\tau = 0$, .43 and .86 seconds; as bandwidth is reduced.

The ECG segment used for the bandpass runs was from X-15 Test 1-48. This same segment was used for one of the cases in each of the other two sets of preliminary autocorrelation runs. To aid in comprehensively studying the effects of the process variations of pre-autocorrelation high pass and band pass filtering and integration time reduction on this same data segment, several parameters of the processes and results are depicted in the chart on the following page. (Figure 14)

The small but regular increase in computed heart rate with bandwidth reduction is probably due to two causes. Recall that

$$x_d(t) = x_c(t) + x_n(t) \tag{2}$$

We also have from our previous analysis:

$$R_d(\tau) = p_c R_c(\tau) + p_n e^{-\beta\tau} = p_c R_c + p_n R_n \tag{47}$$

AUTOCORRELATION

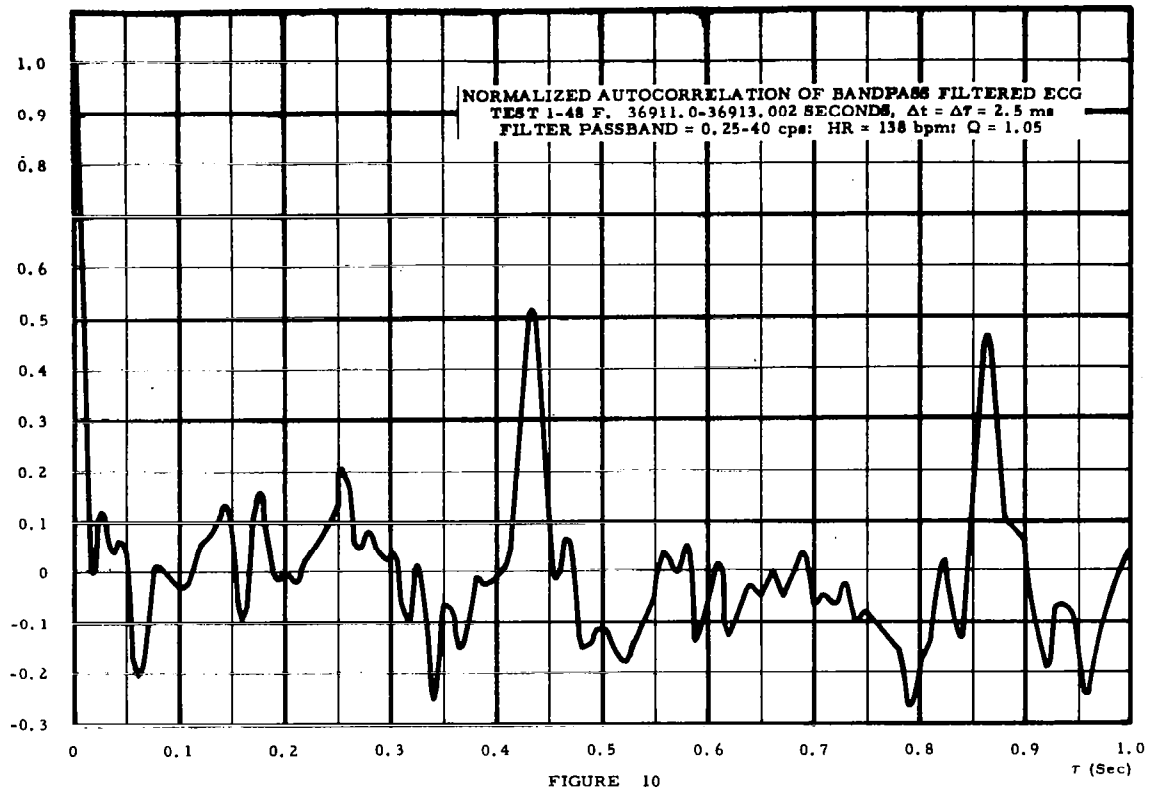

FIGURE 10

AUTOCORRELATION

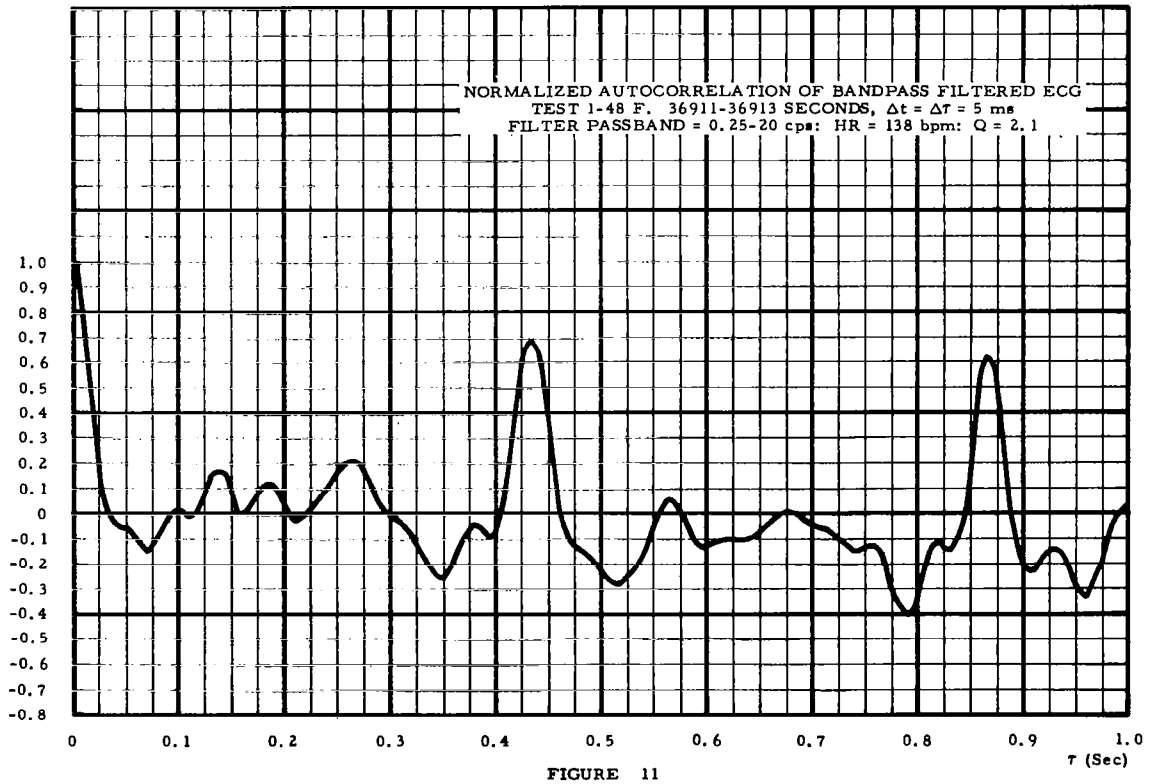

FIGURE 11

Now as degraded signal bandwidth is reduced, we note from the chart an increase in Q or signal-to-noise power ratio through Case 5. From this we can conclude that the noise bandwidth in the degraded signal after filtering is less than it was before filtering, at least until we reach Case 6.

As regards Case 6, we note from the chart that here the highest harmonic of $x_c(t)$ being passed is the second. Now from ECG spectral analysis we find a power peak in $x_c(t)$ at the third harmonic, so that in reducing x_d bandwidth here, we have lost the largest power component of x_c. This not only explains the drop in Q for this case, but also does not eliminate the possibility of a reduction of noise bandwidth even here.

We argue then that there is probably a general reduction in x_n bandwidth accompanying reduction in x_d bandwidth. This means that in expression (47), β becomes smaller as preautocorrelation filtering bandwidth is restricted. From this we see that R_n will take longer to decay, as we go through the cases from 1 to 6. Also, the rate of fall of R_n for τ near τ_o will increase as β becomes smaller. So near the spike peak at $\tau = \tau_o$, the noise component of R_d is larger and falling more quickly when x_d bandwidth is small.

Now, the effect on the shape of the autocorrelation spike tip due to reduction of x_c bandwidth is to blunt it or round it. Combining the x_d bandwidth lowering effects we have, due to R_n, a raising of the left side of the blunt R_c spike relative to the right side. The resultant assymetrical spike shape can be observed well in Figures 11, 12, and 13, the autocorrelation functions for Cases 4, 5, and 6.

The other cause of this spike distortion is due to low frequency periodic noise components still degrading the ECG. They can be seen in Figures 63 and 64, plots of filtered ECG signals. One of these

AUTOCORRELATION

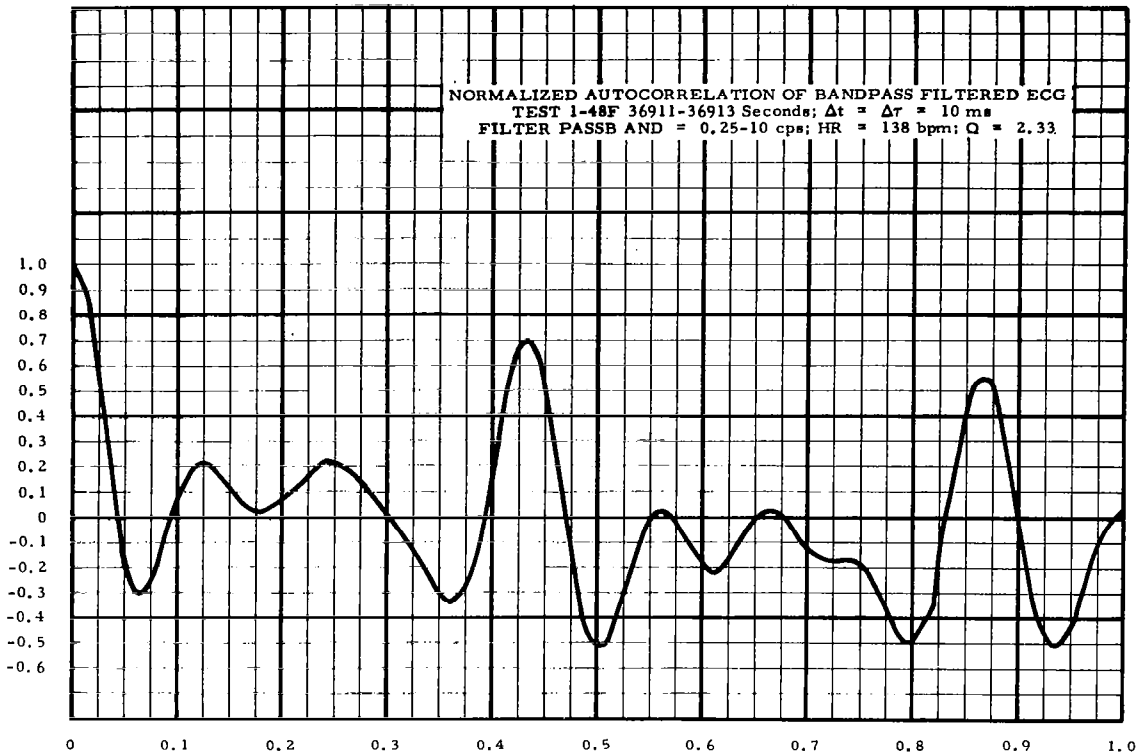

FIGURE 12

AUTOCORRELATION

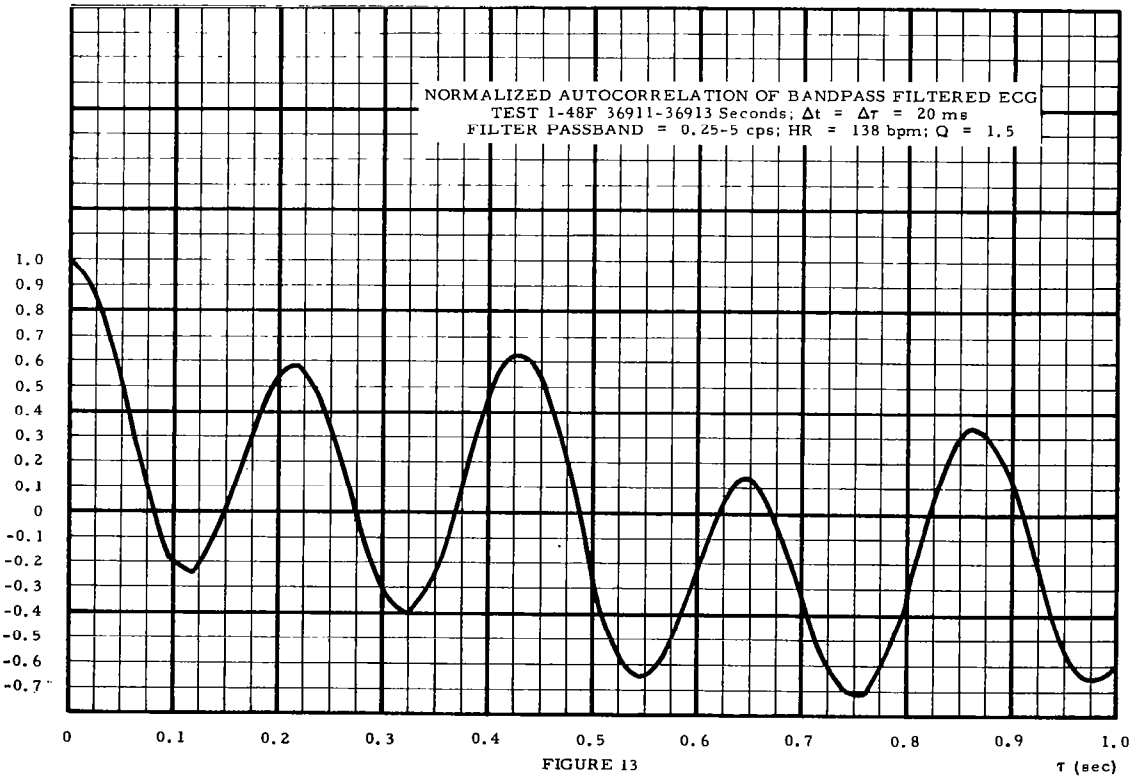

FIGURE 13

periodic noise components has an amplitude roughly equal to the amplitude of second harmonic of an ECG, and a frequency of about .6 cps, a period of 1.6 seconds, and a quarter period of .4 second, which is close to τ_o. This noise component thus has a large negative slope in the neighborhood of the spike peak, and hence will distort the spike shape of $R_d(\tau)$ as did the narrow band white noise exponentially decaying component of $R_d(\tau)$.

With the causes of increased spike assymetry with decreased x_d bandwidth identified, we now turn to the effect of the distortion on the computation of τ_o and HR. Raising the left side of a blunt spike relative to the right side can be seen to displace the maximum amplitude to the left. In other words, the peak value of autocorrelation amplitude $R_d(\tau)$ occurs at a smaller lag with reduced pre-autocorrelation filter bandwidth for the type of degradation present. This means a smaller computed value of τ_o, and a larger computed value of HR as x_d bandwidth is reduced, the effect which required explanation.

The amount of peak left shift is thus dependent on type and amount of degradation, as well as pre-autocorrelation filter parameters. We next note from the chart that several indices of reliability (Spike Amplitude $R_d(\tau_o)$, Spike Width $\Delta\tau_s$, Q, and Spread ΔR_d) are all nearly maximized in Case 5. Since the highest harmonic of x_c passed by the filter is the 4th, the characteristics of Case 5 agree with our predictions from spectral analysis.

3.3.4 Discussion of Optimal High Performance Tachometry

For further development of autocorrelation cardiotachometer technique, we can argue that a coarse or low resolution autocorrelation of bandpass filtered degraded signal x_{dF} will give best economy and reliability for spike detection, since here our spike is wide and of high amplitude with good spread. Once having achieved reliable spike

detection, we can proceed in either or both of two ways.

If our cardiotachometry process is to yield average heart rate, we can simply measure spike occurrence rate by any of several processes familiar to us from conventional cardiotachometry which is based on R-wave detection rather than $R_d(\tau)$ spike detection.

Suppose we wish an accurate measure of individual heart periods, as well as a better estimate of autocorrelation peak amplitude $R_d(\tau_o)$ for purposes which go beyond tachometry. We can then use our coarse value of τ_o as the first approximation to a finer value. With this, we can consider a high resolution autocorrelation process on the unfiltered or wideband degraded signal, but with a limited span of lag variation required now since our coarse approximation is in the neighborhood of the spike peak. Furthermore, we can say something about how rough our coarse value is since we have studied spike width as a function of filtering bandwidth and heart rate.

This two-stage, coarse-fine approach to tachometry signal processes could result in a reliable, economical high performance process design.

3.3.5 Parametric Autocorrelation Runs

To support the development of the sort of autocorrelation processes just described, two sets of parametric autocorrelation runs were made. One set was made on high pass filtered ECG segments from Tests 1-45, 1-41, and 1-48, and contained 45 cases. Previously described bandpass filtered ECG data from Test 1-48 was used in the second run set which included 34 cases.

The purpose of these runs was to determine the effect on the degraded ECG autocorrelation process when sampling resolution Δt, integration

time T, filter passband PB, and signal segment x_d were parametrically varied. These variations were introduced in the hope that examination of run results would help in determining which adjustments of process parameters gave good tradeoffs among reliability, accuracy, and economy.

To make the runs, each case was defined and specified in terms of the x_d segment and process parameters to be used for the computation.

Values of the parameters used are charted below.

Parameter	No. of Values	Values
x_d, ECG Segment	3	Test 1-45, Test 1-41, Test 1-48
Δt, Resolution	15	2.5, 5, 10, 15, 20, 25, 30, 40, 50, 60, 70, 80, 100, 140, 200 ms
T, Integration Time	36	T values ranged from 400 to 1000 ms
PB, Passband	4	High Pass, .5→40 cps, .5→20 cps, .5→10 cps

The .5→5 cps passband was not included in view of the preliminary bandpass run results. The lag increment $\Delta\tau$ was made equal to time sampling resolution $\Delta\tau$ in each run case. Some resolutions were deliverately made very coarse to force cases where the reliability indices would be low. This was done to aid in process trade-off decisions involving high resolution for reliability in spike detection versus low resolution for economy in computation.

Computer outputs from the parametric autocorrelation runs were of

Run Case	1	2	3	4	5	6
Pre-Autocorrelation Filtering	Unfiltered* 0 → 80 cps	Hi-Passed (DC Removed) .3 cps→80 cps	Bandpassed .5 → 40 cps	Bandpassed .5 →20 cps	Bandpassed .5 →10 cps	Bandpassed .5 → 5 cps
Autocorrelation Input Plot Figure No.	5	5 (w/scale shift)	71	72	73	74
Autocorrelation Function Plot Figure No.	6	9	10	11	12	13
T-Integration Time	2.5 sec	1 sec.	1 sec.	1 sec.	1 sec.	1 sec.
Δt - Sampling Interval	.5 ms	.5 ms	2.5 ms	5 ms	10 ms	20 ms
f_s - Sampling Frequency	2000 sps	2000 sps	400 sps	200 sps	100 sps	50 sps
HR - Heart Rate	135.7 bpm	137.9 bpm	138.2 bpm	138.6 bpm	138.9 bpm	140.2 bpm
$R_d(\tau_o)$ - Autocor. Spike Amplitude	.46	.48	.52	.69	.7	.62
$\Delta\tau_s$ - Autocor. Spike Width**	15 ms	13 ms	20 ms	35 ms	55 ms	90 ms
Q - Quality, Signal to Noise	.85	.92	1.05	2.1	2.33	1.5
ΔR_d - Autocor. Spread	.33	.31	.31	.48	.48	.04
H, f_H - Highest Harmonic Passed	34th 78.2 cps	34th 78.2 cps	17th 39.1 cps	8th 18.4 cps	4th 9.2 cps	2nd 4.6 cps

* Unfiltered after Pre-ADC Filtering which had Passband of 0-80 cps
** Measured at $R_d(\tau) = .3$

PROCESS PARAMETERS AND RESULTS OF X-15 TEST 1-48 ECG AUTOCORRELATION
FIGURE 14

Case	x_d	PB (cps)	T (ms)	$\Delta t=\Delta\tau$	N_T	$\hat{\tau}_o$	$R_d(\hat{\tau}_o)$	ΔR_d	$\Delta R'_d$	N_{sphc}	N_{sprs}	E	L-Fig	P-Fig
1	1-45	.54 → 80	560	5	112	490	1.12	1.0		99	7	.071		
2			560	10	56	490	1.09	.98		50	3	.060		
3			555	15	37	495	1.13	1.01		34	2	.059		
4			550	25	22	475	.62	.50		20	2	.100		
5		↓	550	50	11	500	.30	.28		11	1	.091		
6		.4 → 80	765	5	153	495	.94	.75		100	8	.080	17	
7			760	10	76	500	.94	.83		51	4	.078	18	
8			765	15	51	495	.92	.84		34	2	.059	19	
9			750	25	30	500	.58	.46		21	2	.095	20	
10		↓	750	50	15	500	.45	.31		11	1	.091	21	
11		.3 → 80	1000	5	200	495	.93	.82		100	8	.080		
12			1000	10	100	500	.94	.84		51	4	.078		
13			990	15	66	495	.91	.81		34	3	.089		
14			1000	25	40	500	.59	.47		21	2	.095		
15	↓	↓	1000	50	20	500	.49	.39		11	1	.091		

PARAMETRIC HI-PASS ECG AUTOCORRELATION CHART
TEST 1-45
FIGURE 15a

Case	x_d	PB (cps)	T(ms)	$\Delta t=\Delta\tau$	N_T	$\hat{\tau}_o$	$R_d(\hat{\tau}_o)$	ΔR_d	$\Delta R'_d$	N_{sphc}	N_{sprs}	E	L-Fig	P-Fig
16	1-41	.66 → 80	425	5	85	385	.51	.25	.44	78	4	.079		
17			420	10	42	390	.49	.21	.39	40	2	.050		
18			420	15	28	390	.44	.23	.37	27	1	.037		
19			425	25	17	400	.58	.37	.40	17	1	.059		
20		↓	400	50	8	(100)	(.40)			9	-	F	22	
21		.5 → 80	585	5	117	390	.60	.43	.49	79	4	.050	23	
22			580	10	58	390	.60	.44	.48	40	1	.025	24	
23			585	15	39	390	.57	.33	.50	27	1	.037	25	
24			575	25	23	400	.44	.34		17	1	.059	26	
25		↓	550	50	11	(500)	(.41)				-	F	27	
26		.36 → 80	854	5	171	390	.63	.36	.43	79	5	.063		
27			849	10	85	390	.64	.36	.43	40	3	.075		
28			854	15	57	390	.61	.38		27	1	.037		
29			849	25	34	400	.53	.35		17	1	.059		
30	↓	↓	849	50	17	400	.74	.44		11	1	.091		

PARAMETRIC HI-PASS ECG AUTOCORRELATION CHART
TEST 1-41
FIGURE 15b

Case	x_d	PB (cps)	T (ms)	$\Delta t=\Delta\tau$	N_T	$\hat{\tau}_o$	$R_d(\hat{\tau}_o)$	ΔR_d	$\Delta R'_d$	N_{sphc}	N_{sprs}	E	L-Fig	P-Fig
HP-31	1-48	.63 → 80	475	5	95	435	.46	.26	.34	88	3	.041		
32			470	10	47	430	.35	.14		44	2	.045		
33			465	15	31	435	.53	.10*		30	1	.033	28	
34			475	25	19	425	.57	.35		18	1	.056		
35		↓	450	50	9	(350)	(.299)			10	0	M	29	
36		.49 → 80	650	5	130	435	.41	.22	.25	88	1	.011	30	
37			650	10	65	430	.31	.14		44	1	.023	31	
38			645	15	43	435	.48	.09*		30	1	.033	32	
39			650	25	26	425	.47	.22		18	1	.056	33	34
40		↓	650	50	13	450	.60	.35		10	1	.100	35	
41		.33 → 80	956	5	191	435	.43	.26		88	2	.023		
42			951	10	95	430	.42	.16		44	2	.046		
43			946	15	63	435	.42	.07*		30	1	.033		
44			951	25	38	425	.57	.41		18	1	.056		
45	↓	↓	951	50	19	(850)	(.44)			10	-	F	36	

* See Text

PARAMETRIC HI-PASS ECG AUTOCORRELATION CHART
TEST 1-48
FIGURE 15c

Case	PB	T	$\Delta t=\Delta\tau$	N_T	$\hat{\tau}_o$	$R_d(\hat{\tau}_o)$	ΔR_d	$\Delta R'_d$	N_{sphc}	N_{sprs}	E	L-Fig	P-Fig
1	.5 → 40	651	2.5	260	435	.47	.28		175	7	.040		
2	↓	500	2.5	200	435	.53	.32		175	7	.040	37	
3	.5 → 20	651	5	130	435	.62	.41		88	7	.080		
4		500	5	100	435	.63	.40		88	7	.080	38	
5		651	10	65	430	.60	.39		44	4	.091		
6		500	10	50	440	.62	.35		44	4	.091	39	
7		641	20	32	440	.57	.36		23	2	.087		
8		500	20	25	440	.57	.39		23	2	.087	40	41
9		641	40	16	440	.69	.41		12	1	.083		
10		480	40	12	440	.75	.48		12	1	.083		
11		601	60	10	420	.99	.70		8	1	.125		
12		480	60	8	440	1.16	.79*		8	1	.125	42	
13		641	80	8	480	.34	.05		7	2	.286		
14		480	80	6	(80)	(.07)			7	0	M		
15		601	100	6	(300)	(.27)			6	0	M		
16		500	100	5	(300)	(.22)			6	0	M		
17		561	140	4	(140)	(.08)			5	0	M		
18		420	140	3	(280)	(-.13)			5	0	M		
19		601	200	3	(200)	(.30)			4	-	F		
20	↓	400	200	3	(200)	(.24)			4	0	M		

PARAMETRIC BANDPASS TEST 1-48F ECG AUTOCORRELATION CHART

* See Text

FIGURE 16a

Case	PB	T	$\Delta t=\Delta\tau$	N_T	$\hat{\tau}_o$	$R_d(\hat{\tau}_o)$	ΔR_d	$\Delta R'_d$	N_{sphc}	N_{sprs}	E	L-Fig	P-Fig
21	.5 → 10	651	10	65	440	.65	.46	.43	45	6	.133		
22		500	10	50	430	.65	.39		45	5	.111		
23		641	20	32	440	.64	.41		23	3	.130	43	44
24		500	20	25	440	.63	.47		23	2	.087	45	46
25		631	30	21	420	.55	.35		15	2	.133		
26		480	30	16	420	.57	.35		15	2	.133		
27		641	40	16	440	.62	.46		12	1	.083	47	48
28		480	40	12	440	.65	.43		12	1	.083	49	50
29		651	50	13	450	.49	.25		10	2	.200	51	
30		500	50	10	450	.48	.29	.24	10	2	.200		
31		631	70	9	420	.64	.37		8	1	.125	52	
32		490	70	7	420	.64	.26*		8	1	.125	53	54
33		601	100	6	(300)	(.42)			6	-	F	55	56
34	↓	500	100	5	(400)	(.28)			6	0	M	57	58

PARAMETRIC BANDPASS TEST 1-48F ECG AUTOCORRELATION CHART

* See Text

FIGURE 16b

two types. One type was a listing output L containing paired values of τ and $R(\tau)$ for each value of τ from $\tau = 0$ to $\tau = \tau_m$ at increments of $\Delta\tau$. The second type of output was a printer plot P making a graph of the paired values to enable immediate visual comprehension of the autocorrelation function shape. A machine listing and plot were specified as the output for each case.

In view of the extent of the parametric high pass and bandpass runs, involving 79 cases in all, it is not feasible to detail completely all of the results in this report. The specifications and highlights of the results for each case are listed in chart form in Figures 15 and 16, which are discussed below. In addition, sample machine outputs were selected to represent machine output listings and plots of several cases. Replicas of machine outputs appear in Figures 17 through 58.

In the charts, all time and lag values (T, $\Delta t = \Delta\tau$, and $\hat{\tau}_o$ to be defined later), are in milliseconds, ms; all lower and upper cutoff frequencies ($f_{LC} \rightarrow f_{HC}$), specifying the passband PB through which x_d was filtered prior to autocorrelation, are in cycles per second, cps.

The passband for the high pass run cases was determined as follows. The low frequency cutoff due to removal of the mean from x_d can be shown to be $f_{LC} \doteq \frac{.6}{2T}$ cps. The T dependence holds since the mean x_d value was computed as a 2T second average. The high cutoff is due to the preconversion filtering on the analog flight signals. For the ECG analog flight tape playback in conversion, f_{HC} was specified as 80 cps.

Several indices have been defined and applied, which are useful in measuring and evaluating the effect of the parametric variations specified for the run cases. One such index is the number of multiplications required to compute the lagged products ($x_i\, x_{i+j}$) which are

needed to calculate a single value of autocorrelation R_j. This index is measured by the number of sampling increments $\Delta\tau$ in the integration time T. It is called N_T, and so we have

$$N_T = \frac{T}{\Delta t} = f_s T \text{ samples per integration} \tag{48}$$

where

Δt = seconds per sample

$f_s = \frac{1}{\Delta t}$ samples per second

T = seconds per integration

Due to the nature of the discrete autocorrelation algorithm, the maximum lag τ_m is one lag interval $\Delta\tau$ less than integration time T in each run case (τ_m is the largest value of τ for which $R_d(\tau)$ was computed). Also, the number of lag intervals per integration time $N_{\Delta\tau}$ is one less than the number of lag values in T: $N_{\Delta\tau} = N_T - 1$.

Therefore,

$$\tau_m = T - \Delta\tau = (N_T - 1)\Delta\tau = (N_\Delta)(\Delta\tau) \tag{49}$$

$$N_\tau = 1 + \tau_m / \Delta\tau.$$

Chart entries of N_T values are made in the column following the $\Delta\tau$ column.

The $\hat{\tau}_o$ and $R_d(\hat{\tau}_o)$ chart entries are the values corresponding to the peak of the largest spike in $R_d(\tau)$ following the fall of the half-spike centered at the origin ($\tau = 0$). The criteria for proper spike detection were that

$$\left| \hat{\tau}_o - \tau_o \right| < \Delta\tau_s, \text{ the spike width at } R_d = .3 \tag{50}$$

and

$$R_d(\hat{\tau}_o) > .3 \tag{51}$$

where τ_o is a more accurate estimate of heart period than $\hat{\tau}_o$, and τ_o is obtained from the highest resolution autocorrelation.

Whenever condition (50) or (51) is unsatisfied, the $\hat{\tau}_o$ and $R_d(\hat{\tau}_o)$ entries in the charts are enclosed in parentheses.

Two measures of autocorrelation amplitude spread were used. Spread measure ΔR is the spread between $R(\hat{\tau}_o)$ peak and the highest subpeak for any lag following the origin half-spike (i.e., the half-spike peaked at $\tau = 0$) zero-crossing, τ_z. Spread measure $\Delta R'$ is the difference between the $R(\hat{\tau}_o)$ peak and the highest subpeak following the lag value $\tau = 250$ ms. The $\Delta R'$ spread measure is of interest in average rate computation, since $\tau_o < 250$ ms corresponds to HR >240 bpm. Thus, subpeaks at lags less than 250 ms could be excluded from consideration if the autocorrelation cardiotachometer were not required to measure rates above 240 bpm. In the charts, R'_d entries were made only for those cases where its value was significantly different from the R_d value.

Another index is the number of samples per heart cycle, N_{sphc} N_{sphc} is a measure of resolution with respect to heart period, and therefore is useful for comparing cases of the autocorrelation process involving different heart rates. It is readily computed from:

$$N_{sphc} = \frac{\tau_o}{\Delta t} \text{ samples/heart cycle} \tag{52}$$

A different index provides another useful measure in evaluating reliability of spike detection. This index is the number of discrete autocorrelation values contained in the spike width, or the number of "hits" per spike. It is denoted N_{sprs}, the number of samples per autocorrelation spike, and is determined by counting the number of discrete R_d values which are on the spike with amplitudes above some threshold value. In determining spike width $\Delta\tau_s$, the level .3 was used as the normalized autocorrelation value at which to measure it. For consistency, .3 was defined as the spike base level for counting N_{sprs}. Values of N_{sphc} and N_{sprs} for each case are in Figures (15) and (16). From considering the previous two indices, we find that an easily computed measure of efficiency is the ratio

$$E = \frac{N_{sprs}}{N_{sphc}} \tag{53}$$

which is the proportion of "hits" or points on the spike yielded by discrete autocorrelation computations and also is normalized with respect to heart rate. Chart treatment of E is discussed below.

The L-Figure and P-Figure chart columns contain the figure numbers where a replica machine listing (L) or plot (P) for the case appears in this report. Nineteen cases were selected to represent machine outputs of the parametric HP run. These 19 cases illustrate autocorrelations of three x_d signals with five different resolutions for each, plus four additional cases of special interest. Similarly, 14 cases were selected for output detailing from the parametric BP run, covering three passbands and nine resolutions. Listings and plots are in Figures 17 through 58.

To illustrate the manner of determining some of the chart entries fr the computer listings, the plots included from the BP run have b marked as follows: All pairs of (τ, R) values on the spike peaking at

$\hat{\tau}_o$ have been underlined, the number of such pairs being N_{sprs}; the spike peak pair ($\hat{\tau}_o$, R) has been boxed with solid lines; the largest subpeak has been boxed with dashed lines.

The effectiveness of each run is depicted in the E column of the charts. Missed or falsely performed autocorrelation spike detections are identified by the codes M or F, respectively, as the Column E entry. Such M and F cases were determined by applying criteria (50) and (51). An "M" code means inequality (51) did not hold and an "F" code means that inequality (50) did not hold. All other cases resulted in reliable detection. For this majority of cases, the efficiency E was computed from expression (53) and its value entered in Column E.

Having introduced this material on the parametric runs, we can now discuss several interesting features of the results. For example, in run-case HP-20, the spike period is grossly miscalculated as $\hat{\tau}_o$ = 100 ms because $\tau_m = T - \Delta\tau$ = 350 ms was low compared to τ_o = 395 ms.

In HP-25, spike present is detected but period $\hat{\tau}_o$ is indicated as 500 ms which is more than $(1/2)\Delta\tau_s$ from the "true" value of τ_o = 395 ms. The autocorrelation listing values of R_d around τ_o are: R(350) = -.25, R(400) = .36, R(450) = -.14, R(500) = .41. It is seen here that quantization error is large due to the coarse resolution (Δt = 50 ms), since in case HP-21 where $\Delta\tau$ = 5 ms, we have R(500) = .09, from Figure (23) listing.

In run case HP-35, a miss resulted since

$$\tau_o - \tau_m = 442 - 400 = 42 \text{ ms}$$

which is less than a half-spike width, so τ_m was not large enough to penetrate the τ_o spike. In the last HP case, Number 45: the second R_d spike at $\tau = 2\tau_o$ was detectable with an R_d threshold of .3, but the spike at one heart period of lag τ_o was not. From the listing for HP-45, $R(450) = .008 \doteq R(\tau_o)$, but $R(850) = .44 \doteq R(2\tau_o)$. Also of interest is the largest R value in the neighborhood of τ_o, which was $R(550) = .27$.

The missed detection in BP Case 17 was due to excessive quantization error in the sampling ($\Delta\tau$ = 140 ms) of x_{dF}. This was also the cause of the false detection in BP Case 33, and the partial cause of other missed detections in BP cases.

In HP run Cases 33, 38, and 43, for each of which Δt = 15 ms, subpeak amplitudes greater than .3 were observed, making ΔR quite small. In Case 33, R(255) = .43; in Case 38, R(255) = .39; and in Case 43, R(255) = .35. Thus, the highest of these overthreshold subpeaks is lowered with increased integration time T, which agrees with previous results regarding usual ΔR improvement with greater T due to averaging effects.

Subpeak amplitudes were above .3 in the BP Cases 12 and 32:

BP Case 12: R(300) = .37, ΔR = .79, Δt = 60 ms
BP Case 32: R(280) = .38, ΔR = .26, Δt = 70 ms

Here, we see that in contrast to the three HP run cases (33, 38, 43) where a similar thing occurred, we have large spread in the BP cases. These are particular cases of one generally seen advantage of band limiting degraded signals prior to autocorrelation: larger spread. For Δt resolutions as coarse as .60 ms, no ΔR spreads below .25 occurred in the band pass runs. Also seen from these results is that large HP subpeaks resulted at medium resolution (Δt = 15 ms), whereas large BP subpeaks were only found at coarse resolutions (Δt = 60, 70 ms).

Regarding the matter of reliability and economy it was found, for wide band ECG signals, that reliable spike detection with a high quality x_d was possible with a sampling rate f_s of 20 sps with an effectiveness measure of E = .09. For a low quality ECG, reliable detection required an f_s of 40 sps, with E = .06. For a very noisy x_d, an f_s in the range from 100 sps to 200 sps was needed for reliability; where E, which varied from .011 to .046, was quite dependent on f_s and T.

When appreciable bandlimiting of a heavily degraded x_d was applied prior to autocorrelation, reliable detection was possible with a sampling rate as low as f_s = 15 sps, with a high effectiveness measure of E = .125.

3.3.5 Summary of ECG Autocorrelation Investigation

We will nowconclude the discussion of autocorrelation cardiotachometry technique investigation. Fine resolution ECG autocorrelation permits reliable and accurate measurement of heart period τ_o, from which rate HR is easily determined.

If individual ECG period measures are desired, the integration time parameter T of the autocorrelation process must be less than $2\tau_o$ but greater than τ_o. (This can be achieved either by increasing τ_o from small values until a spike is computed, or by determining an approximate period $\hat{\tau}_o$ by other procedures and then checking for positive spread or minimal slope, particularly against any peak or "subpeaks" in the neighborhoods of $\frac{\hat{\tau}_o}{2}, \frac{\hat{\tau}_o}{3}, \frac{\hat{\tau}_o}{4}, \ldots, \tau_{min}$)

To measure average period (and thereby average rate), the individual periods can be averaged. Alternately, a large T equal to the rate

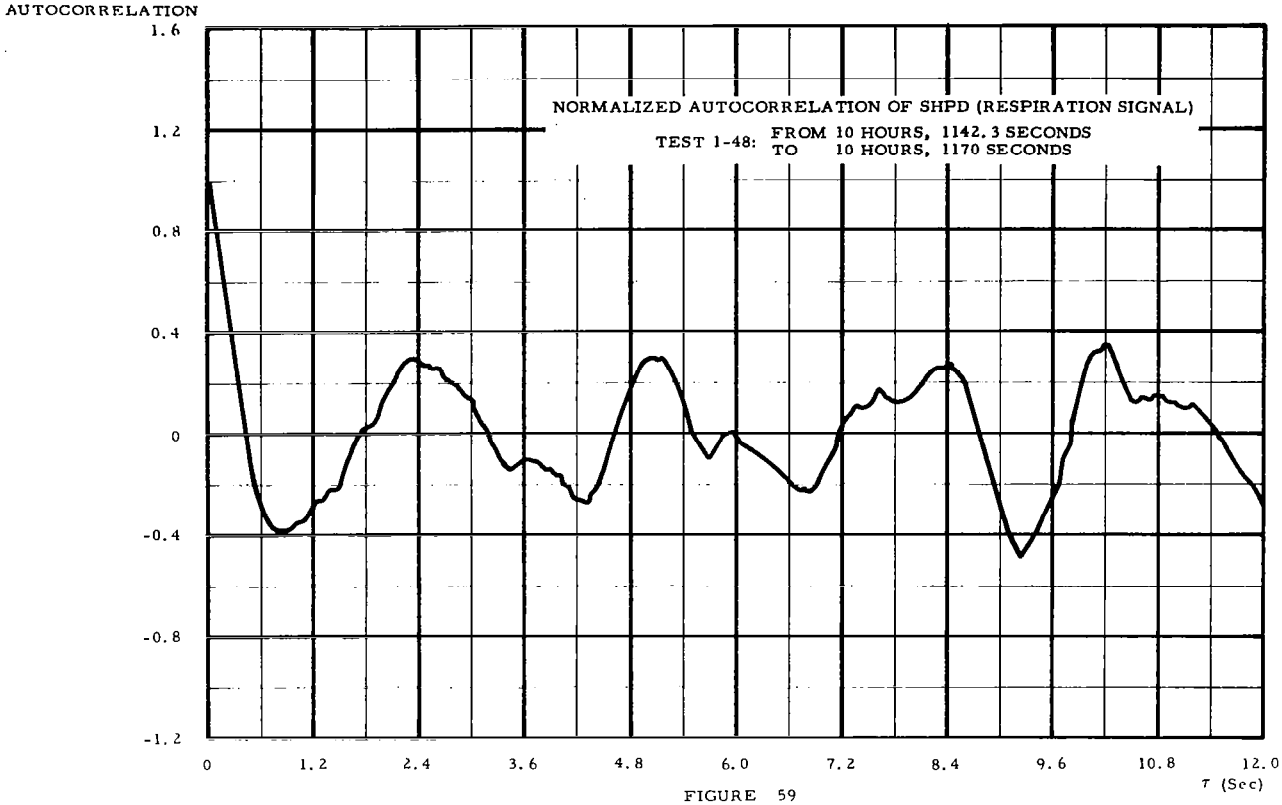
AUTOCORRELATION
1.6
1.2
0.8
0.4
0
-0.4
-0.8
-1.2
NORMALIZED AUTOCORRELATION OF SHPD (RESPIRATION SIGNAL)
TEST 1-48: FROM 10 HOURS, 1142.3 SECONDS
TO 10 HOURS, 1170 SECONDS
0
1.2
2.4
3.6
4.8
6.0
7.2
8.4
9.6
10.8
12.0
τ (Sec)

FIGURE 59

averaging time can be used, and the average period $\bar{\tau}_o$ estimated from the lag interval between successive autocorrelation spikes. This latter method is uneconomical for large HR averaging times.

Without sacrificing reliability, it is possible to bring about a trade-off of some accuracy in τ_o determination for more economy in computation by lowering resolution of the autocorrelation process with clean ECG's, and by a combination of lowered process resolution and band limiting heavily degraded ECG's prior to autocorrelation. Finally, pre-autocorrelation bandpass filtering improves process reliability, particularly with low quality signals.

3.4 Autocorrelation of Respiration Signal

To investigate the utility of autocorrelation for respiration tachometry, a suit-helmet pressure differential (SHPD) signal segment was selected. This SHPD segment, from X-15 Test 1-48, was autocorrelated with the computer program previously described, with a τ_m = 12 seconds. A hand plot was prepared from the machine output listing and appears in Figure 59. The peaks of the normalized autocorrelation are not as spiked as those from the ECG runs. This is due to the narrower bandwidth of the respiration signal as well as to its large aperiodicity. The peaks are well enough defined to permit an easy estimate of respiration rate, which is 24 respirations per minute.

Although the spread ΔR is low at .11, the consistent way in which the peak values exceed an R = .3 threshold indicates that reliable respiration rate determination is possible with autocorrelation of the SHPD signal.

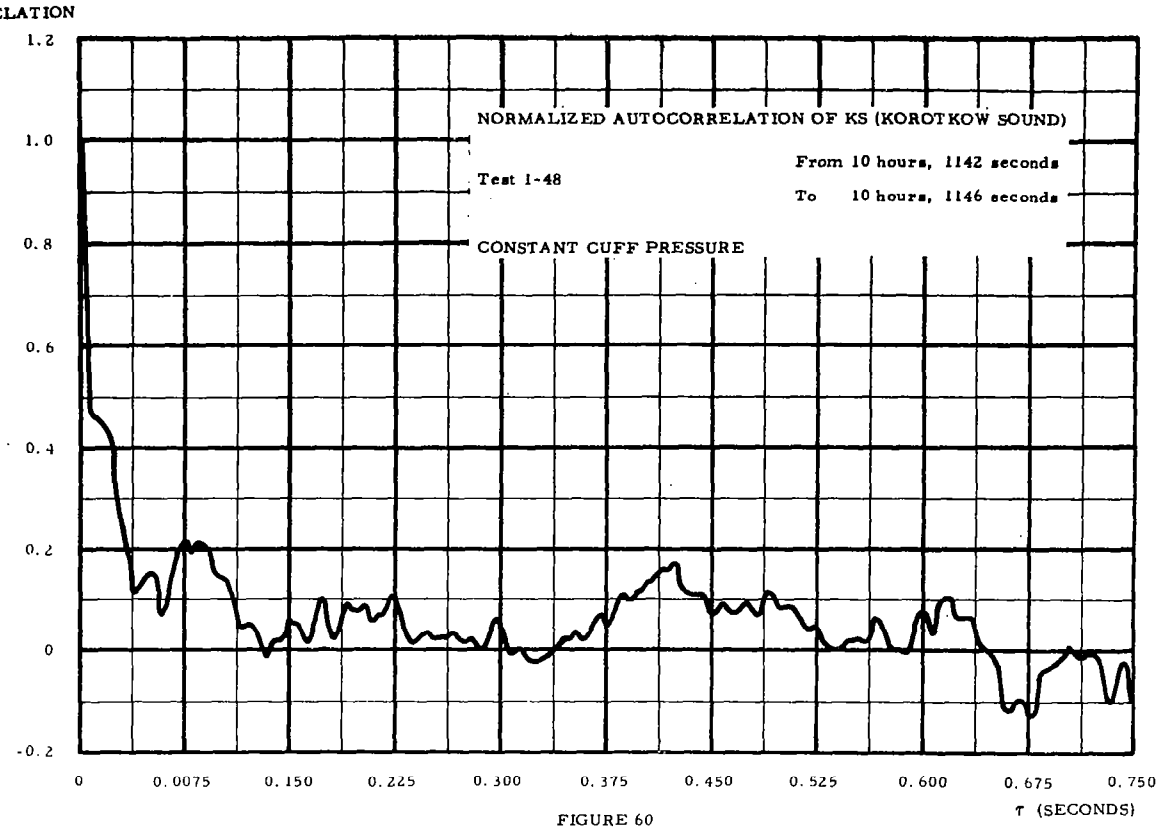

FIGURE 60

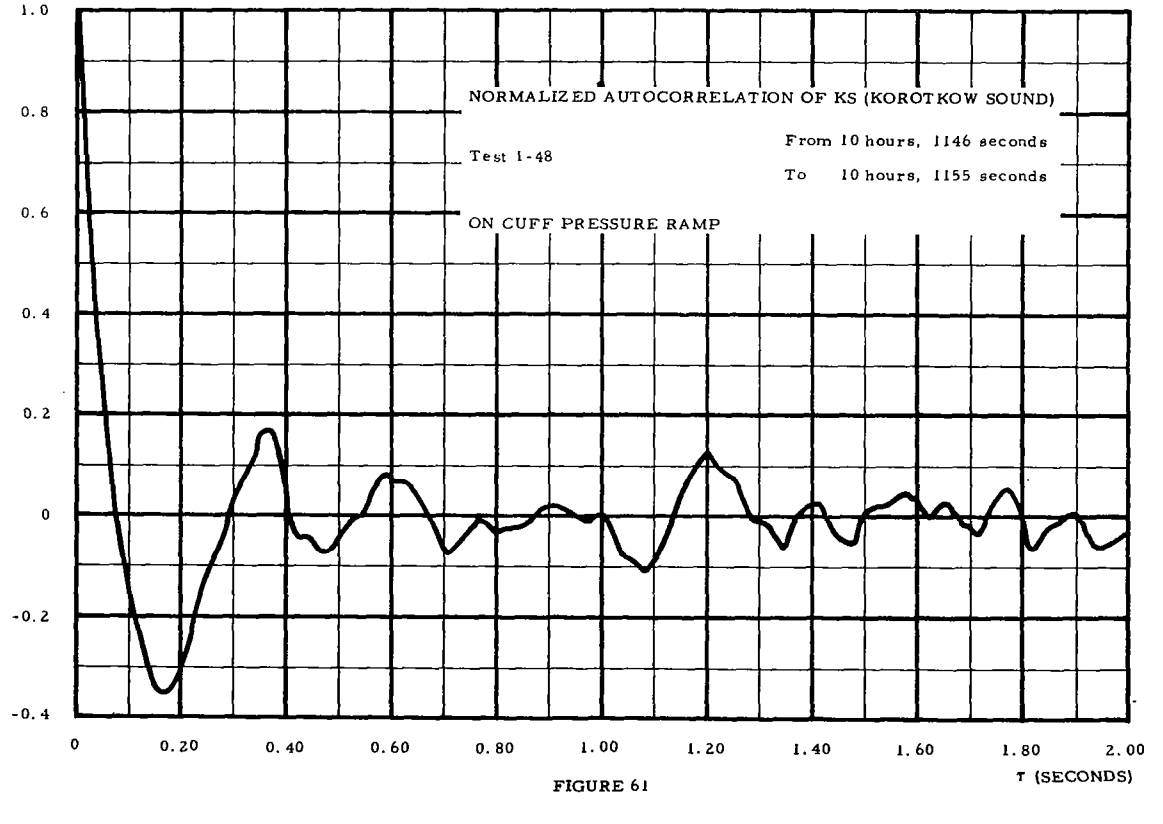

FIGURE 61

3.5 Autocorrelation of Korotkow Sound Signal

The X-15 test data converted and available for study contained no signals in the Korotkow sound channel which could be clearly distinguished from noise. It was decided to attempt to determine whether autocorrelation of this data would help to determine presence of KS signals in the KS channel and thereby aid in blood pressure measurement under such conditions. This attempt was made by autocorrelation runs of two segments of KS channel data. One segment was chosen from a flight portion when the cuff pressure (CP) signal was low and constant, and hence when KS would not be expected. The other segment was chosen from a flight portion for which the cuff pressure signal level would lead one to expect presence of a sound signal in the KS channel, provided the sensor and what followed it were working. The results of these runs are plotted in Figure 60 (CP constant), and Figure 61 (CP Ramp).

The results do not enable any confidence in the statement that sound was present in one case and absent in the other. No discernible periodicity occurs in either case, and similar peak amplitudes appear in the two cases.

Section 4

POWER SPECTRAL DENSITY

The power spectral density function of a signal x(t) gives power density $S_x(f)$ as a function of frequency f. $S_x(f)$ is the frequency domain transform of the autocorrelation function. As in the autocorrelation function, all the basic frequency information in a signal is present and all phase information absent in the spectral density function. Since the autocorrelation function and the power spectral density function are Fourier transform pairs, the power spectral density function, $S_x(f)$, may be obtained through Fourier transforming the autocorrelation function, $\psi_x(\tau)$, into the frequency domain.

$$S_x(f) = 2\int_0^\infty \psi_x(\tau)\cos(2\pi f\tau)d\tau \tag{54}$$

The possible utility of the power spectral density function in period direction applications stems from the fact that a pure cosine component of x(t), having an angular frequency $i\omega_o$ will be transformed into a sharp spike centered at $f_i = \frac{i\omega_o}{2\pi}$ cps in the frequency domain. These sharp spikes are commonly known as "spectral lines" or "delta functions." A band limited white noise component of x(t) appears in $S_x(f)$ as a power base shift; hence, it will not obscure the recognition of sufficiently large periodic constituents. Thus, the power spectral density of a signal plus noise time function $(x_d(t) = x_c(t) + x_n(t) + x_p(t))$function will take the form of a power base shift on which is superimposed power level spikes at the signal harmonics and at the periodic noise frequencies.

In actual applications of power spectral density analysis, we are confronted with the problem that the upper limit of integration in (54) cannot go to infinity, since the autocorrelation function can be computed only to some finite maximum lag, τ_m. Thus (54) is approximated by

$$S_x(f) = 2 \int_0^{\tau_m} \psi_x(\tau) \cos(2\pi f \tau) d\tau \tag{55}$$

which explicitly assumes that $\psi(\tau > \tau_{max}) = 0$, and may imply a discontinuity in $\psi(\tau)$ at $\tau = \tau_{max}$. If a discontinuity in the autocorrelation function exists, which is generally the case, minor power spikes will appear around the period defining spectral lines, thereby indicating erroneous frequencies. This is commonly known as Gibb's Phenomenon, and can be combatted by applying a lag window (Hamming) truncation to the autocorrelation function and making the appropriate amplitude adjustments to (55).

$$\psi'(\tau) = \psi(\tau) \left[.54 + .45 \cos \frac{\tau \pi}{\tau_{max}} \right] \tag{56}$$

$$S(f) = 4 \int_0^{\tau_{max}} \psi'(\tau) \cos(2\pi f \tau) d\tau \tag{57}$$

The digital approximations for equations (11) and (12) are as follows:

$$\psi(r \Delta t) = R_r = R^*_r \left[.54 + .46 \cos \frac{r \pi}{m} \right] \tag{58}$$

$$S(i \Delta f) = S_i = 2 \Delta t \left[R_o + 2 \sum_{r=1}^{m-1} R_r \cos(2 \pi i r \Delta f \Delta t) + R_m \cos(2 \pi i m \Delta f \Delta t) \right] \tag{59}$$

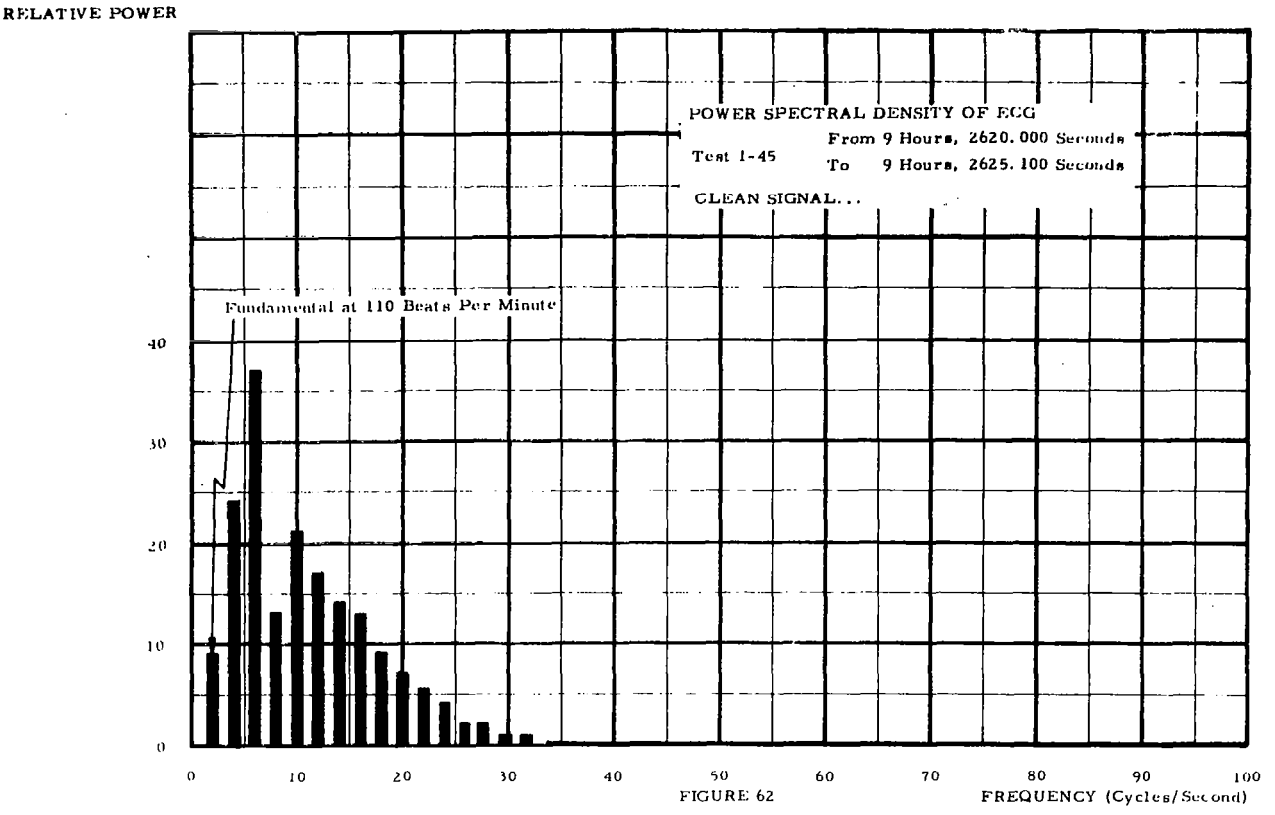

FIGURE 62

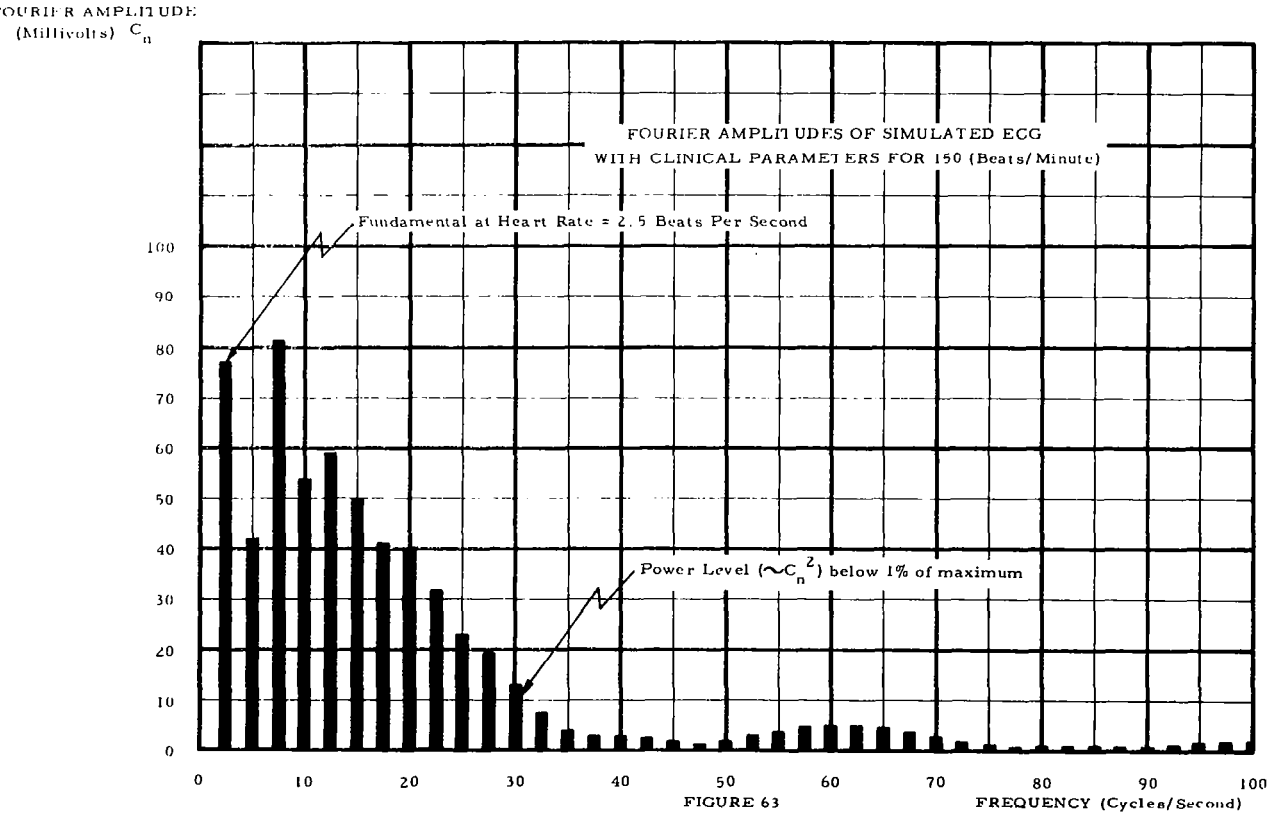

FIGURE 63

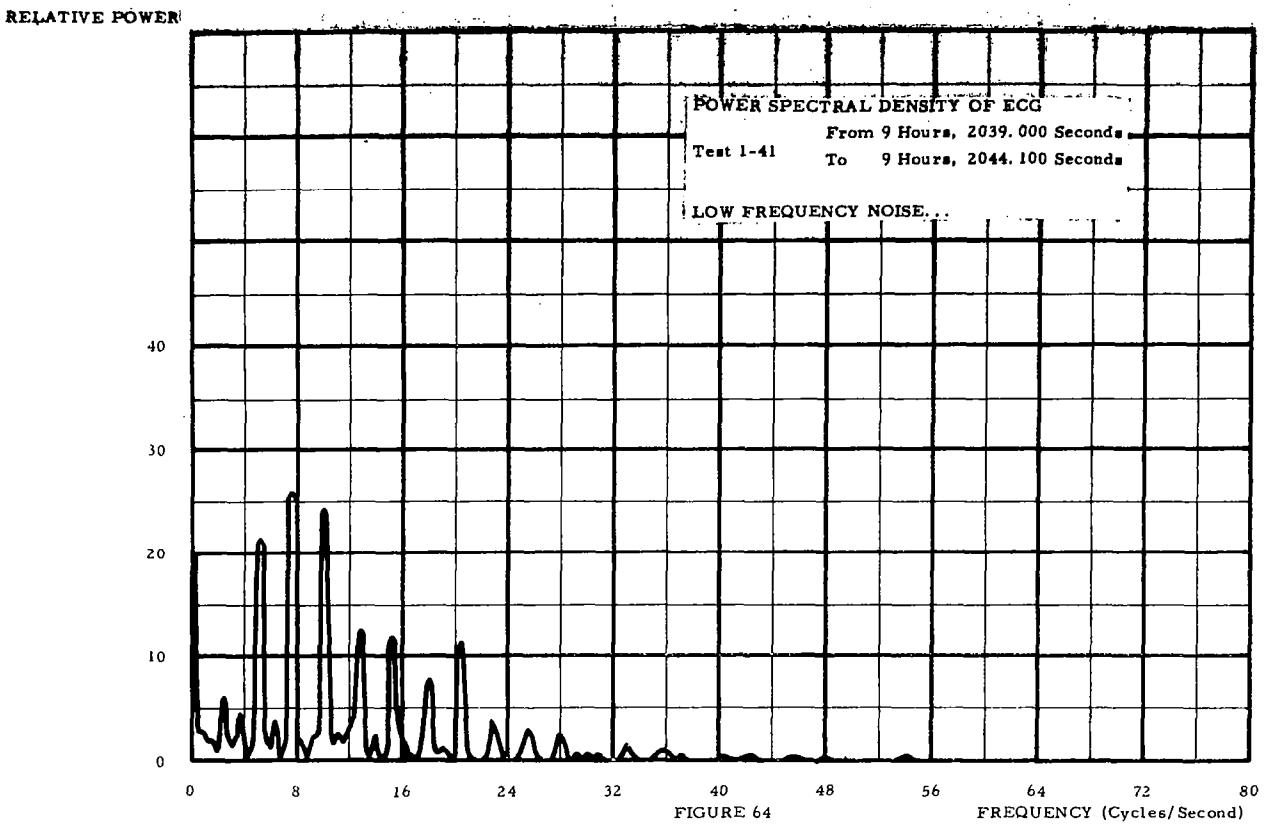

FIGURE 64

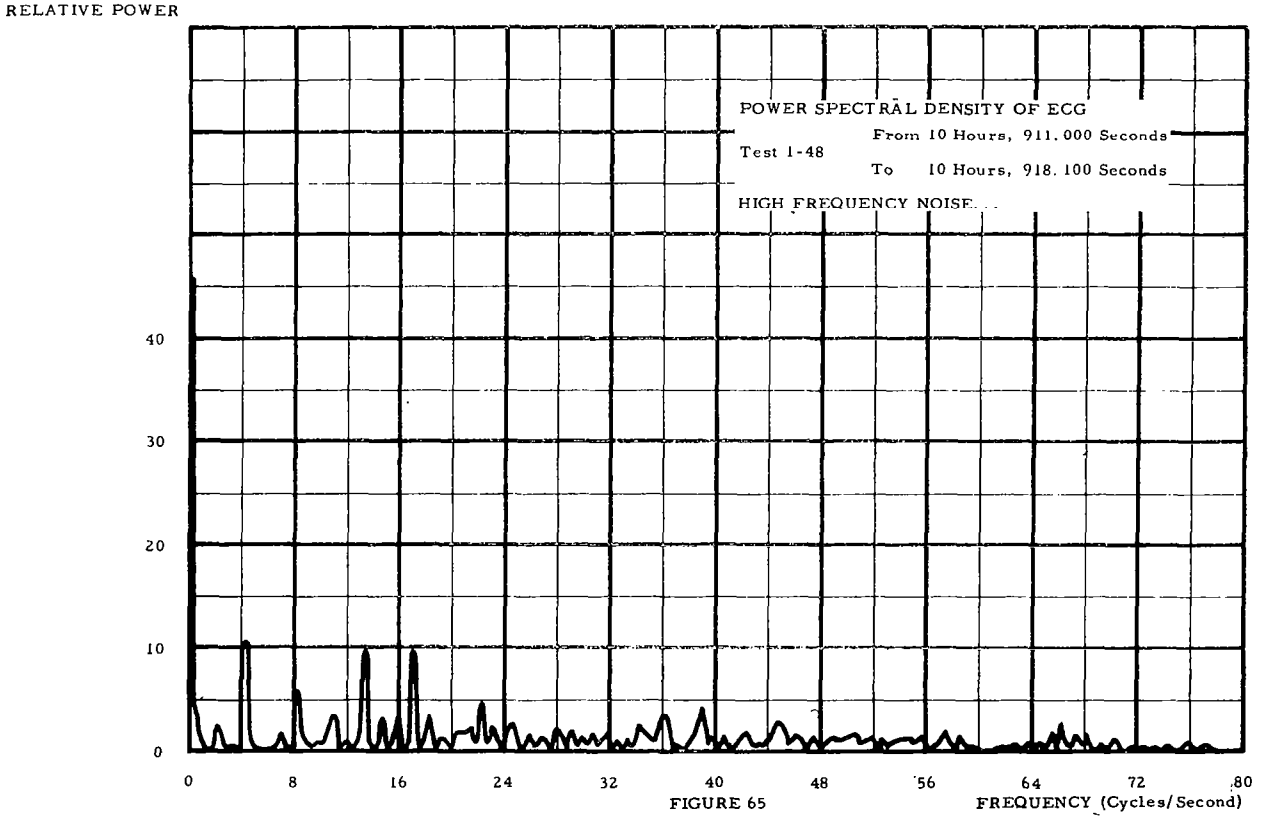

FIGURE 65

where m represents the maximum index in the autocorrelation computation, $m \Delta t = \tau_m$.

The power spectral density functions of several ECG signals were computed in order to investigate rate detection ability afforded by the signals' power spectra. Figure 62 represents the power spectrum of a relatively noise-free ECG signal with a fundamental frequency (heart rate) at 110 beats per minute. To verify the qualitative harmonic power structure of this signal and to investigate the utility of a synthetic ECG signal (to be discussed in Section 8), the power spectrum in the form of Fourier coefficients was constructed for a proposed synthetic ECG signal (see Figure 63). The harmonic structure of the live (flight) ECG and the synthetic ECG were qualitatively similar except for the fundamental power levels. The low fundamental power of the live ECG was attributed to low frequency attentuation in the recording loop.

Figures 64 and 65 represent the power spectral density functions of ECG signals x_d, degraded by low and high bandwidth noise, respectively. The power base shift due to any bandlimited white noise present in x_d cannot be completely presented through digital simulation due to the limiting of sample size and quantizing errors. However, noise corruption does become apparent in these power spectra displays.

A study of flight ECG spectral form was made from the power spectral density plots of the segments of X-15 flight ECG data. Examination of the flight ECG spectra showed that with a high signal to noise power ratio and with the spectra peak at the third harmonic of R-R frequency the power density of the fundamental R-R frequency is about 1/3 that of the peak. Above the third harmonic, power decreases and is more than 20 db below peak level at the 12th harmonic. Thus, the flight ECG appears to have an intelligence bandwidth of about 3-1/2 octaves above the fundamental, the ECG power spectra peaking at the 3rd

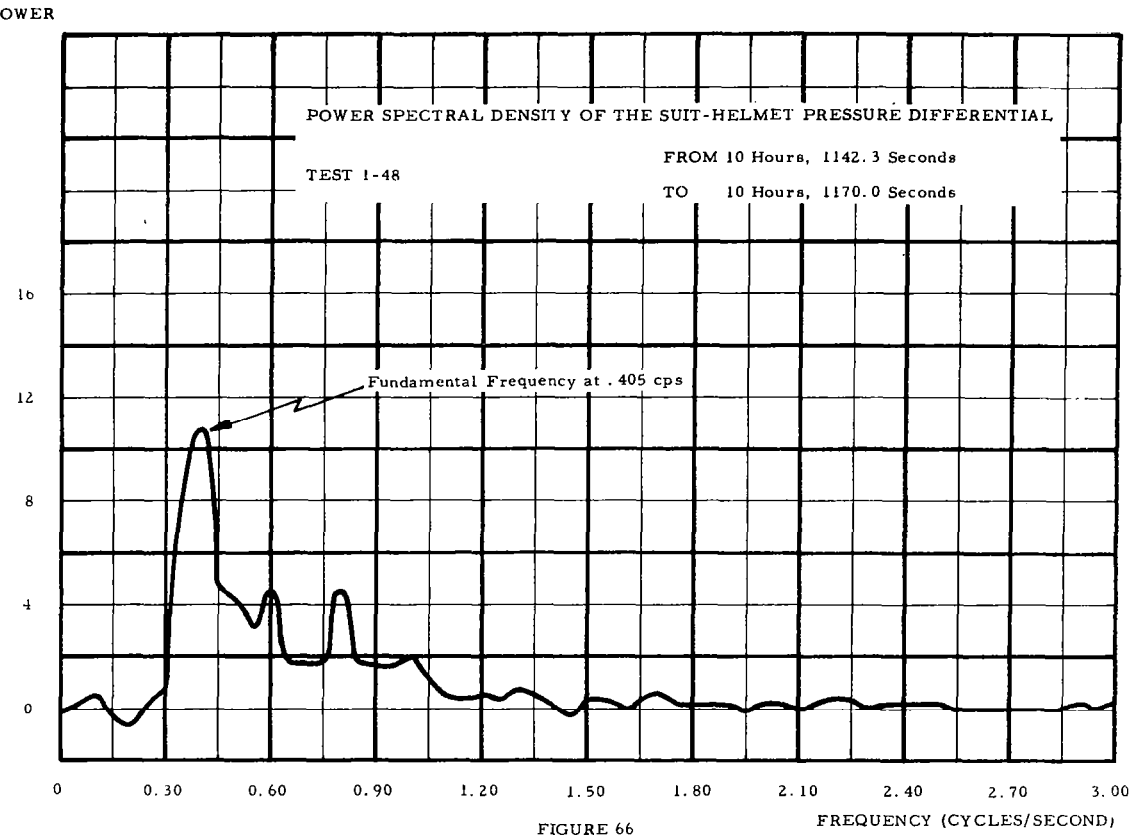
RELATIVE POWER
POWER SPECTRAL DENSITY OF THE SUIT-HELMET PRESSURE DIFFERENTIAL
TEST 1-48
FROM 10 Hours, 1142.3 Seconds
TO 10 Hours, 1170.0 Seconds
Fundamental Frequency at .405 cps
16
12
8
4
0
0
0.30
0.60
0.90
1.20
1.50
1.80
2.10
2.40
2.70
3.00
FREQUENCY (CYCLES/SECOND)

FIGURE 66

harmonic and decreasing at about 10 db/octave above the peak. The noisy-signal spectra extends beyond the clean-signal spectra in bandwidth. In the cases of spectral analysis performed, significant noise power appeared over twice the bandwidth of the signal power.

Heart rate determination from the power spectral density function of x_d appears quite unreliable due to the lack of good discrimination of the fundamental power spike. The higher harmonics of the ECG complex could be utilized in logic circuits to estimate the fundamental frequency, but periodic noise components would probably render this technique unreliable. It seems apparent at this time the additional expense of Fourier transforming the ECG autocorrelation function into the frequency domain is not justified for purposes of heart rate determination.

The power spectral density function of the suit-helmet pressure differential, (see Figure 66 for a typical sample) was investigated with respect to rate measuring utility. The S-HPD signal has the nature of an "almost periodic" function; hence it yields a rather simple harmonic structure. However, due to aperiodicities, the fundamental or rate determining power spike has a large spread but indicates a good discrimination of an averaged respiration rate. Figure 66 shows the average respiration rate over 27.7 seconds to be approximately 24.3 respirations per minute. This value agrees very well with the breathing rate determined by autocorrelation of S-HPD discussed in Section 3 and plotted in Figure 59. If the S-HPD signal were first bandpass filtered (with passband tuned to the respiration rate band), the power spectrum would yield even better rate discrimination than indicated by Figure 66. However, it is felt that in addition to autocorrelation, other techniques, less expensive than spectral density analysis can be formulated without sacrificing reliability for respiration rate determination (see Section 7 on zero-crossing detection).

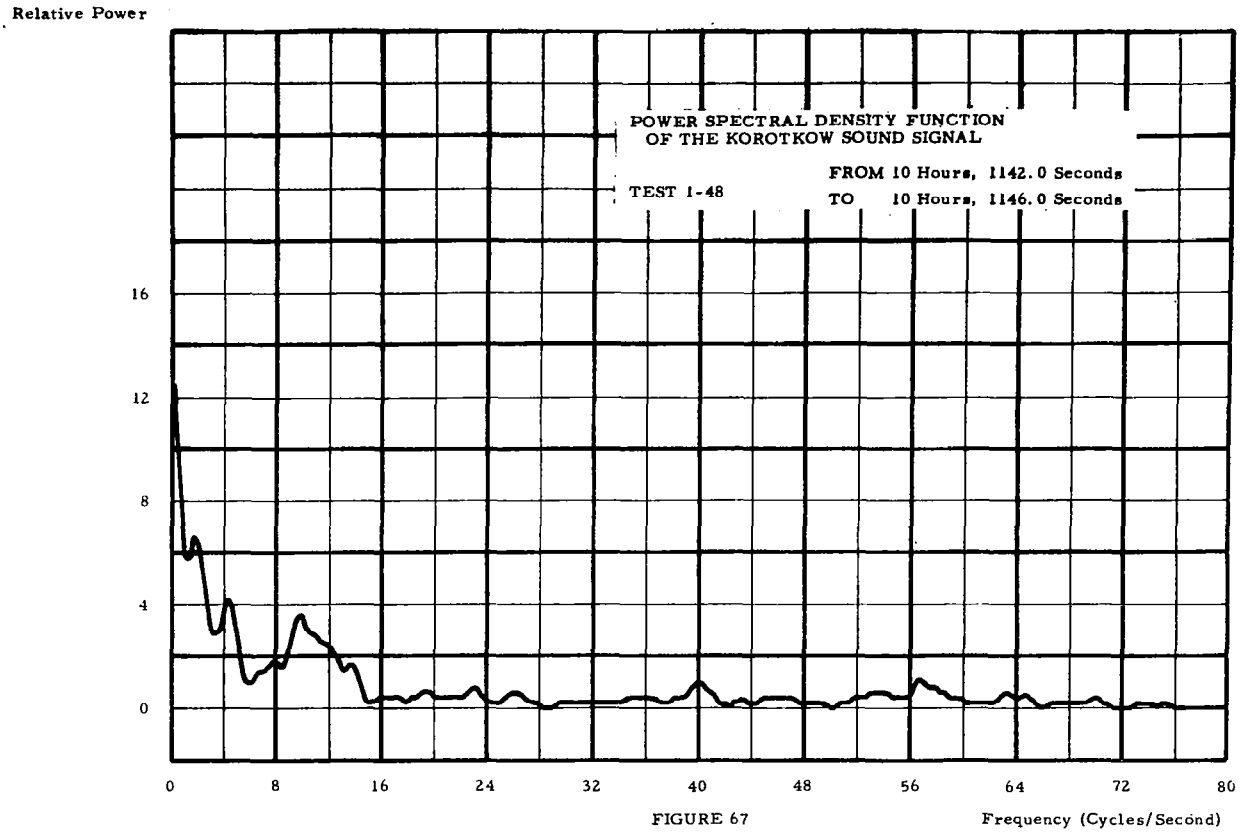

FIGURE 67

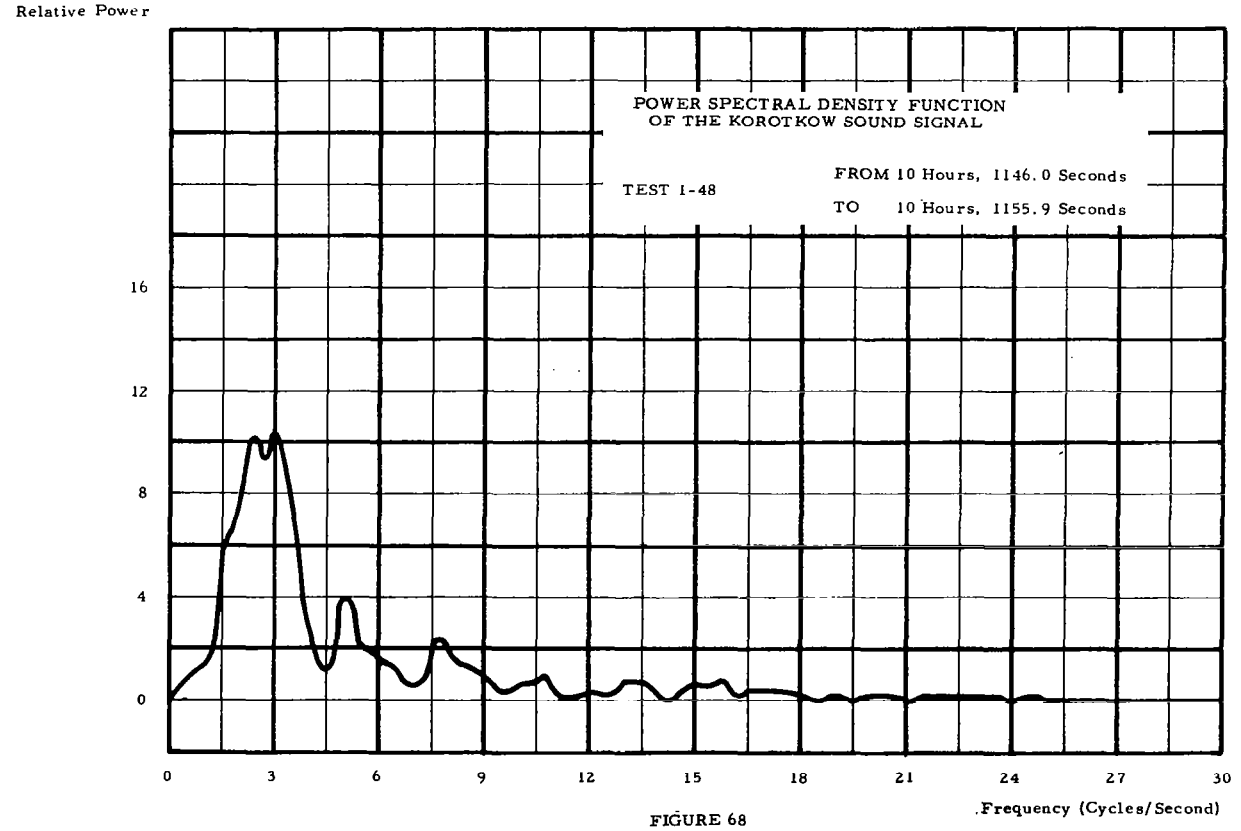

FIGURE 68

The power spectrum of the Korotkow sound signal channel was investigated in an attempt to determine the clean signal characteristics. Two signal segments from test 1 - 48 were chosen in a manner similar to the one used in Korotkow sound autocorrelation for illustration. Figure 67 represents the power spectral density function of a data segment of the Korotkow sound channel where cuff pressure was low and constant and no sound expected, whereas the power spectrum of a segment for which presence of Korotkow sound would be expected (while cuff pressure was on its ramp portion) appears as Figure 68. To aid in studying the Korotkow sound spectrum, it was decided to establish the heart rate in the flight portion for the latter case, and hence the fundamental frequency of any Korotkow sound power components present; and compute the ECG spectral distribution for the same flight portion. To do this, the autocorrelation and power spectral density functions of the time-corresponding ECG segment were computed, and appear as Figures 69 and 70, respectively. The fundamental frequency of the ECG segment f_o is 2.5 cycles per second and should correspond to the fundamental frequency of the Korotkow sound signal. Figure 68 indicated a significant power level around 2.5 cycles per second that did not appear in the first (low constant cuff pressure) case (Figure 67). However, the noise structure of the two Korotkow sound segments were quite dissimilar; hence, no reliable judgment as to the presence of clean signal power can be made.

Due to the extremely low or zero signal to noise ratio of the degraded signals available for test, the utility of power spectral density for locating the presence of Korotkow sound power could not be properly investigated. To establish and apply the necessary criteria of utility, a number of flight Korotkow sound signals ranging from high to low quality would be required, or a substitute set of signals would have to be synthetically generated.

The power spectral density function is in general an expensive technique

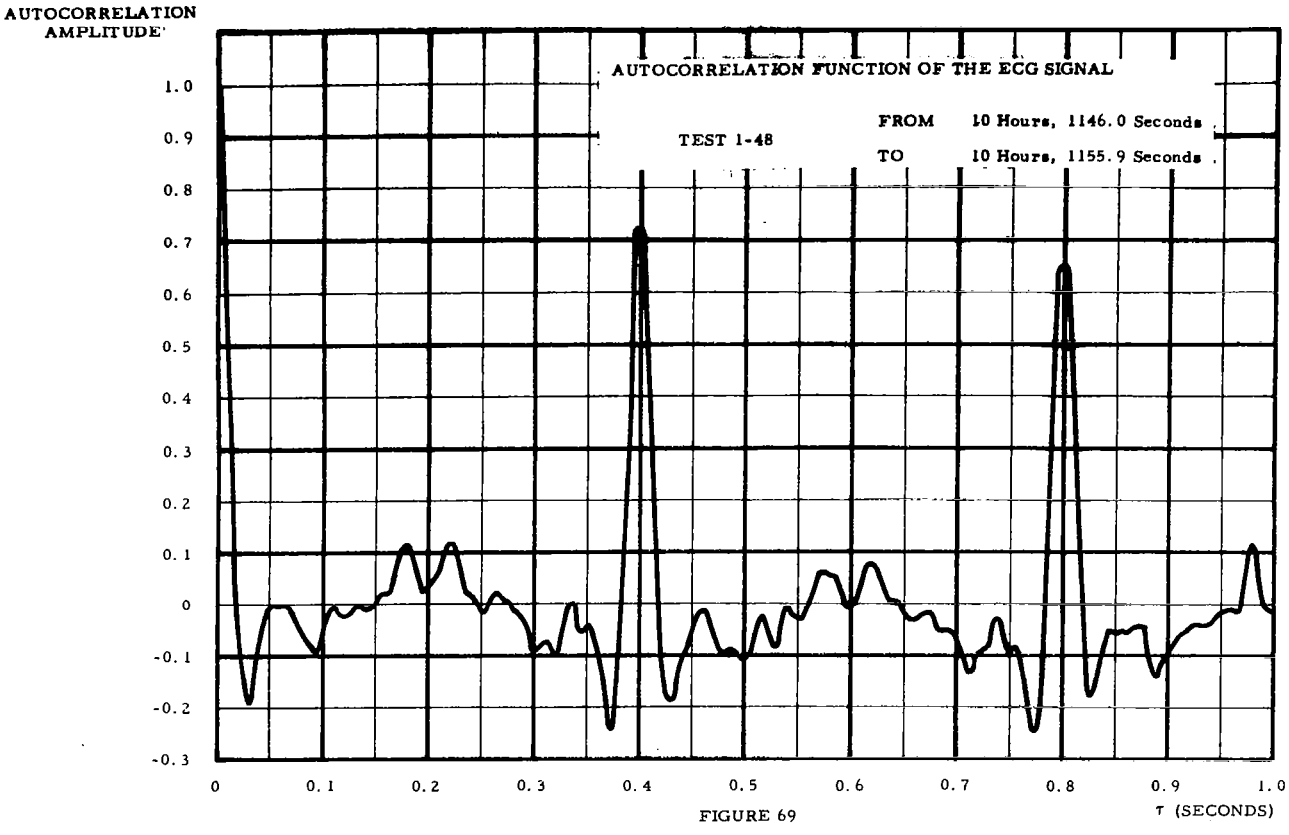

FIGURE 69

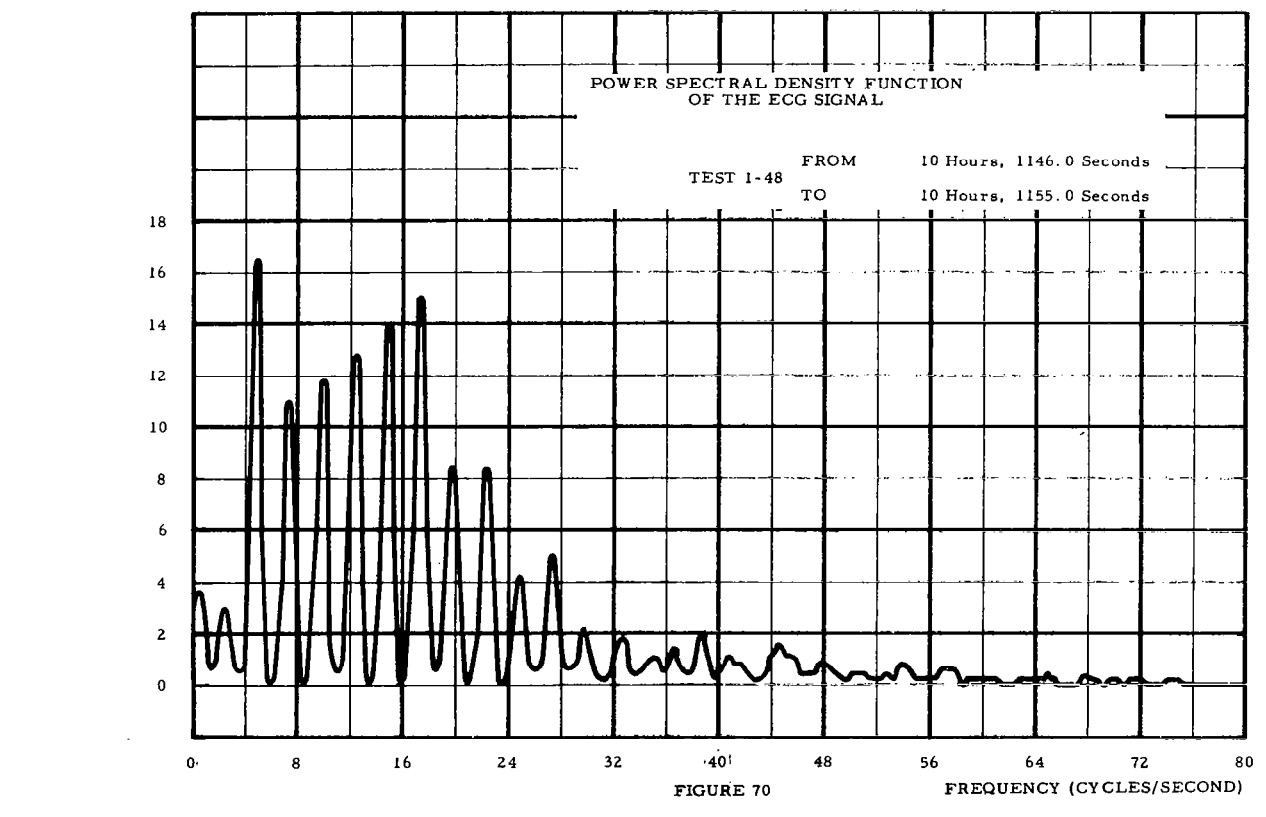

FIGURE 70

for obtaining the fundamental frequency of a signal, but it is of utility in determining harmonic structure. There are many factors which tend to make the power spectrum unreliable:

Round-off errors incurred during large amounts of computation,

Effects of the limitation of the sample size,

Complications due to the harmonic structure of a signal,

Effects of band-limited white and periodic noise.

Excellent knowledge of flight ECG harmonic structure from spectral density runs was obtained. Spectral analysis yielded reliable results in respirotachometry, but was unwieldy in cardiotachometry. Its utility in Korotkow sound detection could not be conclusively studied due to inadequate available data.

Section 5

DIGITAL FILTERING

The effects of digital filtering on noise degraded physiological signals was studied in the context of extracting information known a priori to be contained in a definite frequency band. In some cases, the purpose of the digital filtering was to narrow the limits of an information bandwidth and thus to have the capability of filtering more noise power than signal power when the spectrum of the signal and noise power are of dissimilar shapes or lie in different bands. Digital filtering for these purposes is quite flexible due to the high gain roll-offs attainable and the complete control of filter phase shift possible in digital filter design. In a digital filtering application, two types of computer runs are required: a filter "design" run, and any number of filtering runs in which the "designed" filter is used. The sampled impulse response (weighting sequence) must be determined for the filter having the desired characteristics in the design run. This impulse response must be convolved with the "unfiltered" input signal to produce the reduced bandwidth "filtered" output signal, in the filtering run.

In the filtering applications, a zero phase shift was used throughout; hence, the impulse response was symmetrical and only its positive time values need be computed. The sampled impulse response will be represented by $B_k = B(k\,\Delta t)$ where $k = 0, 1, \cdots, N$ and Δt is the sampling time of the input signal to be filtered. The total number of values in the filter weighting sequence will be $2N + 1$ and the filter time window will be $2N\,\Delta t$. The folding frequency of the input signal is $f_f = f_s/2 = 1/(2\,\Delta t)$. A dimensionless frequency (or frequency ratio)

may be represented by $r = f/f_s$. The problem of filter design now becomes one of finding the sampled impulse response, B_k, which best represent a desired gain function G(r), in the least squares sense. If the root-mean-square error minimization is performed over the frequency band, r=0 to r_2, the following set of linear equations is obtained:

$$\sum_{n=0}^{N} Bn \left[\frac{\sin 2\pi (k-n) r_2}{2\pi(k-n)} + \frac{\sin\left[2\pi(k+n) r_2\right]}{2\pi (k+n)} \right] = \int_0^{r_2} G(r) \cos (2\pi kr)\, dr. \qquad (60)$$

The functional form of G(r) used for low-pass filter design was:

$$(r) = \begin{cases} 1\,, & 0 \le r \le r_c \\ .5 + .5 \cos\left[\dfrac{\pi(r - r_c)}{2h} \right], & r_c < r \le r_c + 2h \\ 0\,, & r > r_c + 2h \end{cases}$$

where r_c is the cut-off frequency and h is the cosine termination quarter period. Using this functional form, G(r), the right hand side of equation (60) becomes

$$\int_0^{r_2} G(r) \cos (2\pi kr)\, dr = \left[\frac{\cos (2\pi kh)}{1 - 16k^2h^2} \right] \left[\frac{\sin \left[2\pi k(r_c + h) \right]}{\pi k} \right] \qquad (61)$$

The resultant set of simultaneous linear equations is very ill conditioned (near singular) and results in large computation errors for an arbitrary r_2 value. If the minimization process is performed to the folding frequency, $r_2 = .5$, the resultant equations for the filter weights become explicit

$$B_k = 2 \left[\frac{\cos (2\pi kh)}{1 - 16 k^2 h^2} \right] \left[\frac{\sin \left[2 \pi k (r_c + h) \right]}{\pi k} \right] \tag{62}$$

These filter weights may then be corrected to insure the actual gain function is unity at zero frequency

$$B_k' = B_k + \frac{1 - B_o - 2 \sum_{i=1}^{N} B_i}{2N + 1} \tag{63}$$

In filter design applications, the parameters N and h were varied until satisfactory agreement was obtained between the desired and actual frequency response of the filter. Since we were dealing with linear filters, high-pass and band-pass filter impulse responses were obtained through appropriate differencing of low-pass responses.

To apply the filtering operation, the impulse response $w(\tau)$ must be convolved with the input signal $y_i(t)$ to obtain the filtered output signal $y_o(t)$

$$y_o(t) = \int_{-\infty}^{\infty} y_i (t + \tau) \, w(\tau) \, d\tau \tag{64}$$

As stated in the Convolution Theorem, this operation is equivalent to taking the product of the signal's power spectrum and the filter gain function in the frequency domain. Since the impulse response of the filter is time-bounded and sampled, equation (64) is approximated by

$$y_i = y(i \, \Delta t) = \sum_{k=-N}^{N} B_k \, x_{i+k} \tag{65}$$

The effects of reduced bandwidth on the ECG signal were studied under varying degrees of degradation. Comparisons of rate discrimination quality of the ECG autocorrelation function and reduced bandwidth ECG were made simultaneously with observations of ECG waveform effects.

Figure 5 indicates a noisy ECG signal (lower plot) input to a low-pass filter whose cut-off frequency was 18 cps, and the filtered ECG output signal (upper plot). It is clear from comparison of the ECG input and output signals that the noise power has been greatly reduced. However, the utility of the R-wave as a trigger in a cardiotachometer is still doubtful. In many instances, in this short segment, the T-wave amplitude exceeded that of an R-wave, due to the variation of the baseline amplitude (respiration effect). To help eliminate the respiration effect, and to remove any DC component and to improve autocorrelation spread, a band-pass filtering operation was done, where the lower cutoff was between the respiration rate and the heart rate.

For the investigation of band-pass techniques, the low cutoff of the filters was chosen to be .5 cycles per second, having infinite attenuation from 0 to .25 cycles per second. The low frequency cutoff f_{LC} was chosen at .5 cps to permit use of the filters for HR $\geq$ 30 bpm. For HR = 30 bpm, $f_o = 1/\tau_o = .5$ cps, and; hence, the fundamental power would not be attenuated by the filters. For higher minimum heart rate cardiotachometer uses, f_{LC} could be raised accordingly. The following table indicates the band-pass filters used for ECG investigations:

Case	Filter Bandwidth	Figure
1	.5 to 40 cps	71
2	.5 to 20 cps	72
3	.5 to 10 cps	73
4	.5 to 5 cps	74

In Cases 1 and 2, there was definite improvement in the R-wave discrimination even though the respiration effect was not completely eliminated. The filter output signals showed a low frequency component at approximately .5 cps, indicating that for its elimination at this heart rate the low pass-band frequency value would have to be around .7 cps. However, this would attenuate an ECG fundamental at HR < 42 bpm. These ECG digital filtering runs indicated severe limitations in the sole use of band-pass filtering for improved performance cardiotachometry. For general application, the range of the respiration rate (assumed .2 to .67 cps) and the range of the heart rate (assumed .5 to 4 cps) overlap from .5 to .67 cycles per second, thus requiring dynamically adjustable frequency-band filters, for the best possible elimination of respiration effect in the filtered ECG. The ECG filtered from .5 to 20 cps (Case 2) showed the best R-wave discrimination and still had many situations where the R-wave to T-wave discrimination ratio was less than 10:7.

The ECG, filtered .5 to 40 cps (Case 1), displayed high noise power in the intelligence band of ECG waveform. The highest noise power was observed around 908 seconds of test 1-48 (See Figure 5 for a sample of the raw signal), and could not be reduced to a reasonable level till the ECG bandwidth was reduced to 10 cps (Case 3). However, at 10 cps, it becomes clear that the ECG waveform has been severely distorted.

In Case 4 (See Figure 74), the pass-band on the ECG signal was .5 to 5 cycles per second. The power spectral density of the ECG segment input to this filter showed a fundamental frequency of approximately 2.3 cycles. Hence, the filter passed only the fundamental and 2nd harmonic power. The zero-crossing rate determination utility of what appears to be two in-phase sinusoids would be quite good if the respiration effect were completely removed. The method of zero-crossing detection for heart rate determination will be discussed in detail in Section 7.

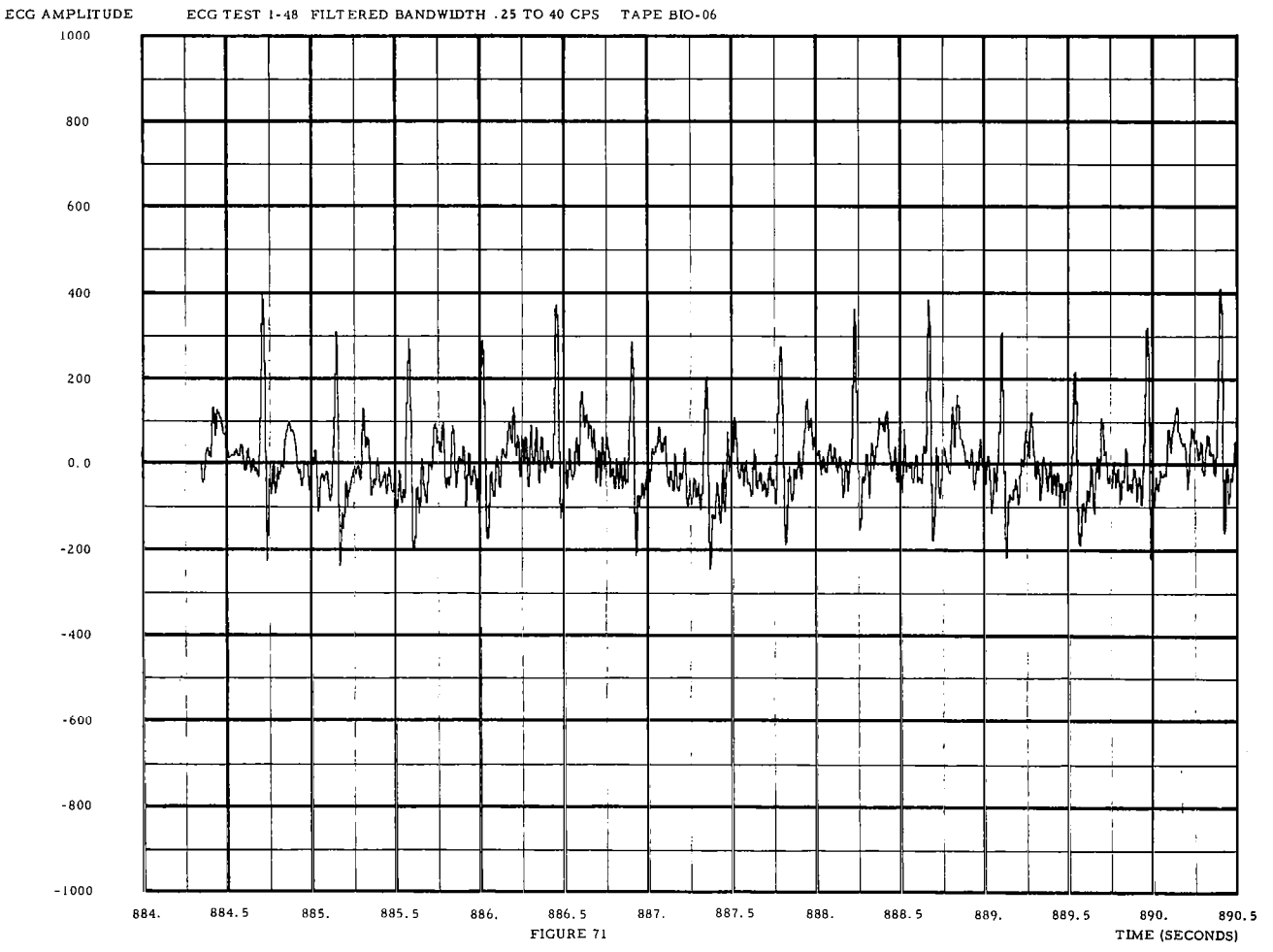
ECG AMPLITUDE
ECG TEST 1-48 FILTERED BANDWIDTH .25 TO 40 CPS TAPE BIO-06
1000
800
600
400
200
0.0
-200
-400
-600
-800
-1000
884.
884.5
885.
885.5
886.
886.5
887.
887.5
888.
888.5
889.
889.5
890.
890.5
TIME (SECONDS)

FIGURE 71

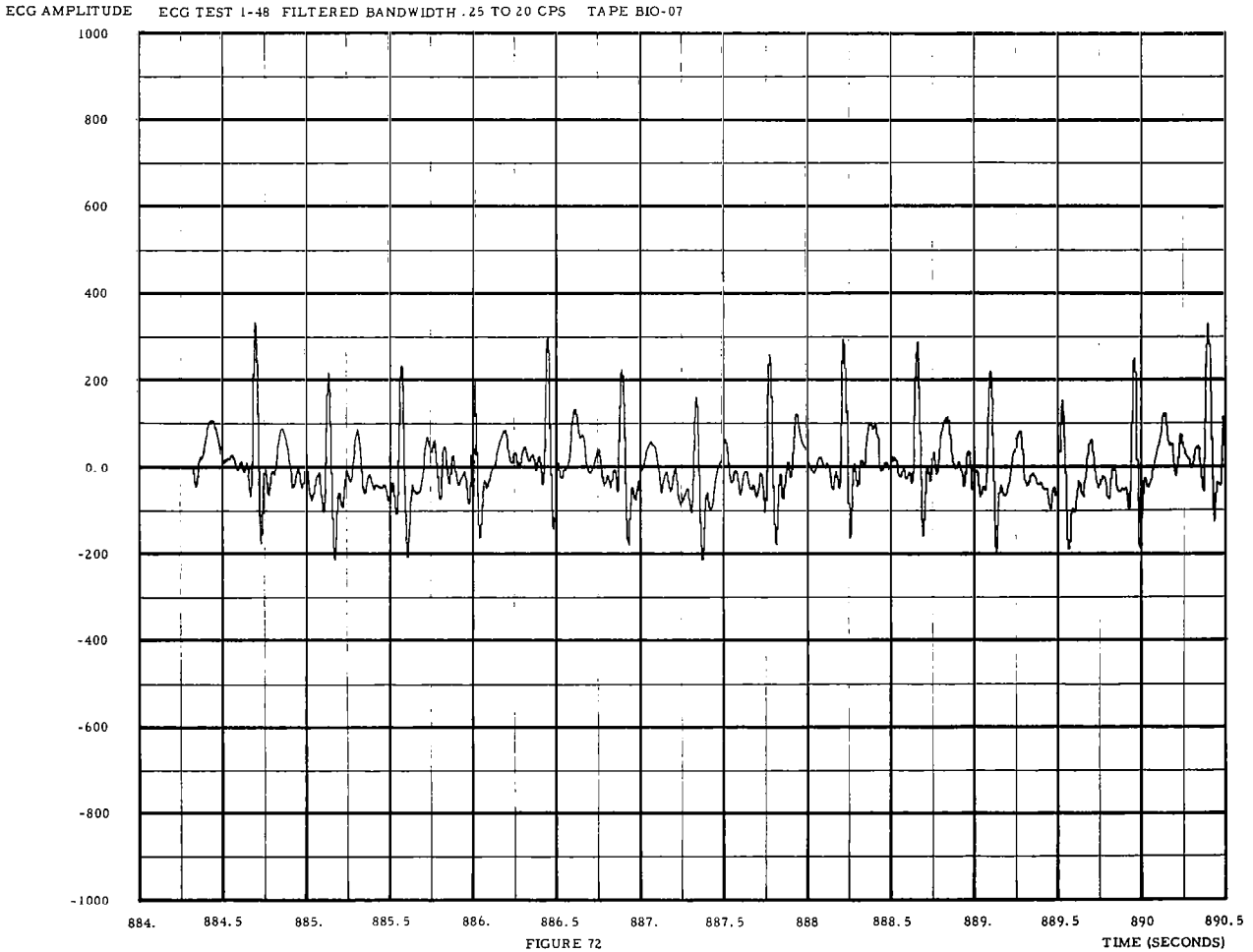
ECG AMPLITUDE
ECG TEST 1-48 FILTERED BANDWIDTH .25 TO 20 CPS TAPE BIO-07
1000
800
600
400
200
0.0
-200
-400
-600
-800
-1000
884.
884.5
885.
885.5
886.
886.5
887.
887.5
888
888.5
889.
889.5
890
890.5
TIME (SECONDS)

FIGURE 72

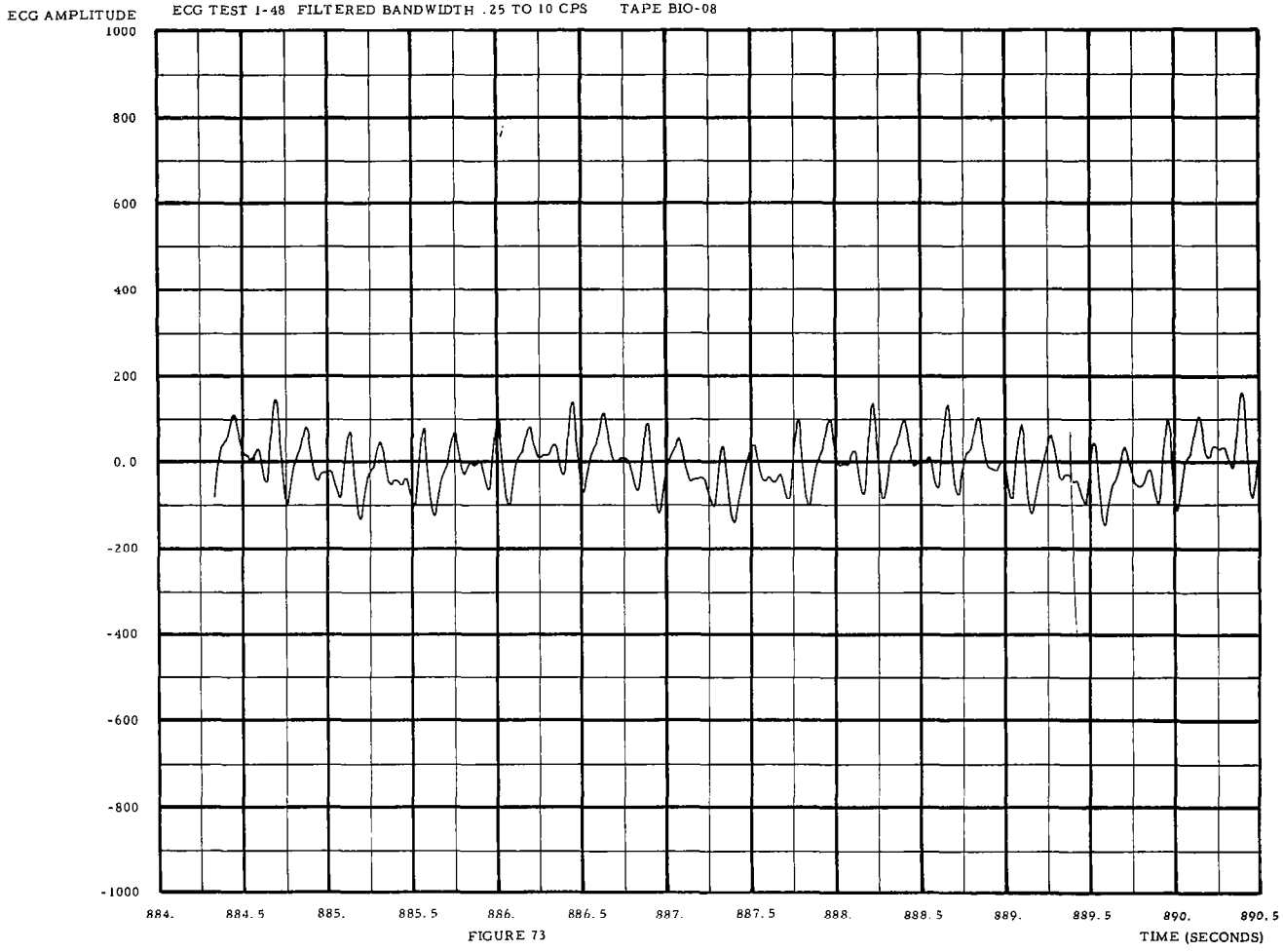
ECG AMPLITUDE
ECG TEST 1-48 FILTERED BANDWIDTH .25 TO 10 CPS TAPE BIO-08
1000
800
600
400
200
0.0
-200
-400
-600
-800
-1000
884.
884.5
885.
885.5
886.
886.5
887.
887.5
888.
888.5
889.
889.5
890.
890.5
TIME (SECONDS)

FIGURE 73

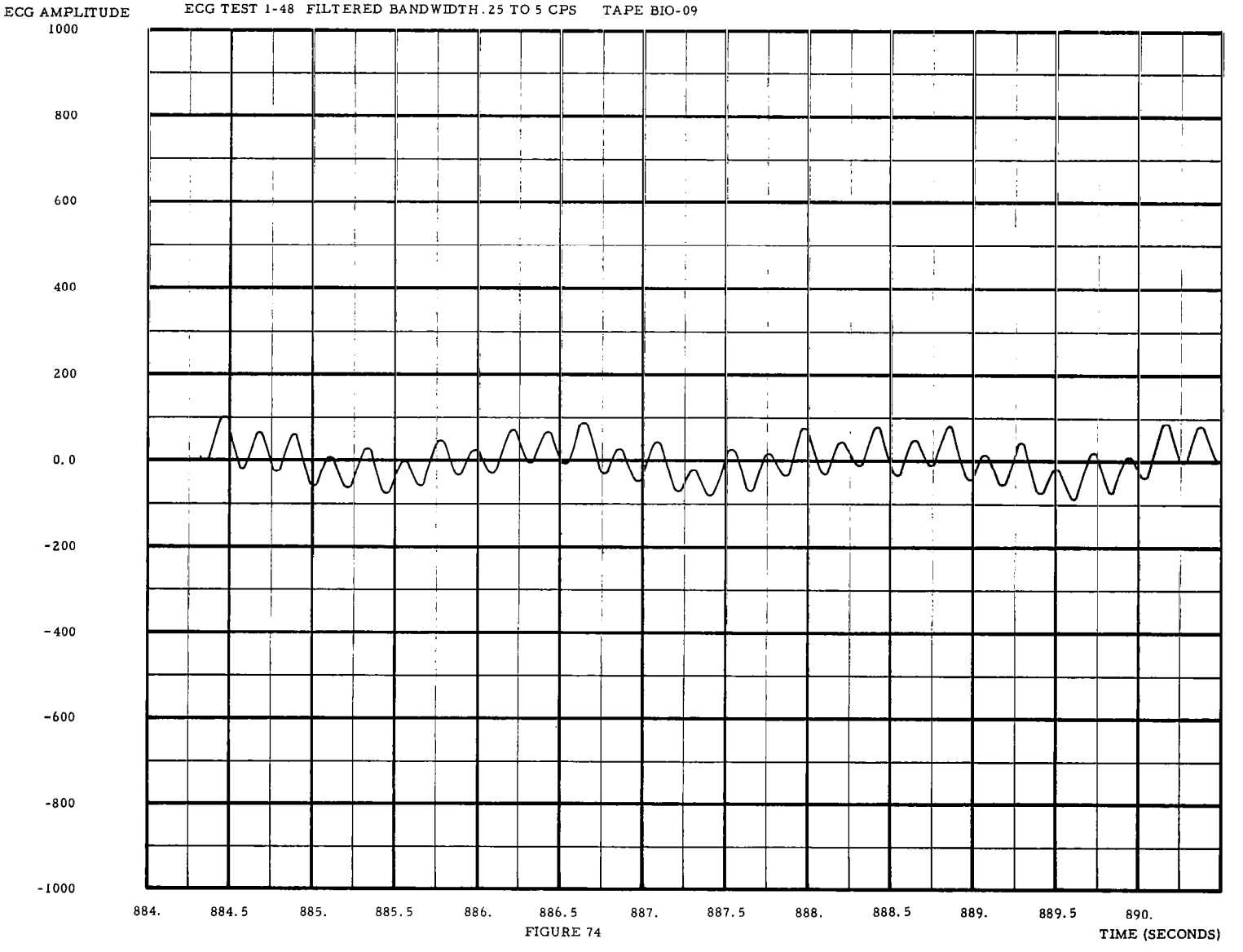
ECG AMPLITUDE
ECG TEST 1-48 FILTERED BANDWIDTH .25 TO 5 CPS TAPE BIO-09
1000
800
600
400
200
0.0
-200
-400
-600
-800
-1000
884.
884.5
885.
885.5
886.
886.5
887.
887.5
888.
888.5
889.
889.5
890.
TIME (SECONDS)

FIGURE 74

A band-pass filtering technique was applied to the suit-helmet pressure differential signal in order to investigate a reliable method of obtaining respiration rate. The digital filtering was applied for the purpose of signal preconditioning, a process required in conjunction with the technique of zero-corssing detection. The digital filtering application was performed on the entire S-HPD signal from Test 1-48 (See Figure 75 for samples of the filter output). The final signal bandwidth obtained was .2 to .67 cycles per second. The erratic nature of the signal was reduced to a smoothed respiration history in the form of a variable rate sinusoid. The application of zero-crossing detection for determination of respiration rate will also be treated in Section 7.

The Korotkow sound signal was passed through three band-pass filters in order to narrow down the signal characteristics. The filters designed and used had pass-bands of 90 to 120 cps, 120 to 150 cps, and 150 to 180 cps. In each case, the signal segment filtered covered the region on the cuff pressure ramp where systole and diastole should have been realized. The signal's fundamental frequency was known from autocorrelation runs on the time-corresponding ECG signal. It was hoped the band-pass techniques would yield the structure of the Korotkow sound complex and, hence, would create some basis for determining signal presence. The filtered signals were studied for the three frequency bands. In all cases no identification could be made of a signal complex repeating at the fundamental period. Autocorrelation and power spectral density functions of the filtered Korotkow sound signals certainly could have been made to support any positive findings.

Digital filtering has proved to be a powerful technique as applied to the enhancement of noise degraded signals. As in analog filtering, the information pass-bands must be known a priori and some of the noise power must lie outside the pass-band for filtering to be useful. For

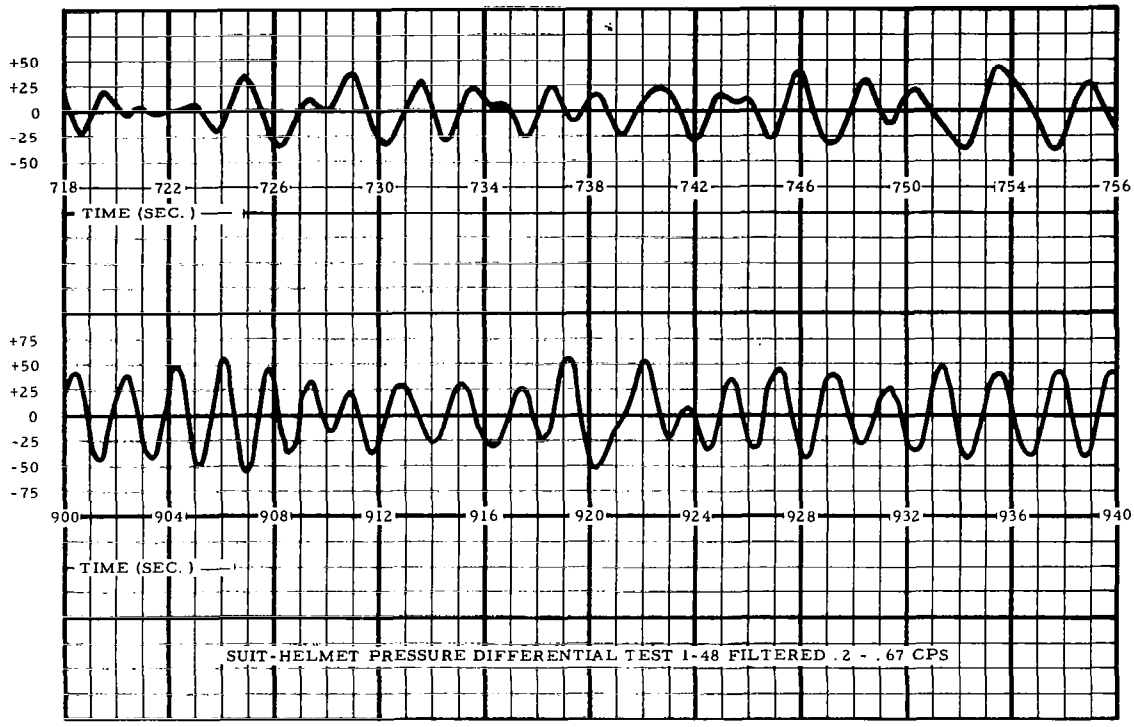
+50
+25
0
-25
-50
718
722
726
730
734
738
742
746
750
754
756
TIME (SEC.)
+75
+50
+25
0
-25
-50
-75
900
904
908
912
916
920
924
928
932
936
940
TIME (SEC.)
SUIT-HELMET PRESSURE DIFFERENTIAL TEST 1-48 FILTERED .2 - .67 CPS

FIGURE 75

accurate filtering, the output data rates for the filtering program utilized in this study were between 2,000 and 4,000 samples per second. For many applications, such as the band-pass filtering of the suit-helmet pressure differential signal, the output data rates could be increased approximately five fold. Also, the ease of redesigning the digital filter makes its application very powerful.

Section 6

WAVEFORM AVERAGING

Averaging techniques were investigated due to their effects in the reduction of random noise power. The process studied was that of computing the arithmetic mean over N ensembles of a noise degraded signal.

$$x_i = \frac{1}{N} \sum_{j=1}^{N} x_{ij} , \quad i = 1, 2, \cdots, n. \tag{66}$$

The sample sizes of each ensemble x_i, $i = 1, 2, \cdots, n$ were forced to be equal to n. If the signal passed through this averager is degraded by random noise whose power is given by σ^2, then the averager triggered over N ensembles will yield a noise power level equal to

$$\sigma_N^2 = \frac{\sigma^2}{(N)} \quad 1/2 \tag{67}$$

The application of the averager expressed by (66) in the context of waveform (the ensembles) enhancement requires the determination of the sample size n, obtained from the waveform period, and appropriate phasing of the waveforms.

Investigations were made as to the effects of averaging on the ECG complex. The sample sizes were determined through the period read-outs of the autocorrelation function combined with the sampling rate. The phasing of the ECG ensembles by lining up R-waves was acccomplished through cross-correlation of a "square" impulse with the current ECG complex.

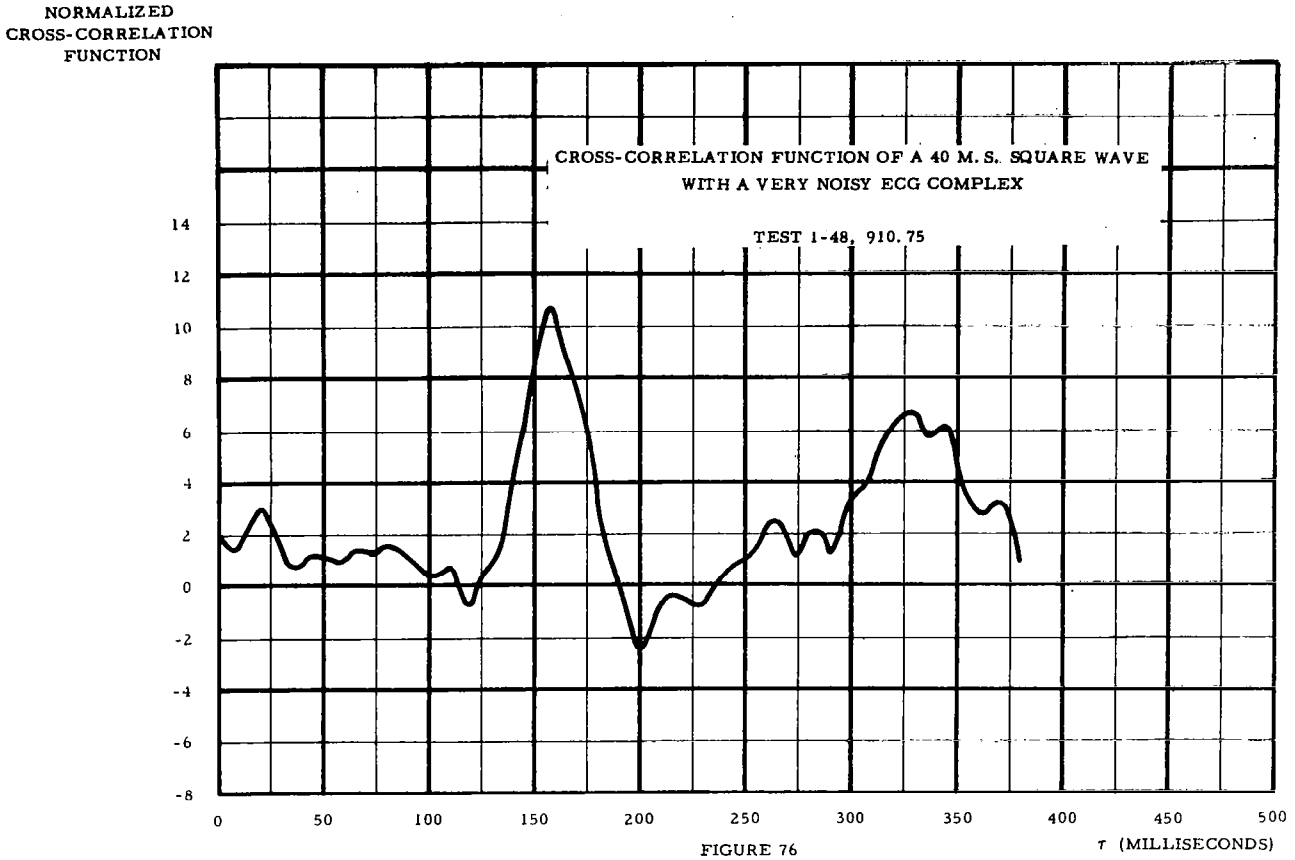

FIGURE 76

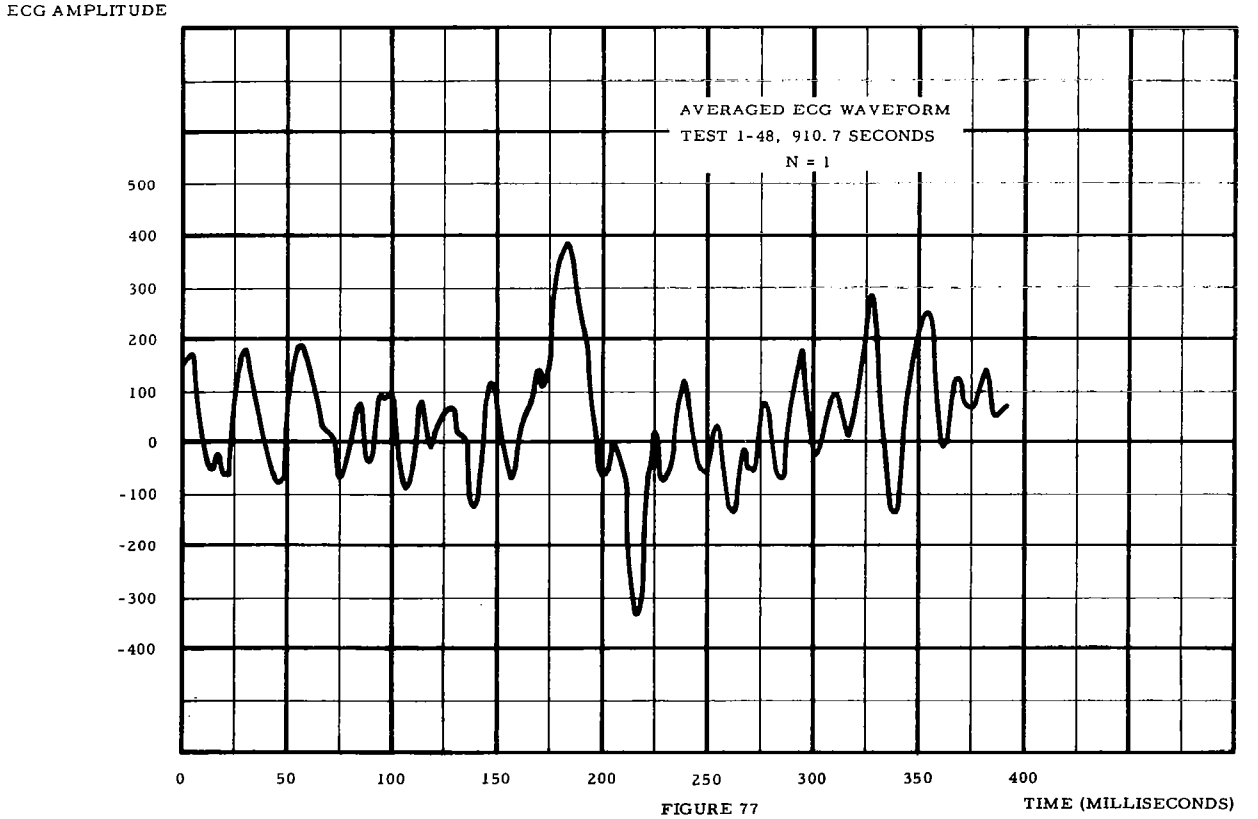

FIGURE 77

A typical cross-correlation function of a noisy ECG complex with a square impulse function is shown in Figure 76. The ECG complex used in the computation appears as Figure 77. The pulse cross-correlation phaser was chosen to be 40 milliseconds wide, and generally yielded better than a 10:7 discrimination ratio between the R-wave and the T-wave. A reduction of the width of the square impulse would certainly increase the R-wave to T-wave discrimination ratio. However, to ensure cancellation of high amplitude noise spikes, the time width of the square impulse must be at least the reciprocal of the noise bandwidth.

The first application of the averager defined by (66), was performed on an ECG signal segment from Test 1-48, 910.7 seconds to 916.2 seconds (See Figure 5, lower plot, for a sample of this segment). This application involved the averaging of 11 ECG waveforms in order to realize the noise power reduction. Figure 78 represents this averaged ECG complex. Comparison of Figures 77 and 78 indicates the noise power has been greatly reduced. Further applications included the averaging of an ECG segment containing clean and noise degraded portions.

Figure 79 represents one of the clean ECG complexes in the signal segments whereas the average waveform is displayed in Figure 80. Since the average waveform over 16 cycles appears relatively noise free, a low noise power is indicated.

The autocorrelation function has been used to estimate the signal-to-noise ratio Q, by suitable computation involving the zero-lag amplitude and the amplitude at a lag of one period. This estimate of S/N ratio is valid if cycle-to-cycle waveform change and aperiodicity are quite small. When S/N ratio is known, equation (77) could be used to obtain the number of ensembles required to obtain an average ECG complex with predetermined noise power. Due to lack of time, this investigation could not be carried out quantitatively; however, with the applications that were performed, the technique appears promising.

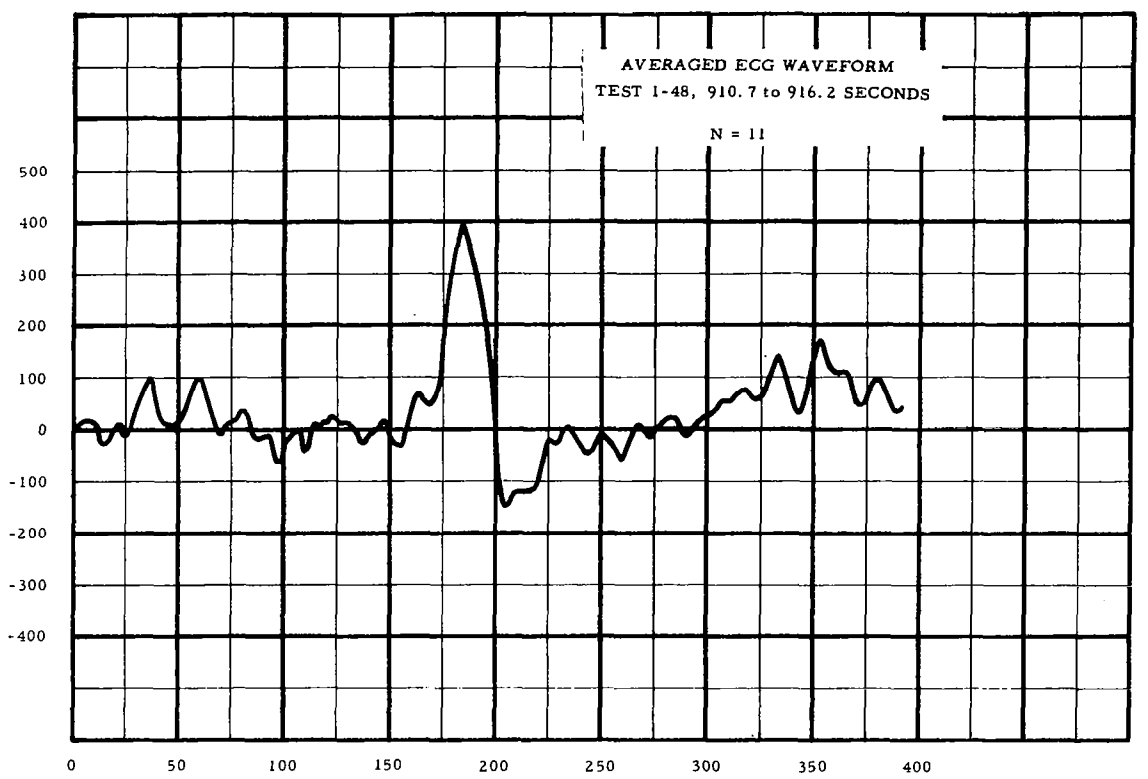
AVERAGED ECG WAVEFORM
TEST 1-48, 910.7 to 916.2 SECONDS
N = 11
500
400
300
200
100
0
-100
-200
-300
-400
0
50
100
150
200
250
300
350
400
FIGURE 78

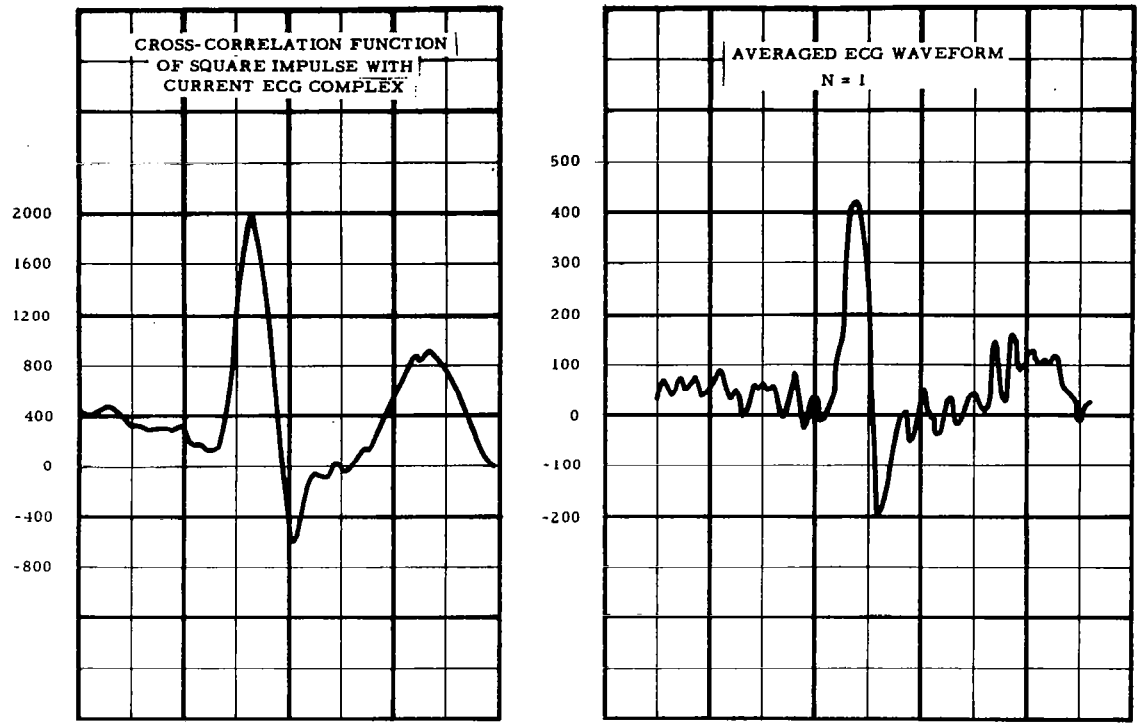

FIGURE 79

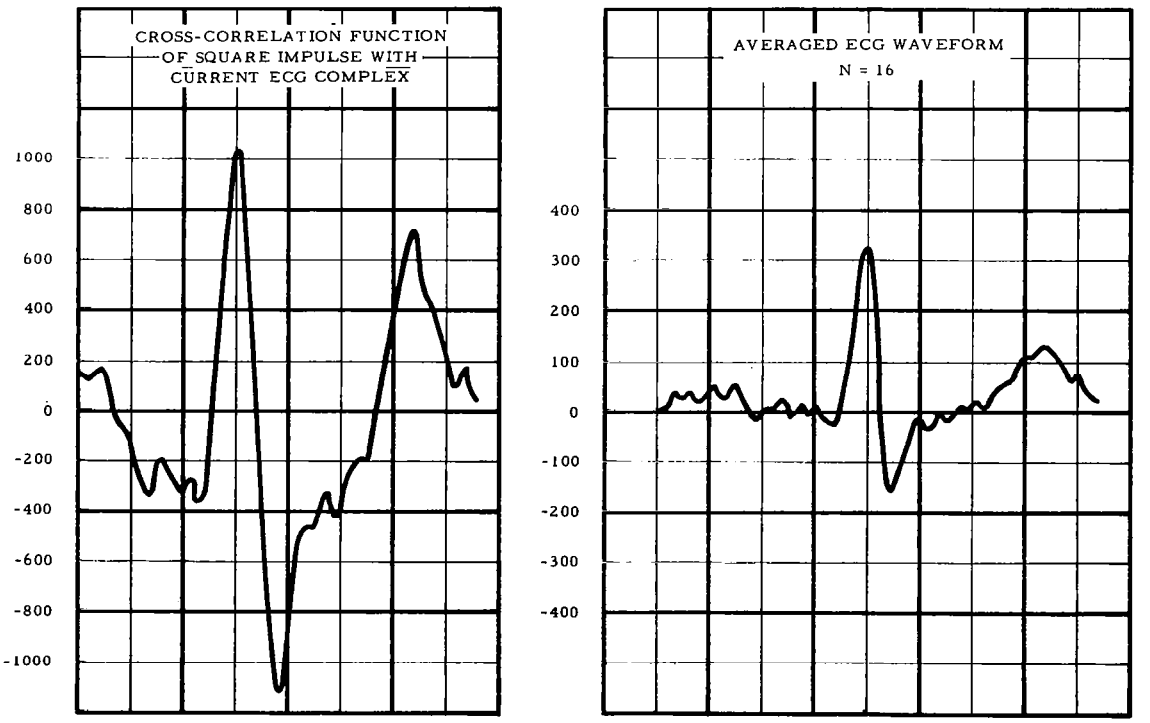

FIGURE 80

Section 7

ZERO-CROSSING DETECTION FOR RATE DETERMINATION

The technique of zero-crossing detection was investigated as a method of fundamental rate determination. It entails counting the number of sign inversions, N, in a given period of time, T. The rate estimate of the phenomena then becomes:

$$R = \frac{N}{2T} \tag{68}$$

This technique is very easily applied in itself, but may require a large amount of signal preconditioning. To apply zero-crossing detection, the signal must be virtually free of any D. C. component and the structure of the signal must be such that a predetermined harmonic always produces the sign inversion. Suitable band-pass techniques can in general meet these requirements in the absence of high power noise in the pass-band.

Zero-crossing counts were used to compute average respiration rates after the S-HPD signal was filtered. The preconditioning bandwidth used was .2 to .67 cycles per second. The rates obtained from the zero-crossing counts were compared to the power spectral density function rate determination. These rates agreed favorably. Figure 75 represents samples of the respiration signal whose bandwidth has been reduced to .2 to .67 cps. The rates determined through zero-crossing counts for the upper and lower plots are 26.04 and 31.56 respirations per minute, respectively. These values are well within reasonable bounds for the respiration rate.

Figure 74 represents a sample of the ECG signal whose bandwidth has been reduced to the point where zero-crossing detection appears

feasible for heart rate determination. The resultant ECG signal contains the first and second harmonic; thus, a zero-crossing count would yield twice the fundamental rate. Due to the low frequency component (respiration effect), a true zero-crossing measure on this signal would yield erroneous results. Therefore, the local maxima were tabulated in order to obtain cycle counts over a given period of time. The average heart rate obtained by this method was 122.4 beats per minute over the time interval 891 seconds to 935.5 seconds. The heart period obtained through local maxima count in the interval 911 to 918.1 seconds was .44 seconds. This value compares favorably with the period yielded by autocorrelation over the same time interval (See Figure 7).

The technique of zero-crossing detection is an economical and reliable method of fundamental rate determination. However, the signal preconditioning required to implement zero-crossing count may be extensive. The suit-helmet pressure differential signal required only fixed bandpass preconditioning. However, the problem of determining concrete prezero-crossing techniques for the ECG signal requires further study.

Section 8

ELECTROCARDIOGRAM SIMULATION

Both to support the program development and effectiveness evaluation portions of each technique investigation, a simulated clean ECG signal $x_c(t)$ has been formulated. This $x_c(t)$ formulation was expressed to permit convenient transformation to a digital generation program. This simulated ECG waveform generation program will permit variations in several ECG parameters, including: heart rate (R-R interval); eight combinations of basic types of period variation (constant, linear, sinusoidal, and random) which can be stipulated at will; P, Q, R, S, and T wave amplitudes and polarities; P, PQ, QRS, ST, and T segment durations. The clean waveform $x_c(t)$ generated by this program permits direct testing of each technique (autocorrelation, spectral, filtering), as to its effectiveness in extracting rate information with varying waveshapes and forms of rate variation. Further, when combined with simulated noise signals, effectiveness of techniques with varying signal-to-noise ratios may be determined.

The computer simulation program will generate ECG waveforms based on the synthesis of 11 segments. Figure 81 represents a sample synthetic ECG waveform where junction point i is represented by (A_i, T_i). The duration of wave-segment i is labeled as τ_i. The segments chosen represent portions of the ECG waveform as indicated in the following chart:

Segment No.	ECG Wave Portion	
1	TP Segment:	Iso - Electric Line from End of T Wave to Beginning of P Wave

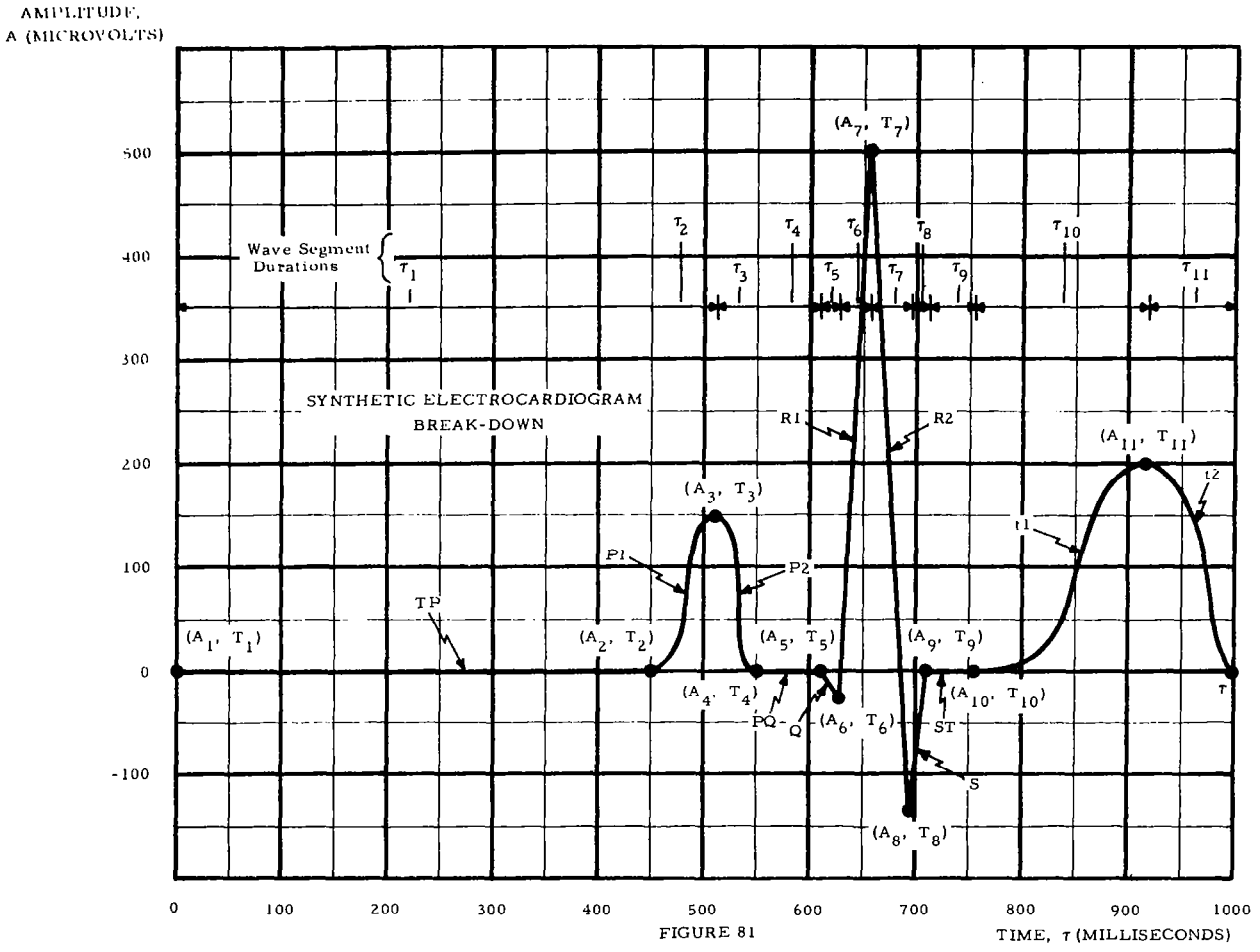
AMPLITUDE,
A (MICROVOLTS)
500
400
300
200
100
0
-100
Wave Segment
Durations
τ_1
τ_2
τ_3
τ_4
τ_5
τ_6
τ_7
τ_8
τ_9
τ_{10}
τ_{11}
SYNTHETIC ELECTROCARDIOGRAM
BREAK-DOWN
(A_1, T_1)
(A_2, T_2)
(A_3, T_3)
(A_4, T_4)
(A_5, T_5)
(A_6, T_6)
(A_7, T_7)
(A_8, T_8)
(A_9, T_9)
(A_{10}, T_{10})
(A_{11}, T_{11})
TP
P1
P2
PQ
Q
R1
R2
S
ST
t1
t2
T
0
100
200
300
400
500
600
700
800
900
1000
TIME, τ (MILLISECONDS)

FIGURE 81

Segment No.	ECG Wave Portion	
2	P1 Segment:	Rise of P Wave
3	P2 Segment:	Fall of the P Wave
4	PQ Segment:	From End of P Wave to Start of Q Wave
5	Q Wave	
6	R1 Segment:	Rise of the R Wave
7	R2 Segment:	Fall of the R Wave
8	S Wave	
9	ST Segment	From end of S to start of T Waves
10	t1 Segment:	Rise of the T Wave
11	t2 Segment:	Fall of the T Wave

This program permits both deterministic and random changes in the cycle-to-cycle heart rate and in each ECG segment amplitude or segment duration. The deterministic variations are either linear or sinusoidal in nature and the random variations (termed exception cycles) permit complete (cycle by cycle) specification of segment amplitudes and duration and heart rate. The program will record the generated signal onto magnetic tape in a format consistent with the converted X-15 flight biodata format. With this philosophy, any type of noise can be injected into the same base signal to evaluate enhancement capabilities.

The ECG program was utilized in the generation of a nominal synthetic ECG signal, which contains heart rate and waveform variations and other anomalies observed in the X-15 flight signals. This synthetic ECG signal consists of 182, 125 sample values, covering a time span of 364.250 seconds and 725 cycles. The time base and all the parameters making up each ECG complex are available in a listing output along with summaries of the signal segments with deterministic variations. An excerpt of the printed output for ECG segment 33 along with

the corresponding signal plot appear as Figures 82 and 83, respectively. Note that cycle 31 (at 250.256 seconds) has dropped the P wave; hence, constitutes an aberrant wave. With the philosophy of the synthetic ECG simulation, the user may generate disrupted waveforms at will and investigate detection techniques or qualities knowing where positive or negative results should occur.

In addition to the simulated waveform generate use, the synthetic ECG, $x_c(t)$, formulation has been analytically investigated to gauge the spectrum of a clean ECG, and to gain an understanding of how the ECG spectrum varies with changes in P, Q, R, S, and T wave amplitudes and durations. The analytical investigation consisted in deriving a Fourier series representation of $x_c(t)$. This representation allows identification of the power composition in any chosen segment of the ECG signal. Also, to determine the validity of the synthetic ECG waveform as a test signal, one criterion chosen was that the synthetic ECG wave spectrum should approximate the flight ECG spectrum. To enable application of this spectral matching criterion, the ability to compute the spectrum of the synthetic ECG was deemed necessary. A mathematical analysis of the synthetic waveform was performed to derive formulas for the Fourier coefficients. The Fourier coefficients are the a_n and b_n which would permit the synthetic ECG signal to be represented arbitrarily well by a truncated Fourier series.

$$x_c(t) = x_c(t + P) = \frac{a_o}{2} + \sum_{n=1}^{H} a_n \sin\left(\frac{2n\pi t}{2}\right) + b_n \cos\left(\frac{2n\pi t}{2}\right) \qquad (69)$$

where P is the period of the signal, and H the number of harmonics.

In the absence of a d. c. component ($a_o = 0$), these coefficients may

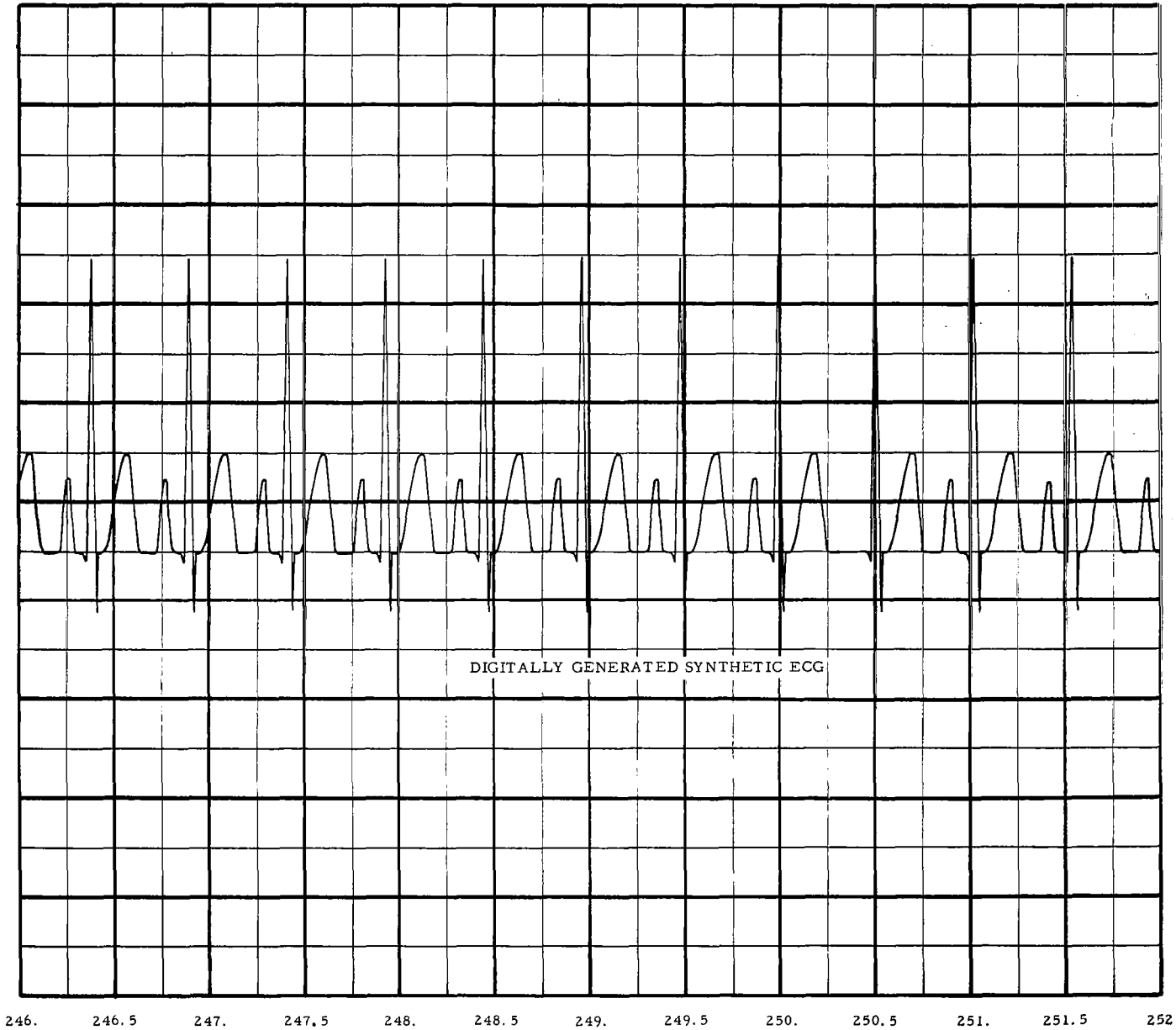
DIGITALLY GENERATED SYNTHETIC ECG
246.
246.5
247.
247.5
248.
248.5
249.
249.5
250.
250.5
251.
251.5
252

FIGURE 83

be computed from the junction point times, T_j, and amplitudes, A_j by the following equations:

$$\tau_j = T_{j+1} - T_j \tag{70}$$

$$\beta_j = A_{j+1} - A_j \tag{71}$$

$$\lambda_j = \frac{P}{2\tau_j} \tag{72}$$

$$\epsilon_j = \frac{1}{\left[2\left(\frac{n}{\lambda_j}\right)^2 - 1\right]} \tag{73}$$

$$\sigma_j = \sin\left[\frac{2\pi n T_j}{P}\right] \tag{74}$$

$$\gamma_j = \cos\left[\frac{2\pi n T_j}{P}\right] \tag{75}$$

$$\begin{aligned} a_n = (n\pi)^{-1} & \left[\epsilon_2\beta_2(\sigma_2 + \sigma_3) + \epsilon_3\beta_3(\sigma_3 + \sigma_4)\right. \\ & \left. + \epsilon_{10}\beta_{10}(\sigma_{10} + \sigma_{11}) + \epsilon_{11}\beta_{11}(\sigma_{11} + \sigma_{12})\right] \\ & - (n\pi)^{-2}\left[\lambda_5\beta_5(\gamma_5 - \gamma_6) + \lambda_6\beta_6(\gamma_6 - \gamma_7)\right. \\ & \left. + \lambda_7\beta_7(\gamma_7 - \gamma_8) + \lambda_8\beta_8(\gamma_8 - \gamma_9)\right] \end{aligned} \tag{76}$$

$$\begin{aligned} b_n = -(n\pi)^{-1} & \left[\epsilon_2\beta_2(\gamma_2 + \gamma_3) + \epsilon_3\beta_3(\gamma_3 + \gamma_4)\right. \\ & \left. + \epsilon_{10}\beta_{10}(\gamma_{10} + \gamma_{11}) + \epsilon_{11}\beta_{11}(\gamma_{11} + \gamma_{12})\right] \end{aligned}$$

$$+ (n\pi)^{-2}\left[\lambda_5 \beta_5 (\sigma_6 - \sigma_5) + \lambda_6 \beta_6 (\sigma_7 - \sigma_6)\right.$$

$$\left. + \lambda_7 \beta_7 (\sigma_8 - \sigma_7) + \lambda_8 \beta_8 (\sigma_9 - \sigma_8)\right] \quad (77)$$

When the a_n and b_n are determined, the autocorrelation, $\psi(\tau)$, and the power spectrum, S(n/P) may be computed from

$$C_n^2 = a_n^2 + b_n^2 \quad (78)$$

$$\psi(\tau) = \sum_{n=1}^{N} \frac{C_n^2}{2} \cos\left(\frac{2\pi n\tau}{P}\right) \quad (79)$$

$$S(f) = S\left(\frac{n}{p}\right) = C_n^2 \quad (80)$$

Relating the expressions (76) and (77) to Figure 81, we find the contribution of j^{th} waveform segment to the n^{th} harmonic Fourier Spectral line is given directly by the term of a_n and the term of b_n which contain β_j as a factor.

A computer program to generate these Fourier coefficients was developed and used to produce a sample power spectrum of the synthetic ECG. The power spectrum of the synthetic and live ECG signals agreed favorably (See Power Spectral Density Function, Section 4).

In addition to the synthetic ECG generation, a program to simulate band-limited white noise has been written. The program generates a normally distributed random sequence, N_i, with a mean of 0 and a standard deviation of 1. For a noise power level of σ, a bandwidth requirement of β cps and a sampling time of T_s, the normally distributed random numbers will be multiplied by a factor

$$\sigma_N = \sigma(1 - e^{-2\beta T_s})^{1/2} \tag{81}$$

Then the bandlimited white noise of power σ is given by the following recursive relationship

$$Y_i = e^{-\beta T_s} y_{i-1} + N_i. \tag{82}$$

Figures 84 and 85 represent the output of a computer implemented statistical analysis of a simulated normally distributed random sequence of mean zero and standard deviation of one. Note that the chi-square test for normality and the run test for randomness yielded positive results. Time did not permit power spectral density runs on the simulated noise.

The synthetic ECG signal has already been useful in the checkout of the waveform averaging process. It is felt that the prime utility would lie in the complete control of the signal for checkout of aberrant wave detection techniques.

Section 9

PATTERN CHANGE DETECTION

The usual methods of displaying ECG waveforms, whether a continuous time record on a strip chart recorder or a beat-by-beat display on an oscilloscope leaves much to be desired. Either display method requires continual monitoring to detect medically significant changes even though the majority of the waveforms are identical to those preceding or following. It has been proposed that the ECG waveform be studied to determine some processing technique which can be used to recognize medically significant changes in the waveform. If this can be done, then a reference waveform can be displayed until a significant change has occurred at which time the abnormal waveform will also be displayed. If this change is a steady state condition, the new waveform can be posted as a reference and subsequent waveforms compared to it.

There are a number of processing techniques which could be employed to recognize significant changes in the ECG waveforms. The most direct and probably the most sophisticated method would be to imitate the action of the human observer by recognizing individual portions of the waveform and comparing them to a large number of stored references. If these segments deviate from pre-programmed limits, a significant change has occurred and the new waveform will be displayed.

This method has an obvious disadvantage in that a large number of reference waveforms must be stored to cover all possible input waveforms and a complex pattern recognition program written to make the necessary decisions. In view of the complexity of this approach, other techniques to detect pattern changes were investigated.

Correlation techniques are discussed more fully elsewhere in this report. Basically, they consist of computing the function

$$R(\tau) = \lim_{T \to \infty} \frac{1}{2T} \int_{-T}^{T} x(t)\ y\ (t+\tau)\ dt$$

where τ is the delay parameter. If x(t) and y(t) are the same function, the resultant function is the autocorrelation function. If they are different functions, the resultant function is the crosscorrelation. The delay time at which the autocorrelation function peaks is equal to the cycle time of a periodic function. The value of this peak is a measure of the similarity between the two functions.

Band limited white noise will have a non-zero autocorrelation function for values of τ around =0. In particular, for an RC low-pass filter

$$R_n(\tau) = \frac{N\omega_o}{4}\ e^{-\omega_o |\tau|} \qquad \omega o = \frac{1}{RC}$$

The particular autocorrelation function which bandlimited white noise produces will, in general, depend on the filter used. However, the value of the autocorrelation function at zero-lag of a signal corrupted by noise will be a function of both the signal and noise. At lag values $\tau \gg \frac{1}{2B}$ where B is the noise bandwidth, the autocorrelation peak will be a function of signal alone. Thus, the ratio of the zero-lag value to other peak values is a measure of the signal to noise ratio as well as the similarity between successive cycles.

Crosscorrelation of an input waveform with a reference waveform also gives a measure of the similarity between the waveforms as well as the signal to noise ratio. However, because the reference waveform is not noisy, the crosscorrelation function degrades more slowly than the autocorrelation function with decreasing signal to noise ratio.

While it has not been shown that correlation techniques are sensitive to medically significant changes in the ECG waveforms, the results of the study to date indicate that further investigation of these techniques is warranted. This is particularly true when the cost of alternative approaches is considered.

Assuming for the moment that correlation techniques will prove to be sensitive pattern change detectors, a discussion of what might be expected is in order. If we perform the normalized incomplete auto and crosscorrelation defined as

$$R_x(\tau) = \frac{\frac{1}{2T}\int_{-T}^{T} x(t)x(t+\tau)\,dt}{\frac{1}{2T}\int_{T}^{T} x^2(t)\,dt} \qquad \text{(autocorrelation)}$$

$$R_{xy}(\tau) = \frac{\frac{1}{2T}\int_{-T}^{T} x(t)y(t+\tau)\,dt}{\left[\frac{1}{4T^2}\int_{-T}^{T} x^2(t)dt \cdot \int_{-T}^{T} y^2(t)\,dt\right]^{1/2}} \qquad \text{(crosscorrelation)}$$

Where T is the half-period, we will find that the peak values will decrease in both functions with decreasing signal to noise ratio. Again, because the reference waveform is not noisy, the crosscorrelation peaks will decrease more slowly than the autocorrelation peaks.

The correlation functions are also used as a measure of the similarity between an incoming waveform and some reference waveform. In our particular use of the autocorrelation function, the reference waveform is the signal waveform immediately preceding the input. This is a reasonable estimate of the input and should produce large correlation values except during rapid waveform changes.

The crosscorrelation function, on the other hand, uses some other estimate of the input as a reference. For example, the average waveform over a number of cycles could be used. This is also a reasonable estimate of the input, particularly if the average was a current one. As the reference becomes older, a decrease in correlation would be expected. Knowing the way in which the auto and crosscorrelation functions vary with signal to noise ratio and pattern changes, some general statements can be made about their combined effect on noisy ECG waveforms.

The effect of decreasing signal to noise ratios and pattern changes on both the auto and crosscorrelation functions is a decrease in the maximum correlation peaks. Since the two functions do not vary in the same manner in either of the two cases, it may be possible to distinguish them and set a decision threshold below which a pattern change will be defined. This decision threshold need not be fixed but could be a function of some measure of the signal to noise ratio.

The situations of interest which could occur for incoming ECG data include:

1. No pattern change
2. Slow pattern change
3. Single aberrant beat
4. Rapid multibeat pattern change
5. Low S/N

The low signal to noise conditions are defined as those which prevent reliable decisions about the type of pattern changes which are occurring. The decision in this case may be to display every beat or to rely on the strip chart display instead.

The following table shows the five possible conditions and their effect on the correlation functions.

Conditions	Auto-Correlation	Crosscorrelation
1. No pattern change	high	high
2. Slow pattern change	high	decreasing
3. Single aberrant beat	low for 2 beats	low for 1 beat
4. Rapid multibeat change	low for 2 beats	low for 1 beat
5. Low S/N	low	low

Figure 86 shows a flow chart of the logical decisions necessary for the detection of ECG pattern change. The decision thresholds T_1 and T_2 depend on the sensitivity of the correlation techniques to significant changes. Implied in this flow chart is some method of determining when a heart beat has occurred even though the signal to noise ratio is so low as to prevent a decision on pattern change. It is also implied that some means of waveform storage will be provided to allow computation of as many as three correlation functions before a decision is made.

Although the decision thresholds T_1 and T_2 are shown in the flow chart as being fixed numbers, it is possible that these can be variable as a function of the auto and crosscorrelation ratio.

The decision process of comparing the normalized correlation functions to some threshold can be directly related to the detection of radar signals in noise. In radar system analysis two probabilities are generally assigned to the detection process; the probability of detection and the probability of false alarm. These two probabilities can also be assigned in our situation although the actual numbers will in general be quite different. In fact, if we consider "detection" as having occurred when a measured value falls below a specified threshold, we are defining our probabilities somewhat differently from the usual radar probabilities. However, if the redefinition is assumed, the decision theory used in radar detection can be applied.

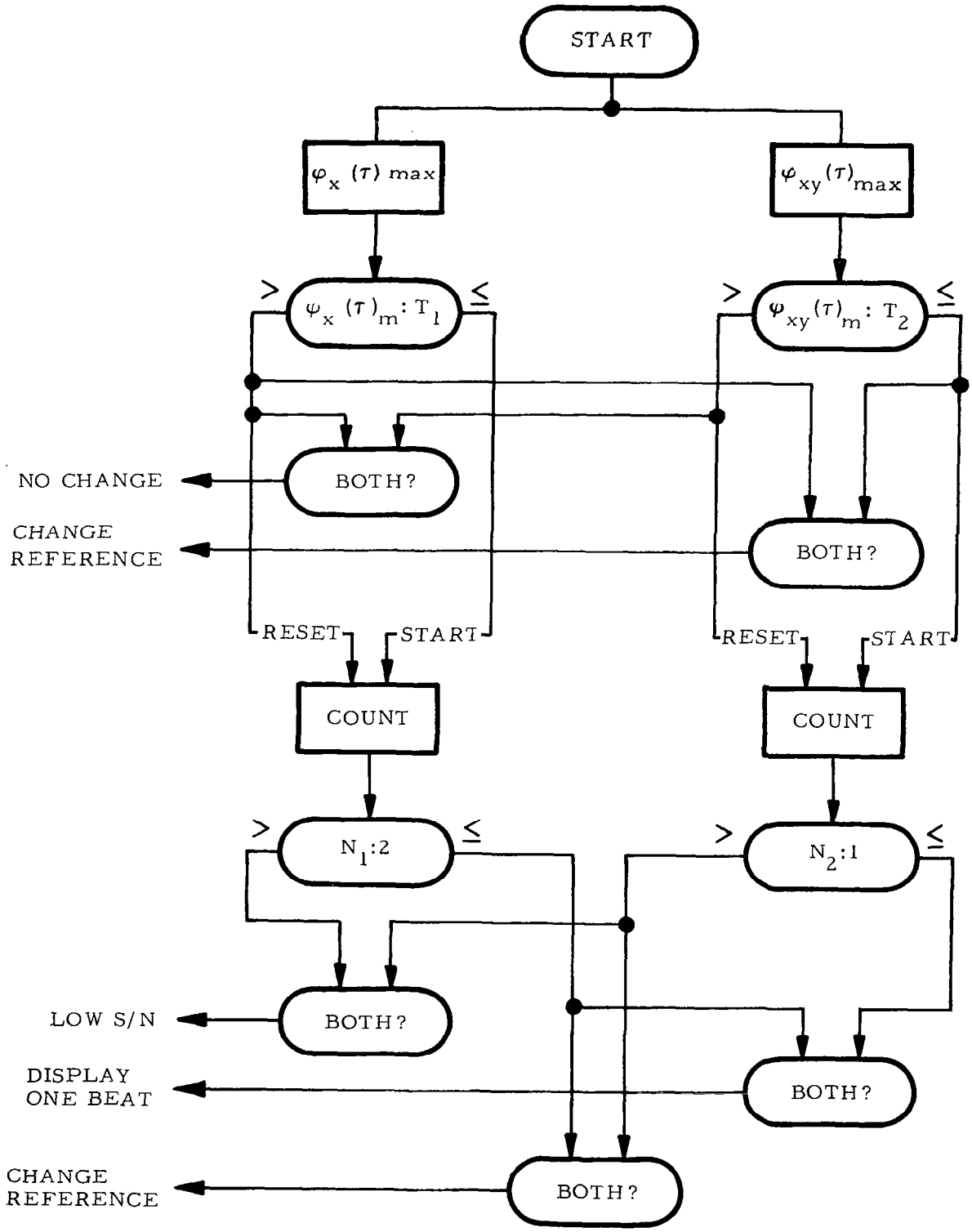

FIGURE 86 ECG PATTERN CHANGE FLOW CHART

Once the necessary decisions have been defined, methods of implementing the sub-system can be investigated. A possible solution is suggested by a commercial special purpose correlation computer available from the Mnemotron Division of the Technical Measurements Corporation. This computer, Model CC-1, was investigated in more detail to evaluate its applicability to our particular requirements. It appears that it is at least technically feasible to modify this equipment to provide continuous auto and crosscorrelation. The basic system would include two CC-1 correlation computers, a model CAT 400B for averaging a reference waveform and special purpose logic for performing the decisions. A rough estimate of purchased hardware cost exclusive of engineering time gives a figure in the $50,000 range. With this figure in mind, consideration might be given to development of special purpose analog or digital devices which perform the required calculations in the most efficient manner for our requirements. The basic difficulty with all analog systems is the storage requirement. Recirculating storage, tape loops and other storage methods present phasing problems. Storage tubes offer a technically feasible approach but the method often used is a hybrid analog-digital scheme. The storage requirement is met by a digital memory while the computations are carried out by analog methods. A device of this type could be developed but it would probably not be economic when the usefulness of the correlation techniques themselves is still to be evaluated.

An economical approach to the evaluation, and possibly the best approach to an operational system, is to program the calculations on a digital computer.

During this Phase I study, correlation techniques were investigated. While the primary objective of these studies was to determine the reliability with which autocorrelation spikes could be used for cardiotachometry, the necessary autocorrelation program was written and a slight addition to the program would enable logical

decisions to be made about pattern change. The crosscorrelation computations are similar to those of autocorrelation and the autocorrelation program could be modified to perform them. Averaging programs have been written which could be used to generate a reference waveform. Two programs which could be used to evaluate the pattern change sub-system were also written during Phase I. These programs, the synthetic ECG and random noise programs, could be used to generate test tapes or to internally generate test signals.

In the light of the availability of these programs as well as the results of the Phase I extension reported in Appendix II, it appears that simulating the pattern change sub-system on a digital computer would be the most economical method of evaluating the usefulness of the correlation techniques. Some evaluation of the trade-offs between the desirability of simulating an operational system and the cost of performing these compilations in real time will have to be made. The computers available for simulation study may not be the most economical ones for real time computing. In an operational system, a more suitable machine could be selected.

With the availability of the simulation programs used to evaluate the pattern change sub-system, the use of a general purpose digital computer in an operational system becomes attractive. A preliminary look indicates that the required computations and decisions could be performed on a machine in the $50,000 price class which puts this approach in direct economic competition with off-the-shelf adaptation and specially developed equipment. Another benefit which may be realized from the use of a general purpose digital computer in an operational system is that extra capability built into the machine may be used to perform claculations and decisions for other sub-systems in the Data Display System.

The pattern change sub-system will eventually be part of a medical data display system, and therefore, some comment is necessary on the display requirements themselves.

Displays are difficult to evaluate analytically and the final decision can only come after a laboratory evaluation. However, the possible display techniques can generally be reduced to a few which are technically and economically feasible. Oscilloscopes and strip chart recorders are common methods of recording complex analog waveforms. Since the data display system is designed to improve on present techniques, the strip chart display can be eliminated from consideration. The choice is now which type of oscilloscope display will most clearly present the required information.

The maximum heart rate of four beats per second and the minimum of one beat every two seconds combine to form a very disagreeable blinking display if the oscilloscope display is initiated only once for each heart beat. In view of the fact that the display is only of a stored reference waveform as long as the current waveform doesn't deviate significantly, there is no reason why an apparently continuous waveform couldn't be displayed. This continuous stationary waveform could be stored either in an external memory or a storage cathode ray tube. Both storage methods have their advantages and should be studied in the laboratory.

The storage oscilloscope requires data only when the waveform is to be changed. This has the advantage of reducing the number of times the memory must be cycled. If the memory forms part of the computer used for the correlation computations, this display requirement may tax the capability of the machine.

The Tektronix model RM564 storage oscilloscope appears suited for this application. This instrument has split screen storage with independent flood guns which allows either half or both halves to be used in the stored or non-stored mode. A rear panel connector allows electrical control over the erase features. The erase time is 0.25

seconds which should be adequate even with rapidly changing waveforms. A modified dual trace pre-amplifier can be used to multiplex the reference and aberrant waveforms.

On the other hand, the storage oscilloscope lacks the contrast and line definition of the usual oscilloscope display. It also suffers in that the waveforms to be compared must be physically displaced due to the split screen erase feature. This may make comparison difficult in certain situations.

If the computer or external storage device has enough unused capability to generate a continuous display, the flexibility of this approach would warrant further investigation. Displaying each waveform at a 20 cps rate should reduce the flicker to an acceptable level with common oscilloscope phosphors. If 250 points per second are displayed for each waveform, the total of 10,000 points per second should be well within the capability of any machine capable of performing the correlation computations in real time. The selection of 250 points per second, a rate which gives five points per cycle of the maximum frequency component, allows the use of simple smoothing filters to produce a continuous display.

Some of the display techniques which should be experimented with would include the relative positions of the two waveforms, intensity modulation of one or both waveforms, and the comparison of the use of a fixed time scale with a variable time scale and electronically generated markers.

The two approaches to waveform display can be evaluated using the oscilloscope mentioned above. This instrument has the capability of being used as a standard oscilloscope as well as a storage oscilloscope.

It would appear that a number of questions are still to be answered in regard to an effective ECG waveform display. The primary one of the sensitivity of correlation techniques to significant waveform changes can be most effectively evaluated by further computer analysis of

artificially generated abnormal waveforms. Since the acceptable costs of false alarms and missed detections can only be evaluated by physically observing a real time display, some form of this display should be generated in the laboratory. This laboratory display should allow operator control over a number of parameters (intensity, position, repitition rate, etc.) in order to select the display which presents the information in the most easily comprehended manner.

Section 10

INVESTIGATION SUMMARY AND RECOMMENDATIONS

10.1 Objective of Investigation

The objective of the investigation was to study advanced signal processing techniques for the Data Display System and the degree to which such techniques could be of help in meeting system requirements.

The general target requirements of the signal processing portion of the Data Display System are to process the ECG, suit-helmet pressure differential, Korotkow sound, and cuff pressure inputs to derive heart rate, respiration rate, blood pressure, and clean typical and aberrant ECG waveforms as output.

10.2 Elements and General Method of Investigation

The investigation was performed to examine the capability of four signal processing techniques in meeting the system requirement; the techniques being filtering, autocorrelation, spectral analysis, and averaging. Both the feasibility and relative utility of the processing techniques were studied. Where application of a technique proved best capable of meeting a system requirement, some study of economical implementation forms was made.

The general procedure followed was conversion of flight data to digital form, mathematical processing technique analysis, digital process programming, program testing and debugging, application of programs with flight input, and study and interpretation of application run results.

10.3 Major Findings

10.3.1 ECG Autocorrelation

ECG autocorrelation achieves reliable heart cycle detection and accurate period or heart rate measurement with highly degraded inputs. For input ECG signals degraded by narrow band white noise or periodic noise unrelated to heart rate, autocorrelation also provides a good measure of signal-to-noise ratio. The economy and reliability of the autocorrelation process can be improved by pre-autocorrelation filtering which produces bandwidth reduction. The high frequency limit of such a pre-autocorrelation passband is determined by the maximum heart cycle frequency to be measured. It was found that a good trade-off between economy and reliability occurred when the ratio of the high frequency limit to the fundamental is three or four. Quantitative findings were that for rates from 120 to 150 bpm, reliable cycle detection of wideband high quality ECG signals was obtained with a sampling frequency f_s of 20 samples per second. For ECG of medium degradation, reliable detection was possible with an f_s of 40 sps. With very noisy ECG, reliable detection was achieved with f_s equal to 100 cps. When pre-autocorrelation bandlimiting was applied to include no more than the fourth harmonic of the heavily degraded ECG, very reliable cycle detection was achieved with a 15 sps sampling frequency. Thus, wideband ECG autocorrelation as a cardiotachometry technique permits reliable and accurate heart period measurement and input signal quality measurement. From these measures, heart rate can be easily determined and the control of an ECG waveform averaging process can be provided. As a supplemental technique to wideband autocorrelation, narrow band autocorrelation preceded by prefiltering improves process reliability and economy.

10.3.2 ECG Digital Filtering

Digital filtering of degraded ECG signals improved signal-to-noise ratio but introduced waveform distortion. Both effects were found when bandwidth was reduced. As contrasted with analog filtering digital filtering permits zero phase shift between filter input and output signals throughout the passband. Since this form of filter was used, the waveform distortion was solely due to attenuation of the higher harmonics and not due to phase distortion. This property of digital filtering gives noise reduction with minimum possible wave shape distortion for a given amount of noise reduction. Thus, for ECG waveform salvaging purposes, digital filtering is an excellent signal processing technique for eliminating noise components of degraded ECG inputs outside of the clean ECG frequency band.

As a sole technique for improving heart rate determination ability, bandpass filtering fails to give reliable performance with degraded inputs. Conventional heart rate determination is based on R-wave detection for heart cycle detection and R-R interval measurement for heart cycle period measurement, and hence fails when R-wave amplitude is less than or insufficiently greater than other portions of the waveform. With wide band degraded input, R-wave detection was very unreliable due to high noise peaks. When narrow bandpass filtering of degraded input passing no more than the fourth harmonic was used, noise was eliminated but R-wave detection was very unreliable due to clean waveform amplitude distortion. This narrow bandwidth distortion resulted in greater relative reduction in R-wave amplitude than in T-wave amplitude. With medium bandwidth filtering, where no more than the eighth harmonic was passed, R-wave detection could be performed, but reliability was only fair due to remaining amplitude distortion. When wideband filtering which passed frequencies to that of the 17th harmonic was used, remaining noise peaks resulted in unreliable detection.

Hence, with a high frequency cutoff either one octave above or below

the eighth harmonic of the heart rate, unreliable and inaccurate operation results. Since the range of heart rate to be determined varies over at least two octaves, from 60 to 240 bpm, bandpass filtering of degraded input cannot alone yield reliable results.

As mentioned before, bandpass filtering as an adjunct to autocorrelation tachometry improves autocorrelation economy. Bandpass filtering as an adjunct to waveform averaging can improve averager economy and permit shorter averaging times.

10.3.3 Spectral ECG Analysis

The flight ECG spectrum has a bandwidth of 3.5 octaves of the fundamental heart cycle frequency, or 12 harmonics. The power peaks at the third harmonic has three times the power of the fundamental. The power difference between adjacent harmonics is too small to permit reliable heart rate determination through spectral analysis of the signal.

10.3.4 Digital Synthetic ECG Waveform Generation

A synthetic ECG waveform generating program was developed which generates digital ECG signals. It enables independent control of rate, all wave-segment amplitudes and durations, and all wave-segment intervals of the simulated ECG. It permits extensive and controlled testing of ECG signal processing techniques.

10.3.5 Electrocardiogram Waveform Averaging

The critical function of any ensemble averaging process is that of proper pacing or establishing of waveform (ensemble) bounds. Depending on the pacing process, it is also necessary to create a

phasing (lining-up)function. If the ECG R-wave were used as a pacing trigger and the ensemble line-up were based on the R-wave, then phasing would be superfluous.

The autocorrelation function may be used with high reliability as an averager pacer where the ensemble bounds are inferred from the time lag corresponding to a peak autocorrelation value. However, in general the phasing function must also be performed since the autocorrelation peak value indicates the lag at which the highest cross-power between successive waveforms occurs. The highest cycle-to-cycle cross-power may well occur at zero phasing of R-waves.

To alleviate costly investigations into cycle-to-cycle cross-power of ECG, a square impulse cross-correlation phaser was utilized.

The phasing process was utilized on the synthetic ECG to establish ability on R-wave line-up. The phasing process had only one failure in all the cursory investigations. This was directly related to excessive width of the square impulse wave.

The techniques, for ensemble averaging, of autocorrelation pacing and cross-correlation phasing look economical and reliable and justify rigorous investigations on the macro-scale.

10.3.6 Respiration Signal Processing

The respiration (suit-helmet pressure differential) signal processing consisted solely of techniques for reliable readout of the average respiration rate. This signal was necessarily erratic due to the breathing mechanism, which is aperiodic, and voice and motion artifact. Frequency or rate analyses generally suggest correlation and

frequency spectrum techniques due to their frequency enhancement capabilities.

Autocorrelation and power spectral density techniques were applied to the respiration signal. Even though the autocorrelation function did not explicitly separate signal from artifact, an average respiration rate could be clearly obtained. Since the artifact generally comprised a different frequency band than pure respiration history, the power spectral density function distinctly separated the two and afforded unobscured respiration rate readout. These processes, however, are quite expensive and their yield did not appear to justify the cost. Therefore, the technique of zero-crossing detection was investigated.

Zero-crossing counting for average respiration rate determination requires only simple band-pass filtering for preconditioning and sign inversion tabulating per some unit of time. It is estimated that zero-crossing detection yields a ten fold saving over autocorrelation and a hundred fold saving over power spectral density with no loss in reliability.

10.3.7 Korotkow Sound Signal Processing

The techniques applied to the Korotkow sound signal were used solely to detect changes in the signal characteristics corresponding to the systolic and diastolic blood pressures. The basic mechanism is that of detecting the presence of acoustic blood flow as opposed to a pure D.C. component in a high noise environment. Due to known advancements in the sensor design and time constraints, only cursory investigations were carried out.

Autocorrelation, power spectral density, and bandpass techniques were

applied to the Korotkow sound signal in order to correlate the acoustic blood flow with the ECG mechanism or for pure sound detection. In no case could any hypothesis be established as to detection success or failure. However, these techniques were overly oriented toward signal structure, whereas the primary concern is merely a signal power change detection.

The total signal power can be obtained from the zero-lag unnormalized autocorrelation. The total power of the two autocorrelation runs made (one segment with no blood flow acoustics and the second suspected to contain blood flow acoustics) was compared and showed variation of two orders of magnitude or a ten percent increase in power. Time limited any further investigations into Korotkow sound signal processing.

10.4 Recommendations

The signal processing techniques described in the preceding text have not received sufficient reliability or economy investigations to warrant implementation into an operational system. Integration of the techniques was not in the scope of the study and may present some problems. Some further areas of work are outlined below:

- Thorough reliability and economy testing.
- Technique integration
- Z-transform (feed-back) digital filtering
- Dynamic quality control averager
- Korotkow sound signal power change detector

Appendix I

PHASE I EXTENSION

1. Introduction

The purpose of this appendix is to present the work accomplished in the Phase I extension studies. Three tasks were performed. The major item was the formulation of a computer program which performs a continuous autocorrelation function for use in the Phase II cardiotachometer and ECG pattern change detector subsystems. An autocorrelation cardiotachometer is a device which processes a physiological input signal containing heart action information by autocorrelating the inputs and utilizes the autocorrelator output to produce heart rate information as final output. If the input signal is electrocardiographic, the device is an autocorrelating electrocardiotachometer and the major process of interest is ECG autocorrelation.

The second task of the Phase I extension studies was the investigation of techniques for generating synthetic waveforms by analog methods. Synthetic ECG waveforms were generated digitally during the Phase I studies (see Section 8) but, since analog waveforms will eventually be required for end-to-end checkout of the complete system, the applicability of commercial function generators was investigated. A number of devices was found which would perform this function to some extent and a comparison of costs and performance is included in this appendix.

The third task performed during the Phase I extension was an investigation of methods for extracting analog outputs from various steps in

the proposed Phase II studies. This is basically a facilities problem and suitable facilities were located where the analog tracings could be generated. The trade-offs involved are also discussed in this appendix.

2. Autocorrelation Input and Output Data Formats

The program development being discussed is one which takes a digitized time sampled ECG as an input time series and produces ordered pairs of normalized autocorrelation peak lag and amplitude values for each heart cycle as primary outputs.

The input samples are called X(I), the input sample rate being f_s samples per second, and the input sample period Δt_s milliseconds per sample. If the analog pre-sampled input is called x(t), and we denote the sampler output by x*(t), we have:

$$x^*(t) = x(t)\Big|_{t=I\,\Delta t_s} = x(I\,\Delta t_s) = X(I) \qquad (1)$$

Thus I is an integer index of time, where a unit increment I corresponds to a Δt_s increment in t.

The normalized autocorrelation is similarly denoted by

$$r^*(\tau) = r(\tau)\Big|_{\tau=j\,\Delta t_s} = r(J\,\Delta t_s) = R(J). \qquad (2)$$

Since R(J) is a function, it can be represented as the ordered pair (J, R).

$$R(J) \leftrightarrow (J,\ R). \qquad (3)$$

Similarly, (1) can be indicated by

$$X(I) \leftrightarrow (I,\ X). \tag{4}$$

For example, if R was .5 at a lag of $\tau = 200\Delta t_s$ milliseconds,

$$r^*(\tau) = r(200)\Delta t_s) = .5$$

$$R(J) = R(200) = .5$$

and

$$(J,\ R) = (.5,\ 200)$$

are equivalent ways of representing the point of the function.

To distinguish the outputs from successive heart cycles, a cycle index K is used, and thus one useful form of representing a program output is the ordered triple

$$(K,\ J,\ R). \tag{5}$$

We will also denote the second and third members of the triple by J_K and R_K, respectively. To easily relate and compare output data (5) to input data (4), it is desirable to key them through a time index relationship. This is done by defining an output time index I'. Since "input time"

$$t = I\Delta t_s,$$

and the period of the Lth cycle is

$$\tau_L = J_L\Delta t_s, \tag{6}$$

We define I' at cycle K by

$$t'_K = I'_K \Delta t_s, \quad I'_K = t'_K / \Delta t_s \tag{7}$$

$$t'_K = \sum_{L=1}^{K} \tau_L = \sum_{L=1}^{K} J_L \Delta t_s \tag{8}$$

$$I'_K = t'_K / \Delta t_s = \left(\sum_{L=1}^{K} J_L \Delta t_s\right) / \Delta t_s = \sum_{L=1}^{K} J_L \tag{9}$$

Thus the other useful forms of output are

$$(K,\ I',\ J,\ R) \tag{10}$$

$$(I',\ J,\ R). \tag{11}$$

In (10) we have K specifying the cycle number; $I' = I'_K$ the time index, or number of elapsed sampling intervals Δt_s, of Kth cycle occurrence; $J = J_K$ the lag index of the autocorrelation; and $R = R_K = R(J_K)$ the amplitude of the normalized autocorrelation. An output of form (11) might be used when the cycle number was of no interest. If the value of J_K in (10) or (11) is the lag index JP for which the first whole spike in $R_K(J)$ peaks, we can indicate this by output forms

$$(K,\ I',\ JP,\ RP) \tag{12}$$

$$(I',\ JP,\ RP) \tag{13}$$

$$(K,\ I',\ RP) \tag{14}$$

$$(I',\ RP) \tag{15}$$

(K, RP) (16)

(I'_K) (17)

Output in the form (17) is all that is required for basic heart rate determination, simply the values of time index at which successive cycles occur. Forms (14), (15), and (16)are useful in that the RP values can be studied to evaluate process reliability, and some of the effects of noise and ECG changes on the autocorrelation output. Since output form (12) contains all the important results of the program, and "contains" the other forms, it was adopted as the desired output format for the autocorrelation program.

3. Heart Rate Computation

To make the final measurement of heart rate from the period lag measures JP_K, we compute the individual cycle rate from (18) and (6)

$$HR_K = (60 \text{ sec/min}) \times (\tau_K^{-1} \text{ beats/sec}) = 60/\tau_K \text{ bpm} \quad (18)$$

$$HR_K = \frac{60}{\tau_K} = \frac{60}{JP_K \Delta t_s} = \frac{60 f_s}{JP_K} \quad (19)$$

where f_s is in samples per second. Since average as well as instantaneous rate is of interest, an average HR over NKA cycles is computed from

$$\overline{HR_K} = \frac{1}{NKA} \sum_{L=K}^{L=K+NKA} HR_K = \frac{60 f_s}{(NKA)} \sum_{L=K}^{L=K+NKA} (JP_L)^{-1} \quad (20)$$

4. Specification and Criteria of Program Development Problem

Combining these rate outputs with those of (12) gives

$$(K,\ I',\ JP,\ RP,\ HR,\ \overline{HR}) \tag{21}$$

$$(K,\ I',\ JP,\ RP,\ HR) \tag{22}$$

Thus, the complete specification for the program is to produce, from input (1), an output of the form (21) for every (NKA)th cycle and an output of form (22) for all other cycles. This is the statement of the program development problem.

The program development problem was analyzed into major subproblems. Various approaches to solving each of the subproblems were sought, found, and studied as to their effectiveness. Four major criteria -- reliability, accuracy, speed, and economy -- were applied in evaluating the effectiveness of the approaches. The reliability criterion is simply to maximize ratio

$$a = \frac{\text{Number of Detected Cycles}}{\text{Number of Input Cycles}}$$

over a given period of operation.

The accuracy criteria were to minimize the errors in determination of J_K and R_K. If $\hat{J}$ and $\hat{R}$ denote approximate values of J and R; ϵJ and ϵR the errors in these estimates; and EJ and ER the maximum allowable error, we have the accuracy specifications

$$|\epsilon J| = |J - \hat{J}| \leq EJ \tag{23}$$

$$|\epsilon R| = |R - \hat{R}| \leq ER \tag{24}$$

The speed criterion was that the rate of computing output be greater than input rate, when input rate is "actual" or measured in "real time", and that the computation delay be less than one minute, which is adequate for most responses the monitor might need to make to sudden ECG changes. For post-flight data reduction program application this requirement could be relaxed. For flight-concurrent monitoring application, a tighter requirement might be useful.

Investigation of the economy criteria in developing a digital computer program involves control of a mixed measure of at least three interdependent factors: minimize machine cost, minimize storage needed for program and data, maximize execution rate of the program. For example, if the storage need is large, the machine cost is increased. If execution rate of the program is increased, more of machine capacity is available for other work, and the allocatable cost of machine utilization for the program is reduced. These are the major complex interdependencies among the cost, storage, and speed factors.

5. Basic Correlation Algorithms

Let $\psi(J)$: IS, NI, DI denote the autocorrelation of X(I) at lag J for a signal segment starting at IS, where NI is the number of data samples used in the integration interval T, and the integration increment is DI units. Then

$$NI = \frac{T}{(DI)\Delta t_s} = \frac{Tf_s}{DI}; \quad T = (NI)\,(DI)\Delta t_s \tag{25}$$

$$J = \frac{\tau}{\Delta t} = \tau f_s \tag{26}$$

$$\psi(J) = \frac{1}{NI} \sum_{I=IS}^{I=IF} X(I)\, X(I + J)\,, \tag{27}$$

where

$$IF = IS + (NI - 1)\, DI \tag{28}$$

For the special case where $\psi(J)$: 1, NI, I; i.e., when

$$IS = DI = 1 \tag{29}$$

$$IF = IS + (NI - 1)\, DI = 1 + (NI - 1) = NI \tag{30}$$

expression (27) becomes

$$\psi(J) = \frac{1}{NI} \sum_{I=1}^{I=NI} X(I)\, X(I + J). \tag{31}$$

The zero lag autocorrelation is given by

$$\psi(0) = \frac{1}{NI} \sum_{I=IS}^{I=IF} X(I)^2 \tag{32}$$

and, when (29) holds, by

$$\psi(0) = \frac{1}{NI} \sum_{1}^{NI} (X(I))^2. \tag{33}$$

Division of (31) by (33) gives the normalized autocorrelation of X(I)

at lag J, denoted by R(J): IS, NI, DI; and for IS = DI = 1 is computed by

$$R(J) = \frac{\sum_{I}^{NI} X(I)\, X(I+J)}{\sum_{I}^{NI} X(I)^2} = \frac{NI * \psi(J)}{NI * \psi(0)} = \frac{A}{B} \qquad (34)$$

The normalized autocorrelation is sometimes referred to as the autocovariance.

6. Extent of Computation of Correlation Functions

From the above algorithms, the extent of computation of autocorrelation and autocovariance functions can be determined. Let $C_a(F)$ denote the number of operations of a type a required to compute a value of function F. Then from (31), (32) and (34) we find:

Computation of A requires NI multiplications: $C_m(A) = C_m(NI*\psi(J)) = NI$

Computation of B requires NI multiplications: $C_m(B) = NI$

Computation of M values of A requires M*NI multiplications.

Having computed B and M values of A, getting M values of $R_N(J)$ requires M divisions: $C_D(A/B) = M$.

Thus over-all computation of M values of R(J), $\underline{R}(J_i) = (RJ1)$, R(J2), $\cdots$, R(JM), requires (M + 1) NI multiplications and M divisions or a total of: $C_o(\underline{R}(J_i)) = M(NI + 1) + NI$ operations. (35)

7. Relationship Between Lag Error and Computation Extent

Now consider the computation required to locate a peak value of R(J) with varying accuracy. As defined in Sections 2 and 4, the lag index value for which R(J) peaks is JP, and EJ is the maximum error in an estimated value J. For $\hat{JP}$ as an estimate of JP we have

$$\epsilon JP = JP - \hat{JP} \tag{36}$$

$$|\epsilon JP| = |JP - \hat{JP}| \leq EJP \tag{37}$$

Now consider an NJ membered sequence of J values spaced DJ units apart, beginning with JS and ending with JF:

$$J = JS,\ JS + DJ,\ JS + 2DJ,\ \cdots,\ JF.$$

Let us define the range or duration of this sequence by

$$JD = (JF - JS) = (NJ - 1)\,DJ\,, \tag{38}$$

and let the Lth value of J be

$$J(L) = JS + (L - 1)\,DJ = J(1) + (L - 1)\,DJ \tag{39}$$

$$DJ = J(L + 1) - J(L) \tag{40}$$

where

$$L = 1,\ 2,\ 3,\ \cdots,\ (NJ - 1)\,.$$

To achieve the desired tolerance in the estimate $\hat{JP}$ of JP requires that

$$(\frac{1}{2} DJ) \leq EJP \tag{41}$$

$$DJ \leq 2\ EJP \tag{42}$$

Since from (38) we have

$$NJ = \frac{JD}{DJ} + 1\ , \tag{43}$$

we can keep M small and conserve computation by choosing DJ as large as the accuracy requirement of (42) permits, which gives

$$DJ = 2\ EJP \tag{44}$$

$$NJ = \frac{JD}{2\ EJP} + 1 \tag{45}$$

Substitution of (45) into (35) yields

$$C_\epsilon = (\frac{JD}{2\ EJP} + 1)\ (NI + 1) + NI \tag{46}$$

Thus for a given time resolution, the extent of computation as a function of allowable maximum lag error EJP is determined.

8. Integration Time and Sampling Frequency Considerations

The maximum number of samples in the integration time T is given by

$$NI_m = \frac{T}{\Delta t_s} = T\ f_s \tag{47}$$

where f_s is the sampling rate in samples per second and Δt_s is the sampling period in seconds per sample. For a given integration time, NI can be reduced by subsampling X(I), which is effected by making DI greater than one. Then DI becomes the sampling period increase ratio. Let Δt_e be the effective sampling period, and f_e the effective sampling frequency. Then we have

$$DI = \frac{\Delta t_e}{\Delta t_s} = \frac{f_s}{f_e} \tag{48}$$

$$NI = \frac{T}{(DI)\Delta t_s} = \frac{T}{\Delta t_e} = Tf_e \tag{49}$$

Reductions of NI can be made by reducing T and f_e as much as allowed by accuracy requirements in determining R(JP).

Usable accuracy in R(JP) can be maintained with

$$T \leq (JF)\ (\Delta t_s) \tag{50}$$

for which NI is smallest if we choose the equality in (50), giving (from (49))

$$NI = \frac{(JF)\ (\Delta t_s)}{(DI)\ (\Delta t_s)} = \frac{JF}{DI} \tag{51}$$

In fact, JP is reliably estimated most easily with a least integration time given by

$$T = (JP)\Delta t_s = \tau P \tag{52}$$

Thus to compute R(JP) with the smallest possible NI, we set $JF = \hat{JP}$,

and from (51) and (48) we have

$$NI = \frac{\hat{JP}}{DI} = \hat{JP}\,(f_e/f_s) \tag{53}$$

After integration time is minimized, further reduction of NI requires an increase in DI or reduction of effective sampling rate f_e.

Now the degree to which f_e can be decreased is limited by aliasing and folding errors as the folding frequency,

$$f_f = \frac{f_e}{2}, \tag{54}$$

becomes so low that the power spectrum of the sampled data becomes badly distorted. This distortion can certainly be avoided by keeping f_f at or above the upper band limit of the data spectrum. For several values of f_s and of the upper band limit f_{HC}, we would have:

f_{HC}	16 cps	32 cps	64 cps	128 cps	
f_e	32 sps	64 sps	128 sps	256 sps	
DI (f_s = 1024)	32	16	8	4	$\Delta t_s \hat{=}$ 1 ms
DI (f_s = 512)	16	8	4	2	$\Delta t_s \hat{=}$ 2 ms
DI (f_s = 256)	8	4	2	1	$\Delta t_s \hat{=}$ 4 ms

This table shows that with a sampling frequency of f_s = 256 sps, $\Delta t_s \hat{=}$ 4 ms, and data filtered to contain little power above f_{HC} = 16 cps, a DI of 8 could be used, giving from (53)

$$NI = \frac{\hat{JP}}{DI} = \frac{\hat{JP}}{8} = \frac{f_s \hat{\tau}}{8} = \frac{256\hat{\tau}}{8} = 32\hat{\tau} \tag{55}$$

Hence if $\hat{T} = T$ were 0.5 second, NI would be 16. By combining (46) and (51), we have

$$C = \left(\frac{JD}{2\ EJP} + 1\right)\left(\frac{JF}{DI} + 1\right) + \frac{JF}{DI} \tag{56}$$

Expression (56) compactly shows several opportunities for reducing C. Some of these are:

a) Keep EJP large, especially when JD is large

b) Keep JD small when EJP is small

c) Increase DI as JF increases, as limited by folding error

9. Bandpass Filtering to Permit f_e Reduction

Earlier investigation indicated that bandlimiting X(I) prior to subsampling not only reduces the folding frequency but increases signal-to-noise ratio as well, if at least the third harmonic of the HR is included in the band-limits. Consider a bandpass filtering of X(I) to produce XF(I) with a filter passband from f_{LC}, the fundamental frequency of the lowest heart rate to be measured, to f_{HC} the third harmonic of the highest heart rate. Subsampling X(F) at an effective rate f_e with no folding error then occurs for f_e as small as

$$f_e = 2f_f = 2f_{HC} \tag{57}$$

To illustrate (57) for HR as high as 240 bpm,

$$f_{HC} = 3\left(\frac{240}{60}\right) = 12 \text{ cps,} \tag{58}$$

$$f_e = 2f_{HC} = 24 \text{ sps} \tag{59}$$

Now from (48) and (57), we get

$$DI = f_s/f_e = f_s/2f_{HC} \tag{60}$$

which is the maximum DI for which no XF(I) folding error results.

Combining (56) and (60) gives

$$C = \left(\frac{JD}{2\,EJP} + 1\right)\left(\frac{2f_{HC}JF}{f_s} + 1\right) + \frac{2f_{HC}JF}{f_s} \tag{61}$$

With the filtering and subsampling arranged as described, expression (61) gives the least computation for a controlled error.

10. Practical Selection of Sampling Frequency f_s

The maximum precision ϵt with which the period measure can be determined is limited by the sampling frequency by

$$\epsilon t \leq \frac{1}{2}\Delta t_s = (1/(2f_s)) \text{ seconds, or } 500/f_s \text{ ms.} \tag{62}$$

From previous definitions we have the following relationship

$$EJP = (\epsilon t)(f_s)/500 \text{ (where } \epsilon t \text{ is in ms)} \tag{63}$$

Combining (62) and (63) gives

$$EJP = \frac{(\epsilon t)(f_s)}{500} \leq 1, \tag{64}$$

Recalling that

$$DJ = 2EJP \tag{44}$$

and that the minimum practical choice of DJ for precision JP determination is 1, one finds the minimum practical value for EJP to be

$$EJP_{min} = \frac{DJ_{min}}{2} = .5 \ . \tag{65}$$

Thus, from (62) and (65), the minimum practical value of f_s needed to permit period determination to a precision of ϵt milliseconds is

$$f_s = \frac{500\ DJP_{min}}{\epsilon t} = \frac{250}{\epsilon t} \quad \text{samples/second} \ . \tag{66}$$

For example, if period is to be determined with a one millisecond tolerance, $\epsilon t = 1$, and the minimum practical sampling rate is

$$f_s = 250 \text{ sps.}$$

11. Computing (JP, RP) by a Multi-Resolution Process

The factors in (56) show extensive computation time is involved if error is held small while a wide number of samples are computed. For example, with

$$2\ EJP = DI = 1 \tag{67}$$

$$JD = JF = JP = f_s \tau_o \ , \tag{68}$$

from (56) we have

$$C = JP^2 + 3JP + 1 . \tag{69}$$

For a τ_o of one second, or an HR of 60 bpm, we have:

$$C = f_s^2 + 3f_s + 1 . \tag{70}$$

At several sampling rates, approximate values of ϵt in ms from (62) and of C in number of operations from (70) are given by:

f_s	10	15	20	30	50	100	500
C	130	270	460	990	2,650	10,300	251,500
ϵt	50	33	25	17	10	5	1

In this example, f_s values of R(J) were computed when DI was 1.

Now let JS be any lag index value on the R(J) spike for which JP is the spike peak lag. Then the extent of computation needed to locate JP can be reduced considerably by first locating through coarse resolution, any lag point on the spike, JS, with an error as large as the spike half-width between JP and JS. Next, with JS taken as a coarse estimate $\hat{\hat{JP}}$[1] of peak lag index JP, a medium resolution tracking of spike values starting

1. That is, we define $\hat{\hat{JP}}$ by: $\hat{\hat{JP}} = JS$

from JS will yield a better estimate $\hat{JP}$ of JP. Finally, JP determination can be made with fine accuracy by a high resolution tracking of the spike peak. Thus, in the first stage there are many steps of each with a small C. In the next stage there are fewer steps of medium extent. And in the last stage, very few steps at highest resolution, where the computation per step is large.

12. Description of Program Design

The over-all purposes of the ECG autocorrelation program are cycle detection, period measurement, and relative clean signal power or signal-to-noise ratio measurement. The general operation of the program is as follows. The sampled ECG input X(I) is passed through a digital bandpass filter whose output is XF(I). Cycle detection is performed by locating the earliest full spike in $R_K(\tau)$, through a coarse resolution spike search process, using XF(I), starting with small search lag values. Following cycle detection, the period of the ECG is then determined by locating the peak of the spike with peak tracking subroutines, first at medium error with XF, then at low error with X. The amplitude of the autocorrelation of the unfiltered input at the peak RP_K, the cycle occurrence time I', and the lag of the peak JP_K are then produced as output. Both the unfiltered and filtered inputs are then updated by advancing the inputs by JP_K sampling intervals, and the next cycle is ready for processing. A power change test is made between cycles, and if the power change between cycles is large, the next cycle detection is performed with spike search as described above, with $XF(I + JP_{K-1})$ as autocorrelator input, and the process continues. If power change is small the cycle detection is done by a spike tracking process with XF, where the tracker oscillates lag values around the last peak location if necessary to track small spike lag changes. For large or small power change, the spike lag for the cycle, JS, is fed to a coarse peak tracker which locates the approximate peak lag JP by autocorrelating the output of the bandpass filter, XF. Fine peak tracking is performed with unfiltered input by tracking from $\hat{JP}$ in either or both directions until RP is determined. Thus, the final period determination is made with as much accuracy as the input sampling rate permits.

This design of the program permits coarse resolution to be used for

spike detection with high reliability, due to the wide autocorrelation spike widths produced by properly bandpassing the input to the autocorrelator. Approximate peak location can be performed very economically at medium resolution by using filtered input for the first stage of peak tracking. Medium resolution can also be used for spike tracking purposes. Accurate or high resolution period determination with a minimum of computation is then possible with unfiltered input in the second stage of peak tracking. The design thus minimizes the over-all number of computations necessary to perform cycle detection, spike tracking, and peak location without sacrificing reliability or accuracy.

In operation, this program design is efficient and will yield reliable and accurate results. Hence, the program design meets all the development criteria.

13. Analog Generations of Synthetic Physiological Waveforms

In certain portions of the data display system study, the availability of a device to generate synthetic physiological waveforms would be an advantage. This device could be used for system pre-flight checkout and, in fact, any time test signals are required at the analog input to the display. For these reasons, a study of methods of generating arbitrary analog functions was undertaken.

The generation of arbitrary function is commonly performed in the analog computer field. Many of the devices referenced in the literature are apparently one of a kind devices. Since the development of a synthetic waveform generating device is beyond the scope of this program, the investigation was confined to devices which are commercially available.

The requirements of this program are for a device which generates ECG waveforms in real time. These waveforms must be adjustable to simulate a variety of abnormalities for testing an ECG pattern change detection sub-system. The specific minimum requirements for ECG waveform generation are detailed in Section 8 of this report. However, in general, deterministic and random changes in the cycle-to-cycle heart rate and in each ECG segment amplitude duration will be required.

One method of generating a continuous train of arbitrary functions is to draw each function on a strip chart and play this chart back using photoelectric sensors. One device which accomplishes this and is commercially available is the F. L. Moseley model 680 strip chart recorder with the model F-3B curve follower attachment. This device, however, has an eight inches per minute maximum chart speed. Assuming a draftsman can produce an ECG waveform in four inches with reasonable accuracy, this limits the simulation to a maximum heart rate of two beats per minute. Or, assuming a real time rate of 200 beats per minute, the system would be operating at 1/100 real time rate. The price of this unit is $1,550.00.

Another device which operates on the same principle is a curve follower attachment to an X-Y plotter. The slewing rate of available plotters allows real time generation of ECG waveforms if some reduction in accuracy is allowed. The Moseley model F-3B can be attached to their model 2D plotter allowing a 20 inches per minute rate on each axis. This system would cost $3,050.00.

A similar X-Y plotter function generator is produced by Electro Instruments, Inc. This system uses an electromagnetic induction method of curve following. The function to be generated is formed out of wire and fastened to the X-Y plotter. The system for function generation is the model 400 plotter with the model 450 curve follower

module. This method of function generation is claimed to be more accurate than the photoelectric method. It has an accuracy of $\pm$ .25% of full scale when limited to slope changes of less than 75°. However, this slope limitation sets a maximum height of 1" on the R wave and all other segments proportionately smaller. It is doubtful that the wire could be formed to the 2.5% accuracy available in this case. The unit cost of this system is about $2,995.00.

The X-Y plotter method of function generation shares a common difficulty with photoformers and most other methods of function generation. That is, the programming of arbitrary changes in the waveform during generation is extremely difficult, if not impossible. This is not generally required in an analog computer system and, therefore, is available only in one of a kind installations. However, by using a tape recorder to record the function and editing out the "dead time" during waveform change over, an analog simulation tape could be generated.

Another commonly used method of synthesizing arbitrary waveforms is by approximating them with a large number of straight line segments. The Exact Electronics model 200 Waveform Synthesizer is designed to do just this. With the type F plug in generator, this unit can produce up to 50 increments with independent slope and duration with each segment starting at the last value of the preceding segment. The type 200 can be triggered externally for rate control. Some manual control of waveform shape may be feasible during generation. This device costs $2,275.00 with plug-in.

Function generators which produce simultaneous sine, cosine, ramp and triangle waveforms are available commercially but, since independent duration control is not available, it does not appear that this approach is economically feasible. The generation of an ECG waveform

would require four independent generators in addition to special purpose timing equipment. The generators cost $685.00 each.

The function generation devices which use a strip chart recorder or X-Y plotter generally assume that the recorder is already part of the facility equipment or could be used for its primary purpose. However, for our application of the unit, it would serve solely as a function generator. Then, from a cost and ease of operation viewpoint, the Exact Electronics type generator becomes the most attractive.

The problem still remains that waveform changes and aberrant beats are difficult to generate. It will probably prove easier and less expensive to generate analog tapes by digital computers and digital to analog converters.

14. Methods for Extracting Analog Outputs

The third task of the Phase I extension was to determine methods of extracting analog outputs for a number of points in the Phase II computer program. These analog outputs would be used for evaluating the effectiveness of the program and to generate an ECG display.

The problem of extracting analog outputs from a digital computer is not one of technical feasibility. Digital to analog conversion is commonly performed in telemetry and hybrid computer installations. The problem is locating a facility in the area which is capable of performing the digital computations, has the digital to analog conversion equipment and is willing to rent time on the equipment to this program.

A survey of the local computer installations failed to locate a facility which could perform the required digital to analog conversion on line in real time. Most installations were capable of performing the digital

computations. However, none of them had the multi-channel high speed digital to analog converters necessary for real time simulation.

Therefore, it was decided to locate off-line digital to analog conversion capability. The most suitable machine for this task which is available locally is the Stromberg-Carlson 4020. This machine produces 35 mm film and hard copy of an internal Charactron oscilloscope tube. While this machine will not allow realistic evaluation of the on-line display, it will produce the necessary analog outputs for evaluation of the programs and allow specification of the final display.

APPENDIX II

RUN CASE HP-6

AUTOCORRELATION OF E K G . TEST NUMBER 1-45 . TAPE NUMBER BIO-03. OCT. 23,1964 PAGE

COMPUTATIONS FROM 9.(HOURS), 2620.000(SECONDS) TO 9.(HOURS), 2621.530(SECONDS) AT EVERY 10 FRAMES.
NUMBER OF FRAMES = 306. NUMBER OF LAGS = 153. DATA TIME RESOLUTION = 0.004999.
AUTOCORRELATION FUNCTION TIME RESOLUTION = 0.005. FROM 0. (SEC) TO 0.765(SEC).
ZERO-LAG AUTOCORRELATION = 0.12708561E 07

TAU	AUTOCOR	TAU	AUTOCOR	TAU	AUTOCOR	TAU	AUTOCOR	TAU	AUTOCOR
-0.	1.000000	0.0050	0.894410	0.0100	0.651284	0.0150	0.370193	0.0200	0.119267
0.0250	-0.056148	0.0300	-0.145103	0.0350	-0.171316	0.0400	-0.168009	0.0450	-0.156836
0.0500	-0.147377	0.0550	-0.136811	0.0600	-0.125801	0.0650	-0.112754	0.0700	-0.103995
0.0750	-0.108445	0.0800	-0.119492	0.0850	-0.127799	0.0900	-0.129999	0.0950	-0.131824
0.1000	-0.137761	0.1050	-0.142097	0.1100	-0.143232	0.1150	-0.142631	0.1200	-0.137561
0.1250	-0.125047	0.1300	-0.105255	0.1350	-0.074643	0.1400	-0.047138	0.1450	-0.024867
0.1500	-0.002943	0.1550	0.014087	0.1600	0.028096	0.1650	0.037159	0.1700	0.043881
0.1750	0.056019	0.1800	0.066603	0.1850	0.067761	0.1900	0.067830	0.1950	0.067521
0.1999	0.062535	0.2049	0.057960	0.2099	0.054192	0.2149	0.050975	0.2199	0.047890
0.2249	-0.009404	0.2299	-0.028106	0.2349	-0.039363	0.2399	-0.046879	0.2449	-0.053994
0.2499	-0.058969	0.2549	-0.058558	0.2599	-0.056592	0.2649	-0.039591	0.2699	-0.029373
0.2749	-0.021082	0.2799	-0.011157	0.2849	0.004203	0.2899	0.016213	0.2949	0.026875
0.2999	0.035072	0.3049	0.038521	0.3099	0.040496	0.3149	0.041603	0.3199	0.034107
0.3249	0.019863	0.3299	0.010839	0.3349	0.007241	0.3399	0.005044	0.3449	-0.002620
0.3499	-0.017941	0.3549	-0.042126	0.3599	-0.073543	0.3649	-0.097286	0.3699	-0.103442
0.3749	-0.099937	0.3799	-0.096803	0.3849	-0.094712	0.3899	-0.094395	0.3949	-0.093659
0.3999	-0.089201	0.4049	-0.081960	0.4099	-0.074731	0.4149	-0.078960	0.4199	-0.094292
0.4249	-0.112195	0.4299	-0.131490	0.4349	-0.147819	0.4399	-0.163916	0.4449	-0.179824
0.4499	-0.201868	0.4549	-0.221902	0.4599	-0.220884	0.4649	-0.182657	0.4699	-0.082058
0.4749	0.097706	0.4799	0.340430	0.4849	0.599389	0.4899	0.819186	0.4949	0.943187
0.4999	0.938968	0.5049	0.810666	0.5099	0.588572	0.5149	0.332542	0.5199	0.106840
0.5249	-0.054325	0.5299	-0.149462	0.5349	-0.185694	0.5399	-0.182614	0.5449	-0.158559
0.5499	-0.129295	0.5549	-0.112290	0.5599	-0.111670	0.5649	-0.126940	0.5699	-0.143634
0.5749	-0.147561	0.5799	-0.141250	0.5849	-0.137069	0.5899	-0.135828	0.5949	-0.129724
0.5998	-0.125758	0.6048	-0.125684	0.6098	-0.123806	0.6148	-0.122140	0.6198	-0.125109
0.6248	-0.121991	0.6298	-0.106769	0.6348	-0.075845	0.6398	-0.039740	0.6448	-0.011755
0.6498	0.004233	0.6548	0.005518	0.6598	0.000855	0.6648	0.007294	0.6698	0.030827
0.6748	0.057050	0.6798	0.073503	0.6848	0.084998	0.6898	0.088133	0.6948	0.077154
0.6998	0.058326	0.7048	0.040626	0.7098	0.023568	0.7148	0.005528	0.7198	-0.004922
0.7248	-0.014519	0.7298	-0.029191	0.7348	-0.042359	0.7398	-0.049772	0.7448	-0.057169
0.7498	-0.066578	0.7548	-0.071616	0.7598	-0.070500				

FIGURE 17

RUN CASE HP-7

AUTOCORRELATION OF E K G . TEST NUMBER 1-45 . TAPE NUMBER BIO-03. OCT. 23,1964 PAGE

COMPUTATIONS FROM 9.(HOURS), 2620.000(SECONDS) TO 9.(HOURS), 2621.530(SECONDS) AT EVERY 20 FRAMES.
NUMBER OF FRAMES = 153. NUMBER OF LAGS = 76. DATA TIME RESOLUTION = 0.009997.
AUTOCORRELATION FUNCTION TIME RESOLUTION = 0.010. FROM 0. (SEC) TO 0.760(SEC).
ZERO-LAG AUTOCORRELATION = 0.62568509E 06

TAU	AUTOCOR	TAU	AUTOCOR	TAU	AUTOCOR	TAU	AUTOCOR	TAU	AUTOCOR
-0.	1.000000	0.0100	0.645599	0.0200	0.107127	0.0300	-0.146611	0.0400	-0.161744
0.0500	-0.136003	0.0600	-0.124935	0.0700	-0.112272	0.0800	-0.132022	0.0900	-0.136209
0.1000	-0.138224	0.1100	-0.138413	0.1200	-0.131350	0.1300	-0.099432	0.1400	-0.042783
0.1500	0.003654	0.1600	0.031869	0.1700	0.038436	0.1800	0.056984	0.1900	0.072382
0.2000	0.065710	0.2099	0.056705	0.2199	0.012586	0.2299	-0.035670	0.2399	-0.061817
0.2499	-0.069668	0.2599	-0.047533	0.2699	-0.026704	0.2799	-0.013401	0.2899	0.014266
0.2999	0.035177	0.3099	0.033643	0.3199	0.021547	0.3299	0.008770	0.3399	0.009365
0.3499	-0.007498	0.3599	-0.071203	0.3699	-0.100959	0.3799	-0.096863	0.3899	-0.094182
0.3999	-0.092234	0.4099	-0.077342	0.4199	-0.080212	0.4299	-0.113305	0.4399	-0.142158
0.4499	-0.197420	0.4599	-0.230986	0.4699	-0.096536	0.4799	0.330860	0.4899	0.814664
0.4999 x	0.944007	0.5099	0.611094	0.5199	0.117375	0.5299	-0.139583	0.5399	-0.170730
0.5499	-0.120705	0.5599	-0.125064	0.5699	-0.171256	0.5799	-0.155974	0.5899	-0.139981
0.5998	-0.113110	0.6098	-0.110184	0.6198	-0.124141	0.6298	-0.114987	0.6398	-0.045886
0.6498	0.009115	0.6598	0.007927	0.6698	0.030465	0.6798	0.071061	0.6898 x	0.090253
0.6998	0.067464	0.7098	0.018435	0.7198	-0.019812	0.7298	-0.041893	0.7398	-0.046668
0.7498	-0.058860								

FIGURE 18

RUN CASE HP-8

AUTOCORRELATION OF E K G . TEST NUMBER 1-45 . TAPE NUMBER BIO-03. OCT. 23,1964 PAGE

COMPUTATIONS FROM 9.(HOURS), 2620.000(SECONDS) TO 9.(HOURS), 2621.530(SECONDS) AT EVERY 30 FRAMES.
NUMBER OF FRAMES = 102. NUMBER OF LAGS = 51. DATA TIME RESOLUTION = 0.014996.
AUTOCORRELATION FUNCTION TIME RESOLUTION = 0.015. FROM 0. (SEC) TO 0.765(SEC).
ZERO-LAG AUTOCORRELATION = 0.43188C10E 06

TAU	AUTOCOR	TAU	AUTOCOR	TAU	AUTOCOR	TAU	AUTOCOR	TAU	AUTOCOR
-0.	1.000000	0.0150	0.337906	0.0300	-0.150422	0.0450	-0.158974	0.0600	-0.110123
0.0750	-0.097728	0.0900	-0.112186	0.1050	-0.145455	0.1200	-0.143977	0.1350	-0.097736
0.1500	-0.015210	0.1650	-0.017850	0.1800	0.049898	0.1950	0.070802	0.2099	0.059491
0.2249	0.026897	0.2399	-0.004483	0.2549	-0.043597	0.2699	-0.029421	0.2849	0.016739
0.2999	0.034149	0.3149	0.047852	0.3299	-0.013066	0.3449	-0.023881	0.3599	-0.067816
0.3749	-0.102445	0.3899	-0.099544	0.4049	-0.069415	0.4199	-0.054086	0.4349	-0.115838
0.4499	-0.183790	0.4649	-0.171750	0.4799	0.280961	0.4949	0.922684	0.5099	0.563247
0.5249	-0.034926	0.5399	-0.193305	0.5549	-0.112724	0.5699	-0.146560	0.5849	-0.121086
0.5998	-0.114627	0.6148	-0.135783	0.6298	-0.093701	0.6448	-0.030541	0.6598	-0.031561
0.6748	0.057423	0.6898	0.084867	0.7048	0.051727	0.7198	-0.011987	0.7348	-0.043060
0.7498	-0.053059								

FIGURE 19

RUN CASE HP-9

AUTOCORRELATION OF E K G . TEST NUMBER 1-45 . TAPE NUMBER BIO-03. OCT. 23,1964 PAGE

COMPUTATIONS FROM 9.(HOURS), 2620.000(SECONDS) TO 9.(HOURS), 2621.530(SECONDS) AT EVERY 50 FRAMES.
NUMBER OF FRAMES = 61. NUMBER OF LAGS = 30. DATA TIME RESOLUTION = 0.024994.
AUTOCORRELATION FUNCTION TIME RESOLUTION = 0.025. FROM 0. (SEC) TO 0.750(SEC).
ZERO-LAG AUTOCORRELATION = 0.19566102E 06

TAU	AUTOCOR	TAU	AUTOCOR	TAU	AUTOCOR	TAU	AUTOCOR	TAU	AUTOCOR
-0.	1.000000	0.0250	0.028466	0.0500	-0.253217	0.0750	-0.106804	0.1000	-0.155677
0.1250	-0.148555	0.1500	-0.038428	0.1750	0.119083	0.2000	0.084987	0.2249	-0.048439
0.2499	-0.100290	0.2749	0.008003	0.2999	0.077201	0.3249	-0.032130	0.3499	-0.055981
0.3749	-0.079950	0.3999	-0.082610	0.4249	-0.126233	0.4499	-0.169980	0.4749	0.392863
0.4999	0.576039	0.5249	0.164547	0.5499	-0.187016	0.5749	-0.204410	0.5999	-0.141706
0.6248	-0.130699	0.6498	0.045547	0.6748	0.031866	0.6998	0.083048	0.7248	-0.024052

FIGURE 20

RUN CASE HP-10

AUTOCORRELATION OF E K G . TEST NUMBER 1-45 . TAPE NUMBER BIO-03. OCT. 23,1964 PAGE

COMPUTATIONS FROM 9.(HOURS), 2620.000(SECONDS) TO 9.(HOURS), 2621.530(SECONDS) AT EVERY100 FRAMES.
NUMBER OF FRAMES = 30. NUMBER OF LAGS = 15. DATA TIME RESOLUTION = 0.049988.
AUTOCORRELATION FUNCTION TIME RESOLUTION = 0.050. FROM 0. (SEC) TO 0.750(SEC).
ZERO-LAG AUTOCORRELATION = 0.13404974E 06

TAU	AUTOCOR	TAU	AUTOCOR	TAU	AUTOCOR	TAU	AUTOCOR	TAU	AUTOCOR
-0.	1.000000	0.0500	-0.280122	0.1000	-0.197772	0.1500	0.063049	0.2000	0.020781
0.2499	-0.098656	0.2999	0.010856	0.3499	-0.014243	0.3999	-0.089782	0.4499	-0.094560
0.4999	0.451028	0.5499	-0.195851	0.5999	-0.182315	0.6498	0.139514	0.6998	0.007151

FIGURE 21

RUN CASE HP-20

AUTOCORRELATION OF E K G . TEST NUMBER 1-41 . TAPE NUMBER A-447 . OCT. 23,1964 PAGE

COMPUTATIONS FROM 9.(HOURS), 2039.000(SECONDS) TO 9.(HOURS), 2039.858(SECONDS) AT EVERY100 FRAMES.
NUMBER OF FRAMES = 17. NUMBER OF LAGS = 8. DATA TIME RESOLUTION = 0.049963.
AUTOCORRELATION FUNCTION TIME RESOLUTION = 0.050. FROM 0. (SEC) TO 0.400(SEC).
ZERO-LAG AUTOCORRELATION = 0.20219933E 06

TAU	AUTOCOR	TAU	AUTOCOR	TAU	AUTOCOR	TAU	AUTOCOR	TAU	AUTOCOR
-0.	1.000000	0.0500	0.407501	0.0999	0.399835	0.1499	-0.280797	0.1999	-0.140992
0.2498	-0.449426	0.2998	-0.029312	0.3497	-0.180606				

FIGURE 22

AUTOCORRELATION OF E K G . TEST NUMBER 1-41 . TAPE NUMBER A-447 . OCT. 23,1964 PAGE

COMPUTATIONS FROM 9.(HOURS), 2039.000(SECONDS) TO 9.(HOURS), 2040.170(SECONDS) AT EVERY 10 FRAMES.
NUMBER OF FRAMES = 234. NUMBER OF LAGS = 117. DATA TIME RESOLUTION = 0.004996.
AUTOCORRELATION FUNCTION TIME RESOLUTION = 0.005. FROM 0. (SEC) TO 0.585(SEC).
ZERO-LAG AUTOCORRELATION = 0.40947854E 07

TAU	AUTOCOR	TAU	AUTOCOR	TAU	AUTOCOR	TAU	AUTOCOR	TAU	AUTOCOR
-0.	1.000000	0.0050	0.842003	0.0100	0.526139	0.0150	0.229145	0.0200	0.013678
0.0250	-0.093867	0.0300	-0.119700	0.0350	-0.110889	0.0400	-0.080492	0.0450	-0.043422
0.0500	-0.020911	0.0550	-0.007769	0.0600	-0.014274	0.0650	-0.050538	0.0699	-0.065289
0.0749	-0.029281	0.0799	0.016296	0.0849	0.041224	0.0899	0.056646	0.0949	0.076240
0.0999	0.110047	0.1049	0.138875	0.1099	0.131319	0.1149	0.081916	0.1199	0.022733
0.1249	-0.006643	0.1299	0.018925	0.1349	0.082971	0.1399	0.135983	0.1449	0.158346
0.1499	0.168936	0.1549	0.154018	0.1599	0.129252	0.1649	0.106482	0.1699	0.062134
0.1749	-0.003749	0.1799	-0.046114	0.1849	-0.049924	0.1899	-0.044897	0.1949	-0.038770
0.1999	-0.037414	0.2048	-0.038589	0.2098	-0.034923	0.2148	-0.042357	0.2198	-0.050675
0.2248	-0.041237	0.2298	-0.029358	0.2348	-0.029031	0.2398	-0.016176	0.2448	-0.000532
0.2498	-0.014326	0.2548	-0.038641	0.2598	-0.045483	0.2648	-0.017376	0.2698	0.044731
0.2748	0.091336	0.2798	0.073688	0.2848	0.012408	0.2898	-0.041038	0.2948	-0.075161
0.2998	-0.083170	0.3048	-0.073883	0.3098	-0.072865	0.3148	-0.084259	0.3198	-0.105108
0.3248	-0.125924	0.3298	-0.124938	0.3347	-0.122491	0.3397	-0.152754	0.3447	-0.191467
0.3497	-0.220031	0.3547	-0.253208	0.3597	-0.284282	0.3647	-0.264944	0.3697	-0.152246
0.3747	0.051025	0.3797	0.304845	0.3847	0.517396	✓0.3897	0.600239	0.3947	0.514724
0.3997	0.288176	0.4047	0.031837	0.4097	-0.154513	0.4147	-0.237030	0.4197	-0.234161
0.4247	-0.201278	0.4297	-0.173287	0.4347	-0.158854	0.4397	-0.153008	0.4447	-0.169739
0.4497	-0.213917	0.4547	-0.258785	0.4597	-0.283621	0.4647	-0.273941	0.4696	-0.221460
0.4746	-0.146748	0.4796	-0.075432	0.4846	-0.024320	0.4896	0.009485	0.4946	0.048544
0.4996	0.094685	0.5046	0.110222	0.5096	0.090165	0.5146	0.070877	0.5196	0.078054
0.5246	0.091209	0.5296	0.093332	0.5346	0.080740	0.5396	0.051748	0.5446	0.002267
0.5496	-0.069018	0.5546	-0.129423	0.5596	-0.149155	0.5646	-0.145713	0.5696	-0.136220
0.5746	-0.117905	0.5796	-0.080325						

FIGURE 23

RUN CASE HP-22

AUTOCORRELATION OF E K G . TEST NUMBER 1-41 . TAPE NUMBER A-447 . OCT. 23,1964 PAGE

COMPUTATIONS FROM 9.(HOURS), 2039.000(SECONDS) TO 9.(HOURS), 2040.170(SECONDS) AT EVERY 20 FRAMES.
NUMBER OF FRAMES = 117. NUMBER OF LAGS = 58. DATA TIME RESOLUTION = 0.009993.
AUTOCORRELATION FUNCTION TIME RESOLUTION = 0.010. FROM 0. (SEC) TO 0.580(SEC).
ZERO-LAG AUTOCORRELATION = 0.20344125E 07

TAU	AUTOCOR	TAU	AUTOCOR	TAU	AUTOCOR	TAU	AUTOCOR	TAU	AUTOCOR
-0.	1.000000	0.0100	0.521767	0.0200	0.008817	0.0300	-0.089186	0.0400	-0.072558
0.0500	-0.011840	0.0600	-0.008686	0.0699	-0.036271	0.0799	0.026089	0.0899	0.053919
0.0999	0.110863	0.1099	0.152601	0.1199	0.007666	0.1299	0.017733	0.1399	0.133185
0.1499	0.156033	0.1599	0.130076	0.1699	0.093007	0.1799	-0.044739	0.1899	-0.057936
0.1999	-0.027894	0.2098	-0.044974	0.2198	-0.038759	0.2298	-0.040817	0.2398	-0.041315
0.2498	-0.032060	0.2598	-0.057831	0.2698	0.039400	0.2798	0.116809	0.2898	-0.028765
0.2998	-0.079702	0.3098	-0.070784	0.3198	-0.110808	0.3298	-0.140390	0.3397	-0.156667
0.3497	-0.215874	0.3597	-0.291939	0.3697	-0.167896	0.3797	0.293445	0.3897	0.596375
0.3997	0.276463	0.4097	-0.146787	0.4197	-0.234061	0.4297	-0.170526	0.4397	-0.159773
0.4497	-0.188822	0.4597	-0.265144	0.4696	-0.226746	0.4796	-0.084938	0.4896	0.023881
0.4996	0.094464	0.5096	0.087734	0.5196	0.082416	0.5296	0.080877	0.5396	0.043475
0.5496	-0.064717	0.5596	-0.137289	0.5696	-0.122080				

FIGURE 24

RUN CASE HP-23

AUTOCORRELATION OF E K G . TEST NUMBER 1-41 . TAPE NUMBER A-447 . OCT. 23,1964 PAGE

COMPUTATIONS FROM 9.(HOURS), 2039.000(SECONDS) TO 9.(HOURS), 2040.170(SECONDS) AT EVERY 30 FRAMES.
NUMBER OF FRAMES = 78. NUMBER OF LAGS = 39. DATA TIME RESOLUTION = 0.014989.
AUTOCORRELATION FUNCTION TIME RESOLUTION = 0.015. FROM 0. (SEC) TO 0.585(SEC).
ZERO-LAG AUTOCORRELATION = 0.13279397E 07

TAU	AUTOCOR	TAU	AUTOCOR	TAU	AUTOCOR	TAU	AUTOCOR	TAU	AUTOCOR
-0.	1.000000	0.0150	0.316434	0.0300	-0.061922	0.0450	0.004733	0.0600	-0.028975
0.0749	-0.024503	0.0899	0.081695	0.1049	0.141661	0.1199	0.012790	0.1349	0.139605
0.1499	0.240495	0.1649	0.166516	0.1799	-0.022299	0.1949	0.026296	0.2098	-0.083385
0.2248	-0.070503	0.2398	0.021471	0.2548	-0.076954	0.2698	-0.020081	0.2848	-0.015534
0.2998	-0.056178	0.3148	-0.130578	0.3298	-0.159069	0.3447	-0.204692	0.3597	-0.303917
0.3747	0.084432	0.3897	0.571124	0.4047	0.067875	0.4197	-0.326878	0.4347	-0.215238
0.4497	-0.266594	0.4647	-0.298265	0.4796	-0.107285	0.4946	0.040335	0.5096	0.073657
0.5246	0.068685	0.5396	0.057452	0.5546	-0.093954	0.5696	-0.101769		

FIGURE 25

RUN CASE HP-24

AUTOCORRELATION OF E K G . TEST NUMBER 1-41 . TAPE NUMBER A-447 . OCT. 23,1964 PAGE

COMPUTATIONS FROM 9.(HOURS), 2039.000(SECONDS) TO 9.(HOURS), 2040.170(SECONDS) AT EVERY 50 FRAMES.
NUMBER OF FRAMES = 46. NUMBER OF LAGS = 23. DATA TIME RESOLUTION = 0.024981.
AUTOCORRELATION FUNCTION TIME RESOLUTION = 0.025. FROM 0. (SEC) TO 0.575(SEC).
ZERO-LAG AUTOCORRELATION = 0.88338723E 06

TAU	AUTOCOR	TAU	AUTOCOR	TAU	AUTOCOR	TAU	AUTOCOR	TAU	AUTOCOR
-0.	1.000000	0.0250	-0.006989	0.0500	0.069629	0.0749	-0.017896	0.0999	0.082525
0.1249	0.011949	0.1499	0.254878	0.1749	-0.012017	0.1999	-0.097329	0.2248	-0.005080
0.2498	0.082472	0.2748	0.105102	0.2998	-0.088220	0.3248	-0.210299	0.3497	-0.237981
0.3747	-0.027328	0.3997	0.443795	0.4247	-0.285397	0.4497	-0.309236	0.4746	-0.238226
0.4996	0.092832	0.5246	0.015769	0.5496	0.018023				

FIGURE 26

RUN CASE HP-25

AUTOCORRELATION OF E K G . TEST NUMBER 1-41 . TAPE NUMBER A-447 . OCT. 23,1964 PAGE

COMPUTATIONS FROM 9.(HOURS), 2039.000(SECONDS) TO 9.(HOURS), 2040.170(SECONDS) AT EVERY100 FRAMES.
NUMBER OF FRAMES = 23. NUMBER OF LAGS = 11. DATA TIME RESOLUTION = 0.049963.
AUTOCORRELATION FUNCTION TIME RESOLUTION = 0.050. FROM 0. (SEC) TO 0.550(SEC).
ZERO-LAG AUTOCORRELATION = 0.25361706E 06

TAU	AUTOCOR	TAU	AUTOCOR	TAU	AUTOCOR	TAU	AUTOCOR	TAU	AUTOCOR
-0.	1.000000	0.0500	0.217018	0.0999	0.410609	0.1499	-0.266079	0.1999	0.006232
0.2498	-0.594688	0.2998	0.120926	0.3497	-0.253878	0.3997	0.364143	0.4497	-0.143256
0.4996	0.413257								

FIGURE 27

RUN CASE HP-33

AUTOCORRELATION OF E K G . TEST NUMBER 1-48 . TAPE NUMBER A-153 . OCT. 23,1964 PAGE

COMPUTATIONS FROM 10.(HOURS), 911.000(SECONDS) TO 10.(HOURS), 911.957(SECONDS) AT EVERY 30 FRAMES.
NUMBER OF FRAMES = 63. NUMBER OF LAGS = 31. DATA TIME RESOLUTION = 0.015011.
AUTOCORRELATION FUNCTION TIME RESOLUTION = 0.015. FROM 0. (SEC) TO 0.465(SEC).
ZERO-LAG AUTOCORRELATION = 0.503412306 06

TAU	AUTOCOR	TAU	AUTOCOR	TAU	AUTOCOR	TAU	AUTOCOR	TAU	AUTOCOR
-0.	1.000000	0.0150	0.009295	0.0300	0.026919	0.0450	0.155903	0.0600	-0.257183
0.0751	-0.093547	0.0901	-0.015224	0.1051	-0.264540	0.1201	-0.065227	0.1351	0.092649
0.1501	-0.083653	0.1651	0.052709	0.1801	0.098017	0.1951	-0.261574	0.2102	0.325992
0.2252	-0.052816	0.2402	0.120854	0.2552	0.425820	0.2702	-0.229118	0.2852	0.196501
0.3002	0.148121	0.3152	-0.254083	0.3302	-0.067055	0.3453	-0.196138	0.3603	-0.093069
0.3753	-0.205819	0.3903	0.152028	0.4053	-0.084954	0.4203	-0.015513	0.4353	0.529559
0.4503	0.082258								

FIGURE 28

RUN CASE HP-35

AUTOCORRELATION OF E K G . TEST NUMBER 1-48 . TAPE NUMBER A-153 . OCT. 23,1964 PAGE

COMPUTATIONS FROM 10.(HOURS), 911.000(SECONDS) TO 10.(HOURS), 911.957(SECONDS) AT EVERY100 FRAMES.
NUMBER OF FRAMES = 19. NUMBER OF LAGS = 9. DATA TIME RESOLUTION = 0.050038.
AUTOCORRELATION FUNCTION TIME RESOLUTION = 0.050. FROM 0. (SEC) TO 0.450(SEC).
ZERO-LAG AUTOCORRELATION = 0.99247999E 05

TAU	AUTOCOR	TAU	AUTOCOR	TAU	AUTOCOR	TAU	AUTOCOR	TAU	AUTOCOR
-0.	1.000000	0.0500	-0.196870	0.1001	-0.099156	0.1501	-0.209979	0.2002	0.164215
0.2502	-0.195621	0.3002	-0.186392	0.3503	0.299311	0.4003	-0.517814		

FIGURE 29

RUN CASE HP-36

AUTOCORRELATION OF E K G . TEST NUMBER 1-48 . TAPE NUMBER A-153 . OCT. 23,1964 PAGE

COMPUTATIONS FROM 10.(HOURS), 911.000(SECONDS) TO 10.(HOURS), 912.305(SECONDS) AT EVERY 10 FRAMES.
NUMBER OF FRAMES = 261. NUMBER OF LAGS = 130. DATA TIME RESOLUTION = 0.005004.
AUTOCORRELATION FUNCTION TIME RESOLUTION = 0.005. FROM 0. (SEC) TO 0.650(SEC).
ZERO-LAG AUTOCORRELATION = 0.19151508E 07

TAU	AUTOCOR	TAU	AUTOCOR	TAU	AUTOCOR	TAU	AUTOCOR	TAU	AUTOCOR
-0.	1.000000	0.0050	0.535511	0.0100	0.052160	0.0150	0.044039	0.0200	0.084408
0.0250	0.100152	0.0300	0.074381	0.0350	-0.011437	0.0400	0.080124	0.0450	0.144134
0.0500	-0.055889	0.0550	-0.195931	0.0600	-0.179245	0.0650	-0.127268	0.0701	-0.046124
0.0751	0.004092	0.0801	-0.000570	0.0851	0.070118	0.0901	0.082027	0.0951	-0.019560
0.1001	-0.023277	0.1051	-0.014839	0.1101	-0.040465	0.1151	-0.013001	0.1201	0.008084
0.1251	0.036462	0.1301	0.060109	0.1351	0.018954	0.1401	0.080686	0.1451	0.187733
0.1501	0.056968	0.1551	-0.082801	0.1601	-0.087640	0.1651	-0.036942	0.1701	0.034943
0.1751	0.095350	0.1801	0.070693	0.1851	0.066023	0.1901	0.032036	0.1951	-0.063336
0.2002	-0.057014	0.2052	-0.027200	0.2102	-0.074461	0.2152	-0.037412	0.2202	0.001406
0.2252	0.015579	0.2302	0.028986	0.2352	0.015714	0.2402	-0.036184	0.2452	-0.015920
0.2502	0.073766	0.2552	0.161579	0.2602	0.157596	0.2652	0.082733	0.2702	0.067231
0.2752	0.073186	0.2802	0.090169	0.2852	0.095680	0.2902	0.020611	0.2952	-0.071429
0.3002	0.000612	0.3052	0.015008	0.3102	-0.151724	0.3152	-0.162488	0.3202	-0.057533
0.3252	-0.061746	0.3302	-0.048669	0.3353	-0.139554	0.3403	-0.286249	0.3453	-0.148531
0.3503	0.063101	0.3553	0.015115	0.3603	-0.058561	0.3653	-0.104241	0.3703	-0.083221
0.3753	-0.023504	0.3803	-0.064540	0.3853	-0.079950	0.3903	0.071972	0.3953	0.075511
0.4003	-0.052125	0.4053	-0.041975	0.4103	0.058061	0.4153	0.099991	0.4203	0.093469
0.4253	0.138546	0.4303	0.293153	0.4353	0.410499	0.4403	0.277420	0.4453	0.119664
0.4503	0.099815	0.4553	-0.019992	0.4603	-0.031235	0.4653	0.092614	0.4704	0.066652
0.4754	-0.004239	0.4804	-0.082213	0.4854	-0.172459	0.4904	-0.123370	0.4954	-0.057496
0.5004	-0.129923	0.5054	-0.160192	0.5104	-0.144937	0.5154	-0.087222	0.5204	-0.029274
0.5254	-0.073047	0.5304	-0.135093	0.5354	-0.052626	0.5404	0.006076	0.5454	-0.122676
0.5504	-0.121808	0.5554	0.041182	0.5604	0.058089	0.5654	-0.009709	0.5704	-0.015363
0.5754	0.031507	0.5804	0.067787	0.5854	-0.013439	0.5904	-0.176757	0.5954	-0.180091
0.6005	-0.061360	0.6055	0.020405	0.6105	0.017929	0.6155	-0.041951	0.6205	-0.108990
0.6255	-0.164503	0.6305	-0.118715	0.6355	-0.058958	0.6405	-0.032381	0.6455	-0.009025

FIGURE 30

RUN CASE HP-37

AUTOCORRELATION OF E K G . TEST NUMBER 1-48 . TAPE NUMBER A-153 . OCT. 23,1964 PAGE

COMPUTATIONS FROM 10.(HOURS), 911.000(SECONDS) TO 10.(HOURS), 912.305(SECONDS) AT EVERY 20 FRAMES.
NUMBER OF FRAMES = 130. NUMBER OF LAGS = 65. DATA TIME RESOLUTION = 0.010008.
AUTOCORRELATION FUNCTION TIME RESOLUTION = 0.010. FROM 0. (SEC) TO 0.650(SEC).
ZERO-LAG AUTOCORRELATION = 0.90819484E 06

TAU	AUTOCOR	TAU	AUTOCOR	TAU	AUTOCOR	TAU	AUTOCOR	TAU	AUTOCOR
-0.	1.000000	0.0100	0.051064	0.0200	0.033316	0.0300	0.110968	0.0400	0.092092
0.0500	-0.035188	0.0600	-0.097167	0.0701	-0.156242	0.0801	0.064900	0.0901	0.094957
0.1001	-0.105103	0.1101	-0.058190	0.1201	-0.030692	0.1301	0.070340	0.1401	0.140805
0.1501	0.014465	0.1601	-0.097232	0.1701	0.058983	0.1801	0.143391	0.1901	0.000974
0.2002	-0.133066	0.2102	-0.009218	0.2202	-0.006991	0.2302	0.053851	0.2402	-0.096175
0.2502	0.074866	0.2602	0.272429	0.2702	0.011234	0.2802	0.060151	0.2902	0.003774
0.3002	-0.008115	0.3102	-0.148040	0.3202	-0.105962	0.3302	-0.053228	0.3403	-0.287264
0.3503	0.023879	0.3603	-0.010931	0.3703	-0.126081	0.3803	-0.078970	0.3903	0.122859
0.4003	-0.069678	0.4103	0.117258	0.4203	0.064985	0.4303	0.312981	0.4403	0.289955
0.4503	0.089411	0.4603	-0.008440	0.4704	-0.000413	0.4804	-0.041614	0.4904	-0.125857
0.5004	-0.097769	0.5104	-0.133011	0.5204	0.035051	0.5304	-0.168957	0.5404	-0.004049
0.5504	-0.167348	0.5604	-0.007797	0.5704	-0.055978	0.5804	0.122828	0.5904	-0.185925
0.6005	-0.074560	0.6105	0.066926	0.6205	-0.065058	0.6305	-0.137303	0.6405	-0.000759

FIGURE 31

RUN CASE HP-38

AUTOCORRELATION OF E K G . TEST NUMBER 1-48 . TAPE NUMBER A-153 . OCT. 23,1964 PAGE

COMPUTATIONS FROM 10.(HOURS), 911.000(SECONDS) TO 10.(HOURS), 912.305(SECONDS) AT EVERY 30 FRAMES.
NUMBER OF FRAMES = 87. NUMBER OF LAGS = 43. DATA TIME RESOLUTION = 0.015011.
AUTOCORRELATION FUNCTION TIME RESOLUTION = 0.015. FROM 0. (SEC) TO 0.645(SEC).
ZERO-LAG AUTOCORRELATION = 0.6544377CE 06

TAU	AUTOCOR	TAU	AUTOCOR	TAU	AUTOCOR	TAU	AUTOCOR	TAU	AUTOCOR
-0.	1.000000	0.0150	-0.060711	0.0300	0.040157	0.0450	0.215702	0.0600	-0.259540
0.0751	0.014540	0.0901	-0.045895	0.1051	-0.210695	0.1201	-0.070880	0.1351	0.082273
0.1501	0.032755	0.1651	-0.122192	0.1801	0.144495	0.1951	-0.096520	0.2102	0.176377
0.2252	0.072467	0.2402	0.113702	0.2552	0.387998	0.2702	-0.240844	0.2852	0.171539
0.3002	0.110333	0.3152	-0.254296	0.3302	-0.023050	0.3453	-0.244732	0.3603	-0.078637
0.3753	-0.144002	0.3903	0.136050	0.4053	-0.073933	0.4203	-0.064086	0.4353	0.479550
0.4503	0.039397	0.4653	0.042214	0.4804	-0.000459	0.4954	-0.042100	0.5104	-0.085883
0.5254	-0.085609	0.5404	0.005004	0.5554	-0.076697	0.5704	0.000243	0.5854	-0.055254
0.6005	-0.172642	0.6155	0.194302	0.6305	-0.113286				

FIGURE 32

RUN CASE HP-39

AUTOCORRELATION OF E K G . TEST NUMBER 1-48 . TAPE NUMBER A-153 . OCT. 23,1964 PAGE

COMPUTATIONS FROM 10.(HOURS), 911.000(SECONDS) TO 10.(HOURS), 912.305(SECONDS) AT EVERY 50 FRAMES.
NUMBER OF FRAMES = 52. NUMBER OF LAGS = 26. DATA TIME RESOLUTION = 0.025019.
AUTOCORRELATION FUNCTION TIME RESOLUTION = 0.025. FROM 0. (SEC) TO 0.650(SEC).
ZERO-LAG AUTOCORRELATION = 0.34993771E 06

TAU	AUTOCOR	TAU	AUTOCOR	TAU	AUTOCOR	TAU	AUTOCOR	TAU	AUTOCOR
-0.	1.000000	0.0250	0.130375	0.0500	-0.296917	0.0751	-0.058576	0.1001	0.084154
0.1251	-0.117756	0.1501	-0.082188	0.1751	-0.091189	0.2002	-0.025276	0.2252	0.044420
0.2502	0.093491	0.2752	0.072969	0.3002	-0.294681	0.3252	-0.104224	0.3503	0.247222
0.3753	-0.174721	0.4003	0.020525	0.4253	0.469428	0.4503	0.085017	0.4754	-0.052506
0.5004	-0.210302	0.5254	-0.010396	0.5504	-0.142292	0.5754	-0.139575	0.6005	-0.069741
0.6255	0.193784								

FIGURE 33

RUN CASE HP-39

INDEPENDENT VARIABLE---TAU (SECONDS)
VALUE = A*SCALE + B , A = 10**-1 B = 0.

DEPENDENT VARIABLE-----NORMALIZED AUTOCORRELATION FUNCTION
VALUE = A*SCALE + B , A = 10** 0 B = -0.4000E-00.

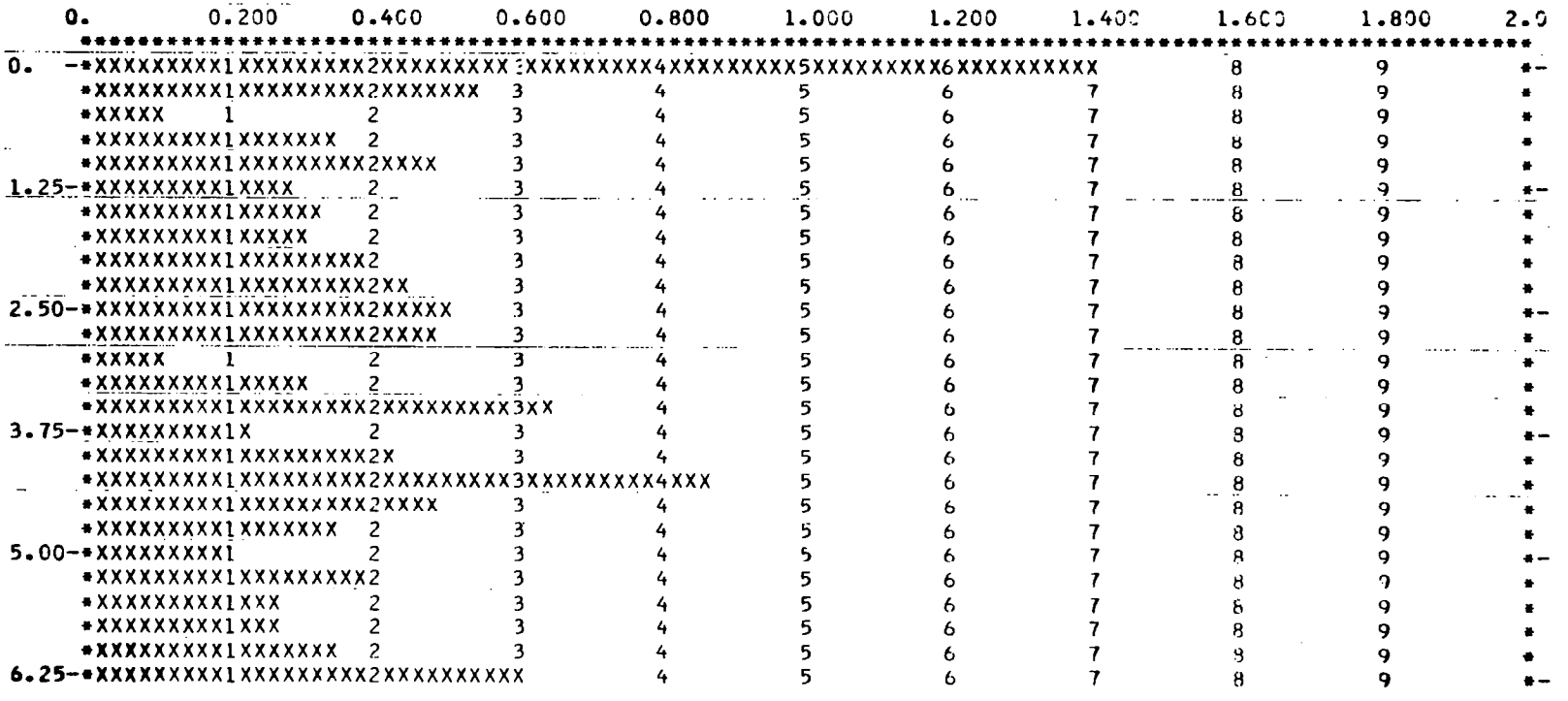

FIGURE 34

RUN CASE HP-40

AUTOCORRELATION OF E K G . TEST NUMBER 1-48 . TAPE NUMBER A-153 . OCT. 23,1964 PAGE

COMPUTATIONS FROM 10.(HOURS), 911.000(SECONDS) TO 10.(HOURS), 912.305(SECONDS) AT EVERY100 FRAMES.
NUMBER OF FRAMES = 26. NUMBER OF LAGS = 13. DATA TIME RESOLUTION = 0.050038.
AUTOCORRELATION FUNCTION TIME RESOLUTION = 0.050. FROM 0. (SEC) TO 0.650(SEC).
ZERO-LAG AUTOCORRELATION = 0.11170463E 06

TAU	AUTOCOR	TAU	AUTOCOR	TAU	AUTOCOR	TAU	AUTOCOR	TAU	AUTOCOR
-0.	1.000000	0.0500	-0.114041	0.1001	-0.133894	0.1501	-0.228569	0.2002	0.098428
0.2502	-0.077173	0.3002	-0.141438	0.3503	0.251153	0.4003	-0.402984	0.4503	0.598011
0.5004	0.012982	0.5504	0.229939	0.6005	-0.976042				

FIGURE 35

RUN CASE HP-45

AUTOCORRELATION OF E K G . TEST NUMBER 1-48 . TAPE NUMBER A-153 . OCT. 23,1964 PAGE

COMPUTATIONS FROM 10.(HOURS), 911.000(SECONDS) TO 10.(HOURS), 912.914(SECONDS) AT EVERY100 FRAMES.
NUMBER OF FRAMES = 38. NUMBER OF LAGS = 19. DATA TIME RESOLUTION = 0.050038.
AUTOCORRELATION FUNCTION TIME RESOLUTION = 0.050. FROM 0. (SEC) TO 0.951(SEC).
ZERO-LAG AUTOCORRELATION = 0.26975431E 06

TAU	AUTOCOR	TAU	AUTOCOR	TAU	AUTOCOR	TAU	AUTOCOR	TAU	AUTOCOR
-0.	1.000000	0.0500	-0.328205	0.1001	-0.177349	0.1501	-0.006001	0.2002	0.215353
0.2502	-0.263954	0.3002	-0.043157	0.3503	0.168802	0.4003	-0.028030	0.4503	0.008027
0.5004	-0.018335	0.5504	0.270854	0.6005	-0.276117	0.6505	0.098945	0.7005	-0.201082
0.7506	-0.002212	0.8006	-0.012590	0.8506	0.437714	0.9007	-0.132843		

FIGURE 36

RUN CASE BP-2

AUTOCORRELATION OF O K G . TEST NUMBER 1-48 F. TAPE NUMBER BIO-06. NOV. 11,1964 PAGE

COMPUTATIONS FROM 10.(HOURS), 911.000(SECONDS) TO 10.(HOURS), 912.000(SECONDS) AT EVERY 1 FRAMES.
NUMBER OF FRAMES = 401. NUMBER OF LAGS = 200. DATA TIME RESOLUTION = 0.002502.
AUTOCORRELATION FUNCTION TIME RESOLUTION = 0.003. FROM 0. (SEC) TO 0.500(SEC).
ZERO-LAG AUTOCORRELATION = 0.25103329E 07

TAU	AUTOCOR	TAU	AUTOCOR	TAU	AUTOCOR	TAU	AUTOCOR	TAU	AUTOCOR
-0.	1.000000	0.0025	0.947828	0.0050	0.800239	0.0075	0.589907	0.0100	0.361390
0.0125	0.158458	0.0150	0.012723	0.0175	-0.062986	0.0200	-0.074827	0.0225	-0.042496
0.0250	0.009176	0.0275	0.058404	0.0300	0.091730	0.0325	0.105268	0.0350	0.102354
0.0375	0.089228	0.0400	0.070808	0.0425	0.048308	0.0450	0.019319	0.0475	-0.020047
0.0500	-0.072090	0.0526	-0.135021	0.0551	-0.202140	0.0576	-0.262928	0.0601	-0.305663
0.0626	-0.320746	0.0651	-0.303619	0.0676	-0.256226	0.0701	-0.187082	0.0726	-0.108917
0.0751	-0.035528	0.0776	0.021604	0.0801	0.055890	0.0826	0.066608	0.0851	0.058128
0.0876	0.037712	0.0901	0.012754	0.0926	-0.011367	0.0951	-0.032115	0.0976	-0.049217
0.1001	-0.063146	0.1026	-0.073576	0.1051	-0.078745	0.1076	-0.076099	0.1101	-0.063890
0.1126	-0.042781	0.1151	-0.016485	0.1176	0.009099	0.1201	0.028024	0.1226	0.036735
0.1251	0.035812	0.1276	0.029954	0.1301	0.025936	0.1326	0.029457	0.1351	0.042221
0.1376	0.060655	0.1401	0.076984	0.1426	0.082252	0.1451	0.073052	0.1476	0.039366
0.1501	-0.004690	0.1526	-0.052488	0.1552	-0.093171	0.1577	-0.118147	0.1602	-0.123337
0.1627	-0.109457	0.1652	-0.080573	0.1677	-0.042001	0.1702	0.001496	0.1727	0.045991
0.1752	0.087826	0.1777	0.122643	0.1802	0.145018	0.1827	0.149365	0.1852	0.131934
0.1877	0.093018	0.1902	0.038128	0.1927	-0.022774	0.1952	-0.077931	0.1977	-0.117503
0.2002	-0.136798	0.2027	-0.137498	0.2052	-0.126234	0.2077	-0.111315	0.2102	-0.098868
0.2127	-0.090308	0.2152	-0.082366	0.2177	-0.069612	0.2202	-0.048264	0.2227	-0.019379
0.2252	0.010323	0.2277	0.030612	0.2302	0.032050	0.2327	0.019700	0.2352	-0.028888
0.2377	-0.073980	0.2402	-0.107504	0.2427	-0.114108	0.2452	-0.086034	0.2477	-0.026451
0.2502	0.051218	0.2527	0.127699	0.2552	0.184392	0.2578	0.209549	0.2603	0.201728
0.2628	0.169431	0.2653	0.127219	0.2678	0.090034	0.2703	0.067918	0.2728	0.063246
0.2753	0.071148	0.2778	0.082670	0.2803	0.089098	0.2828	0.085469	0.2853	0.071863
0.2878	0.052182	0.2903	0.031309	0.2928	0.012227	0.2953	-0.005478	0.2978	-0.025052
0.3003	-0.050273	0.3028	-0.082597	0.3053	-0.119241	0.3078	-0.153264	0.3103	-0.175834
0.3128	-0.179935	0.3153	-0.163908	0.3178	-0.133212	0.3203	-0.099368	0.3228	-0.076319
0.3253	-0.075529	0.3278	-0.101574	0.3303	-0.149955	0.3328	-0.208126	0.3353	-0.259409
0.3378	-0.288318	0.3403	-0.285420	0.3428	-0.250043	0.3453	-0.190092	0.3478	-0.119298
0.3503	-0.052992	0.3528	-0.003949	0.3553	0.020406	0.3578	0.018889	0.3604	-0.004314
0.3629	-0.041545	0.3654	-0.083740	0.3679	-0.122113	0.3704	-0.149272	0.3729	-0.160202
0.3754	-0.152712	0.3779	-0.127913	0.3804	-0.090294	0.3829	-0.047032	0.3854	-0.006523
0.3879	0.023705	0.3904	0.039084	0.3929	0.039289	0.3954	0.028188	0.3979	0.012429
0.4004	-0.000791	0.4029	-0.006014	0.4054	-0.000925	0.4079	0.013656	0.4104	0.035087
0.4129	0.060853	0.4154	0.090202	0.4179	0.124740	0.4204	0.167673	0.4229	0.221930
0.4254	0.287917	0.4279	0.361714	0.4304	0.434546	0.4329	0.493864	0.4354	0.526057
0.4379	0.520102	0.4404	0.471054	0.4429	0.382423	0.4454	0.266602	0.4479	0.142903

FIGURE 37 (1 of 2)

RUN CASE BP-2

AUTOCORRELATION OF O K G . TEST NUMBER 1-48 F. TAPE NUMBER BIO-06. NOV. 11,1964 PAGE

COMPUTATIONS FROM 10.(HOURS), 911.000(SECONDS) TO 10.(HOURS), 912.000(SECONDS) AT EVERY 1 FRAMES.
NUMBER OF FRAMES = 401. NUMBER OF LAGS = 200. DATA TIME RESOLUTION = 0.002502.
AUTOCORRELATION FUNCTION TIME RESOLUTION = 0.003. FROM 0. (SEC) TO 0.500(SEC).
ZERO-LAG AUTOCORRELATION = 0.25103329E 07

TAU	AUTOCOR	TAU	AUTOCOR	TAU	AUTOCOR	TAU	AUTOCOR	TAU	AUTOCOR
0.4504	0.033496	0.4529	-0.042010	0.4554	-0.071966	0.4579	-0.056354	0.4604	-0.007335
0.4630	0.053878	0.4655	0.103219	0.4680	0.121051	0.4705	0.098522	0.4730	0.040174
0.4755	-0.037812	0.4780	-0.113475	0.4805	-0.167057	0.4830	-0.188110	0.4855	-0.178868
0.4880	-0.152642	0.4905	-0.127886	0.4930	-0.120280	0.4955	-0.136183	0.4980	-0.170259

FIGURE 37 (2 of 2)

RUN CASE BP-4

AUTOCORRELATION OF O K G . TEST NUMBER 1-48 F. TAPE NUMBER BIO-57. NOV. 11,1964 PAGE

COMPUTATIONS FROM 10.(HOURS), 911.003(SECONDS) TO 10.(HOURS), 912.000(SECONDS) AT EVERY 1 FRAMES.
NUMBER OF FRAMES = 201. NUMBER OF LAGS = 100. DATA TIME RESOLUTION = 0.005005.
AUTOCORRELATION FUNCTION TIME RESOLUTION = 0.005. FROM 0. (SEC) TO 0.500(SEC).
ZERO-LAG AUTOCORRELATION = 0.75734331E 06

TAU	AUTOCOR	TAU	AUTOCOR	TAU	AUTOCOR	TAU	AUTOCOR	TAU	AUTOCOR
-0.	1.000000	0.0050	0.934493	0.0100	0.761822	0.0150	0.529853	0.0200	0.297062
0.0250	0.111239	0.0300	-0.005862	0.0350	-0.062018	0.0400	-0.085535	0.0450	-0.108501
0.0500	-0.150362	0.0551	-0.209399	0.0601	-0.265553	0.0651	-0.292361	0.0701	-0.271738
0.0751	-0.204286	0.0801	-0.110414	0.0851	-0.021829	0.0901	0.032586	0.0951	0.039687
0.1001	0.087537	0.1051	-0.039071	0.1101	-0.070675	0.1151	-0.066983	0.1201	-0.026145
0.1251	0.034675	0.1301	0.087610	0.1351	0.107371	0.1401	0.083264	0.1451	0.024409
0.1501	-0.044107	0.1552	-0.092228	0.1602	-0.098107	0.1652	-0.058043	0.1702	0.012905
0.1752	0.085850	0.1802	0.130718	0.1852	0.128370	0.1902	0.077671	0.1952	-0.005084
0.2002	-0.093516	0.2052	-0.161755	0.2102	-0.193471	0.2152	-0.186355	0.2202	-0.150320
0.2252	-0.101124	0.2302	-0.052672	0.2352	-0.011651	0.2402	0.023268	0.2452	0.057950
0.2502	0.097440	0.2552	0.141728	0.2603	0.184604	0.2653	0.215800	0.2703	0.225145
0.2753	0.206765	0.2803	0.161502	0.2853	0.096560	0.2903	0.022732	0.2953	-0.049356
0.3003	-0.112278	0.3053	-0.162993	0.3103	-0.202093	0.3153	-0.231891	0.3203	-0.254427
0.3253	-0.270126	0.3303	-0.277932	0.3353	-0.276024	0.3403	-0.263180	0.3453	-0.239730
0.3503	-0.207863	0.3553	-0.171309	0.3604	-0.134678	0.3654	-0.103053	0.3704	-0.080291
0.3754	-0.069407	0.3804	-0.070737	0.3854	-0.080470	0.3904	-0.089786	0.3954	-0.085630
0.4004	-0.053792	0.4054	0.016121	0.4104	0.125658	0.4154	0.264425	0.4204	0.410765
0.4254	0.536413	0.4304	0.614060	0.4354	0.625679	0.4404	0.568606	0.4454	0.456696
0.4504	0.315637	0.4554	0.174230	0.4604	0.055237	0.4655	-0.030642	0.4705	-0.085739
0.4755	-0.121575	0.4805	-0.152026	0.4855	-0.186487	0.4905	-0.226060	0.4955	-0.264304

FIGURE 38

RUN CASE BP-6

AUTOCORRELATION OF O K G . TEST NUMBER 1-48 F. TAPE NUMBER BIO-07. NOV. 11,1964 PAGE

COMPUTATIONS FROM 10.(HOURS), 911.003(SECONDS) TO 10.(HOURS), 912.000(SECONDS) AT EVERY 2 FRAMES.
NUMBER OF FRAMES = 100. NUMBER OF LAGS = 50. DATA TIME RESOLUTION = 0.010010.
AUTOCORRELATION FUNCTION TIME RESOLUTION = 0.010. FROM 0. (SEC) TO 0.500(SEC).
ZERO-LAG AUTOCORRELATION = 0.37772671E 06

TAU	AUTOCOR	TAU	AUTOCOR	TAU	AUTOCOR	TAU	AUTOCOR	TAU	AUTOCOR
-0.	1.000000	0.0100	0.764679	0.0200	0.300630	0.0300	-0.003726	0.0400	-0.085231
0.0500	-0.150786	0.0601	-0.266461	0.0701	-0.273687	0.0801	-0.113586	0.0901	0.029491
0.1001	0.005756	0.1101	-0.071513	0.1201	-0.027074	0.1301	0.086319	0.1401	0.082310
0.1501	-0.044408	0.1602	-0.098630	0.1702	0.011020	0.1802	0.127780	0.1902	0.075286
0.2002	-0.095111	0.2102	-0.196362	0.2202	-0.155674	0.2302	-0.058185	0.2402	0.019204
0.2502	0.093474	0.2603	0.180545	0.2703	0.224939	0.2803	0.168945	0.2903	0.034410
0.3003	-0.104996	0.3103	-0.203736	0.3203	-0.261015	0.3303	-0.283372	0.3403	-0.266663
0.3503	-0.212034	0.3604	-0.139333	0.3704	-0.082623	0.3804	-0.071137	0.3904	-0.091168
0.4004	-0.056789	0.4104	0.124151	0.4204	0.412827	0.4304	0.616844	0.4404	0.569680
0.4504	0.316426	0.4604	0.058171	0.4705	-0.081334	0.4805	-0.148971	0.4905	-0.225279

FIGURE 39

RUN CASE BP-8

AUTOCORRELATION OF O K G . TEST NUMBER I-48 F. TAPE NUMBER BIO-07. NOV. 11,1964 PAGE

COMPUTATIONS FROM 10.(HOURS), 911.003(SECONDS) TO 10.(HOURS), 912.000(SECONDS) AT EVERY 4 FRAMES.
NUMBER OF FRAMES = 50. NUMBER OF LAGS = 25. DATA TIME RESOLUTION = 0.020020.
AUTOCORRELATION FUNCTION TIME RESOLUTION = 0.020. FROM 0. (SEC) TO 0.500(SEC).
ZERO-LAG AUTOCORRELATION = 0.19005774E 06

TAU	AUTOCOR	TAU	AUTOCOR	TAU	AUTOCOR	TAU	AUTOCOR	TAU	AUTOCOR
-0.	1.000000	0.0200	0.295877	0.0400	-0.074945	0.0601	-0.268726	0.0801	-0.114392
0.1001	0.001776	0.1201	-0.028659	0.1401	0.092660	0.1602	-0.134016	0.1802	0.134401
0.2002	-0.110352	0.2202	-0.153933	0.2402	0.006257	0.2603	0.184212	0.2803	0.170068
0.3003	-0.086219	0.3203	-0.263449	0.3403	-0.273972	0.3604	-0.140784	0.3804	-0.080345
0.4004	-0.054670	0.4204	0.408937	0.4404	0.571855	0.4604	0.059748	0.4805	-0.142796

FIGURE 40

RUN CASE BP-8

INDEPENDENT VARIABLE---TAU (SECONDS)
VALUE = A*SCALE + B , A = 10**-1 B = 0.

DEPENDENT VARIABLE-----NORMALIZED AUTOCORRELATION FUNCTION
VALUE = A*SCALE + B , A = 10** C B = -0.4000E-00.

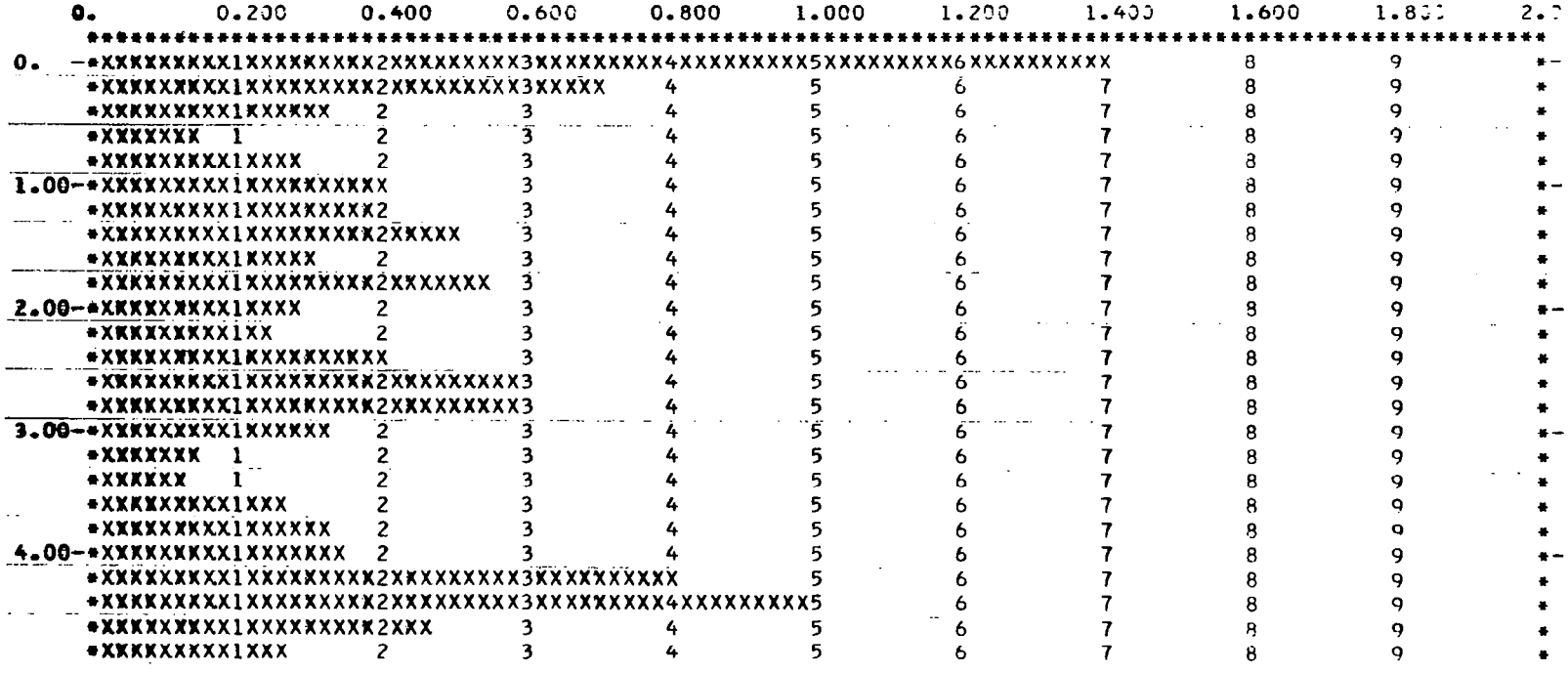

FIGURE 41

RUN CASE BP-12

AUTOCORRELATION OF O K G . TEST NUMBER 1-48 F. TAPE NUMBER BIO-07. NOV. 11,1964 PAGE

COMPUTATIONS FROM 10.(HOURS), 911.003(SECONDS) TO 10.(HOURS), 912.000(SECONDS) AT EVERY 12 FRAMES.
NUMBER OF FRAMES = 16. NUMBER OF LAGS = 8. DATA TIME RESOLUTION = 0.060059.
AUTOCORRELATION FUNCTION TIME RESOLUTION = 0.060. FROM 0. (SEC) TO 0.480(SEC).
ZERO-LAG AUTOCORRELATION = 0.28875643E 05

TAU	AUTOCOR	TAU	AUTOCOR	TAU	AUTOCOR	TAU	AUTOCOR	TAU	AUTOCOR
-0.	1.000000	0.0601	-0.365094	0.1201	-0.207497	0.1802	0.222655	0.2402	-0.271076
0.3003 ✓	0.370429	0.3604	-0.859447	0.4204	1.163488				

FIGURE 42

RUN CASE 23

AUTOCORRELATION OF O K G . TEST NUMBER 1-48 F. TAPE NUMBER BIO-08. NOV. 11,1964 PAGE

COMPUTATIONS FROM 10.(HOURS), 911.008(SECONDS) TO 10.(HOURS), 912.300(SECONDS) AT EVERY 2 FRAMES.
NUMBER OF FRAMES = 65. NUMBER OF LAGS = 32. DATA TIME RESOLUTION = 0.020020.
AUTOCORRELATION FUNCTION TIME RESOLUTION = 0.020. FROM 0. (SEC) TO 0.641(SEC).
ZERO-LAG AUTOCORRELATION = 0.13070867E 06

TAU	AUTOCOR	TAU	AUTOCOR	TAU	AUTOCOR	TAU	AUTOCOR	TAU	AUTOCOR
-0.	1.000000	0.0200	0.678407	0.0400	0.027263	0.0601	-0.353302	0.0801	-0.263751
0.1001	0.008768	0.1201	0.155214	0.1401	0.138044	0.1602	0.059015	0.1802	-0.021277
0.2002	-0.052561	0.2202	0.020176	0.2402	0.162208	0.2603	0.216960	0.2803	0.089760
0.3003	-0.124413	0.3203	-0.275292	0.3403	-0.325357	0.3604	-0.300979	0.3804	-0.155031
0.4004	0.170404	0.4204	0.536630	0.4404	0.634887	0.4604	0.316077	0.4805	-0.189995
0.5005	-0.482981	0.5205	-0.393911	0.5405	-0.111811	0.5605	0.050772	0.5806	-0.027571
0.6006	-0.205026	0.6206	-0.258733						

FIGURE 43

RUN CASE BP-23

INDEPENDENT VARIABLE---TAU (SECONDS)
VALUE = A*SCALE + B , A = 10**-1 B = 0.

DEPENDENT VARIABLE-----NORMALIZED AUTOCORRELATION FUNCTION
VALUE = A*SCALE + B , A = 10** 0 B = -0.6000E 00.

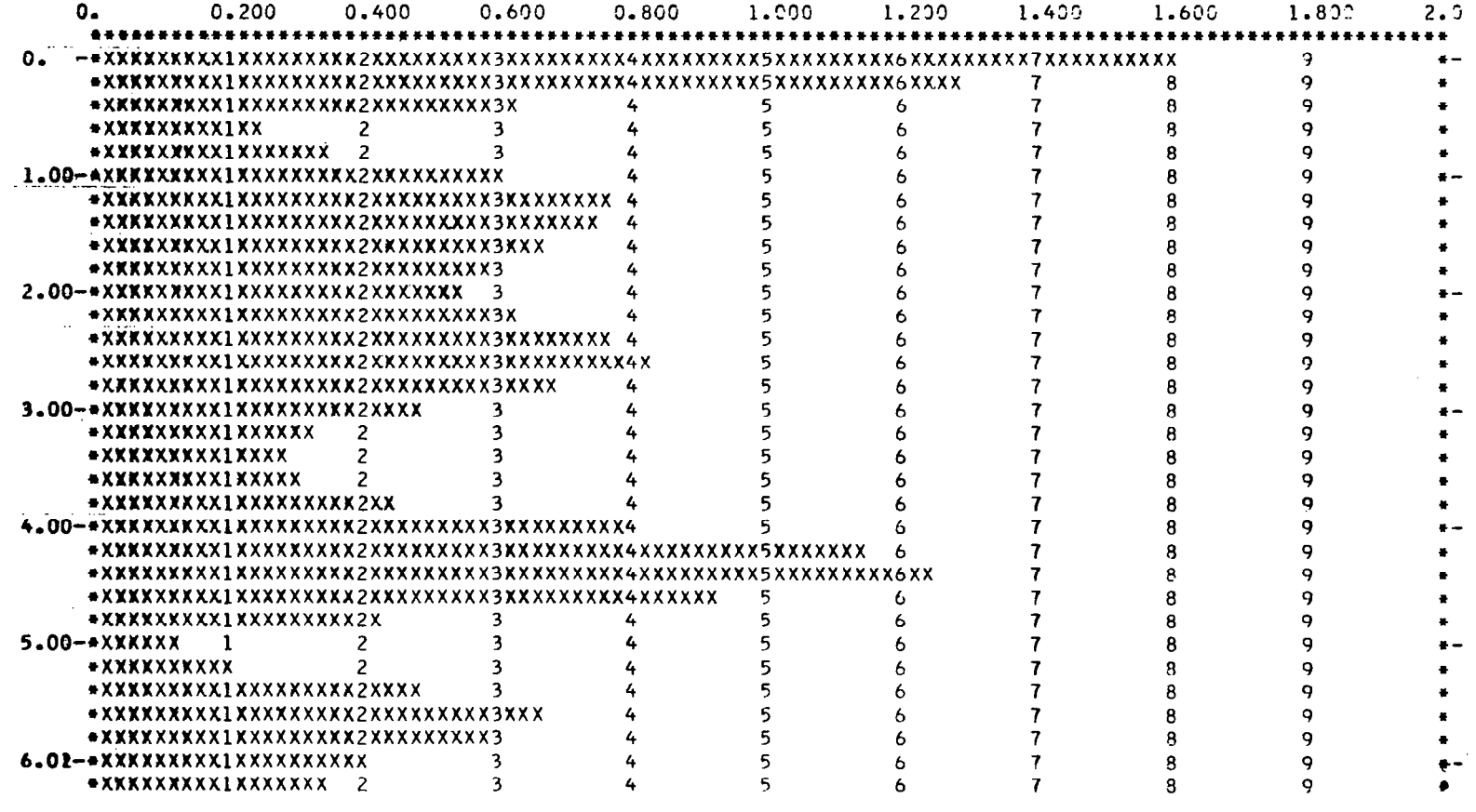

FIGURE 44

RUN CASE BP-24

AUTOCORRELATION OF O K G . TEST NUMBER 1-48 F. TAPE NUMBER BIO-08. NOV. 11,1964 PAGE

COMPUTATIONS FROM 10.(HOURS), 911.008(SECONDS) TO 10.(HOURS), 912.000(SECONDS) AT EVERY 2 FRAMES.
NUMBER OF FRAMES = 50. NUMBER OF LAGS = 25. DATA TIME RESOLUTION = 0.020020.
AUTOCORRELATION FUNCTION TIME RESOLUTION = 0.020. FROM 0. (SEC) TO 0.500(SEC).
ZERO-LAG AUTOCORRELATION = 0.12218028E 06

TAU	AUTOCOR	TAU	AUTOCOR	TAU	AUTOCOR	TAU	AUTOCOR	TAU	AUTOCOR
-0.	1.000000	0.0200	0.650069	0.0400	-0.033199	0.0601	-0.416440	0.0801	-0.301119
0.1001	-0.018312	0.1201	0.098562	0.1401	0.048907	0.1602	-0.022999	0.1802	-0.070234
0.2002	-0.090162	0.2202	-0.039536	0.2402	0.086822	0.2603	0.164129	0.2803	0.076479
0.3003	-0.121302	0.3203	-0.284987	0.3403	-0.353888	0.3604	-0.333595	0.3804	-0.170434
0.4004	0.185137	0.4204	0.561464	0.4404	0.626846	0.4604	0.260536	0.4805	-0.249443

FIGURE 45

RUN CASE BP-24

INDEPENDENT VARIABLE---TAU (SECONDS)
VALUE = A*SCALE + B , A = 10**-1 B = 0.

DEPENDENT VARIABLE-----NORMALIZED AUTOCORRELATION FUNCTION
VALUE = A*SCALE + B , A = 10** 0 B = -0.6000E 00.

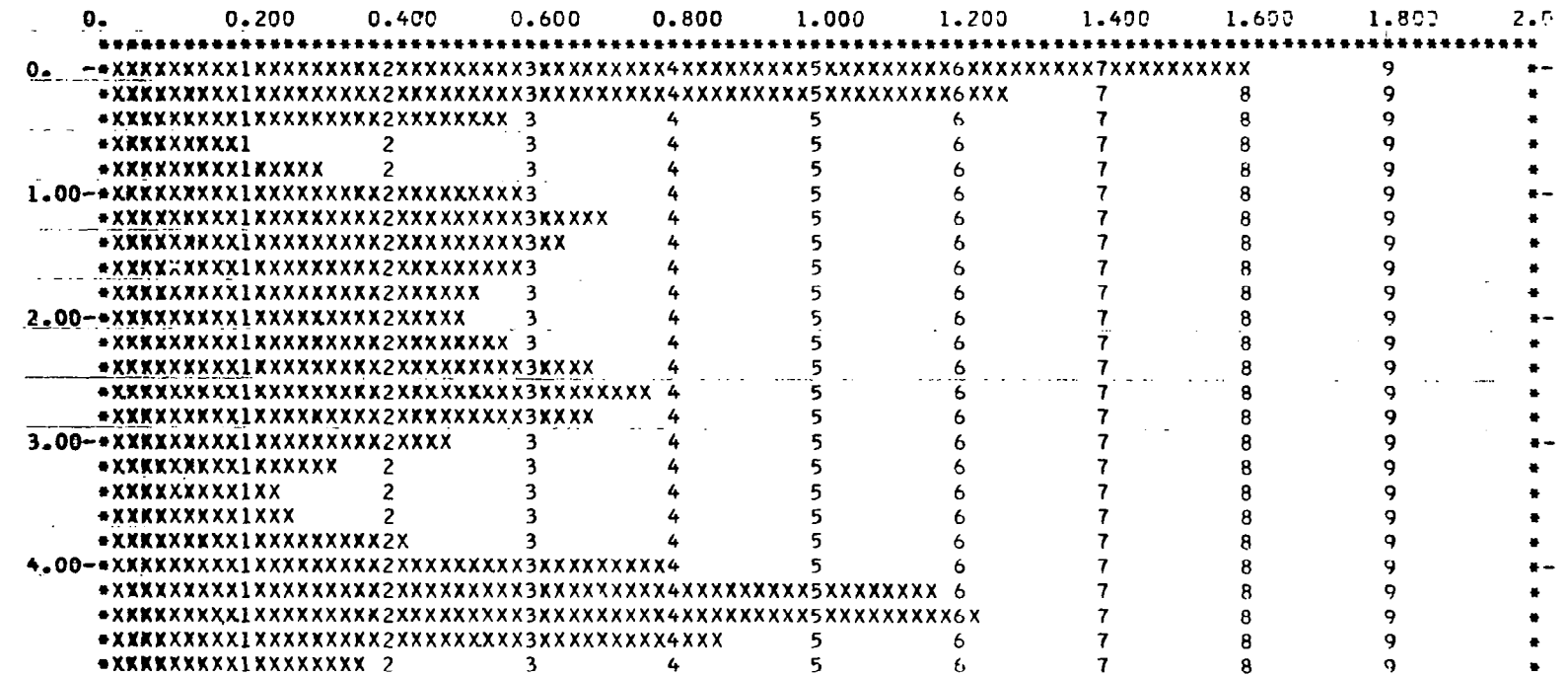

FIGURE 46

RUN CASE BP-28

AUTOCORRELATION OF O K G . TEST NUMBER 1-48 F. TAPE NUMBER BIO-08. NOV. 11,1964 PAGE

COMPUTATIONS FROM 10.(HOURS), 911.008(SECONDS) TO 10.(HOURS), 912.000(SECONDS) AT EVERY 4 FRAMES.
NUMBER OF FRAMES = 25. NUMBER OF LAGS = 12. DATA TIME RESOLUTION = 0.040039.
AUTOCORRELATION FUNCTION TIME RESOLUTION = 0.040. FROM 0. (SEC) TO 0.480(SEC).
ZERO-LAG AUTOCORRELATION = 0.55126327E 05

TAU	AUTOCOR	TAU	AUTOCOR	TAU	AUTOCOR	TAU	AUTOCOR	TAU	AUTOCOR
-0.	1.000000	0.0400	0.044714	0.0801	-0.328708	0.1201	0.142655	0.1602	0.059628
0.2002	-0.078250	0.2402	0.021168	0.2803	0.222603	0.3203	-0.179498	0.3604	-0.414596
0.4004	0.187944	0.4404	0.653827						

FIGURE 49

RUN CASE BP-28

INDEPENDENT VARIABLE---TAU (SECONDS)
VALUE = A*SCALE + B , A = 10**-1 B = 0.

DEPENDENT VARIABLE-----NORMALIZED AUTOCORRELATION FUNCTION
VALUE = A*SCALE + B , A = 10** 0 B = -0.6000E 00.

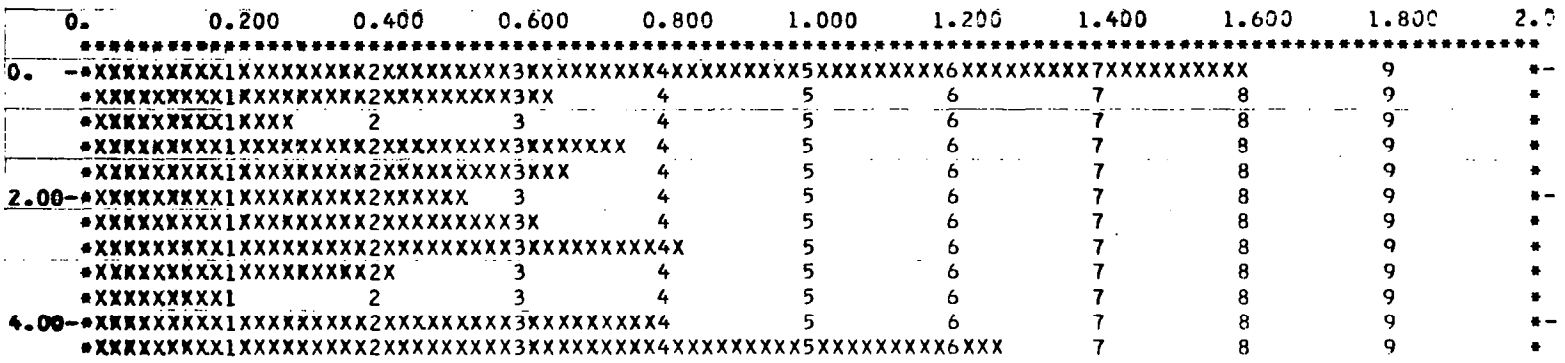

FIGURE 50

RUN CASE BP-29

AUTOCORRELATION OF O K G . TEST NUMBER 1-48 F. TAPE NUMBER BIO-08. NOV. 11,1964 PAGE

COMPUTATIONS FROM 10.(HOURS), 911.008(SECONDS) TO 10.(HOURS), 912.300(SECONDS) AT EVERY 5 FRAMES.
NUMBER OF FRAMES = 26. NUMBER OF LAGS = 13. DATA TIME RESOLUTION = 0.050049.
AUTOCORRELATION FUNCTION TIME RESOLUTION = 0.050. FROM 0. (SEC) TO 0.651(SEC).
ZERO-LAG AUTOCORRELATION = 0.37683857E 05

TAU	AUTOCOR	TAU	AUTOCOR	TAU	AUTOCOR	TAU	AUTOCOR	TAU	AUTOCOR
-0.	1.000000	0.0500	0.081409	0.1001	-0.230645	0.1501	0.285602	0.2002	-0.129276
0.2502	0.236409	0.3003	-0.008570	0.3503	-0.639096	0.4004	0.431073	0.4504	0.485327
0.5005	-0.382777	0.5505	-0.257445	0.6006	-0.110826				

FIGURE 51

RUN CASE BP-31

AUTOCORRELATION OF O K G . TEST NUMBER I-48 F. TAPE NUMBER BIO-08. NOV. 11,1964 PAGE

COMPUTATIONS FROM 10.(HOURS), 911.008(SECONDS) TO 10.(HOURS), 912.300(SECONDS) AT EVERY 7 FRAMES.
NUMBER OF FRAMES = 18. NUMBER OF LAGS = 9. DATA TIME RESOLUTION = 0.070068.
AUTOCORRELATION FUNCTION TIME RESOLUTION = 0.070. FROM 0. (SEC) TO 0.631(SEC).
ZERO-LAG AUTOCORRELATION = 0.43558576E 05

TAU	AUTOCOR	TAU	AUTOCOR	TAU	AUTOCOR	TAU	AUTOCOR	TAU	AUTOCOR
0.	1.000000	0.0701	-0.528002	0.1401	0.190349	0.2102	-0.031913	0.2803	0.269603
0.3503	-0.551601	0.4204	0.636425	0.4905	-0.517367	0.5605	0.089853		

FIGURE 52

RUN CASE BP-32

AUTOCORRELATION OF O K G . TEST NUMBER 1-48 F. TAPE NUMBER BIO-08. NOV. 11,1964 PAGE

COMPUTATIONS FROM 10.(HOURS), 911.008(SECONDS) TO 10.(HOURS), 912.000(SECONDS) AT EVERY 7 FRAMES.
NUMBER OF FRAMES = 14. NUMBER OF LAGS = 7. DATA TIME RESOLUTION = 0.070068.
AUTOCORRELATION FUNCTION TIME RESOLUTION = 0.070. FROM 0. (SEC) TO 0.490(SEC).
ZERO-LAG AUTOCORRELATION = 0.40786717E 05

TAU	AUTOCOR	TAU	AUTOCOR	TAU	AUTOCOR	TAU	AUTOCOR	TAU	AUTOCOR
-0.	1.000000	0.0701	-0.595005	0.1401	0.246072	0.2102	-0.102449	0.2803	0.383493
0.3503	-0.583596	0.4204	0.635263						

FIGURE 53

RUN CASE BP-32

INDEPENDENT VARIABLE---TAU (SECONDS)
VALUE = A*SCALE + B , A = 10**-1 B = 0.

DEPENDENT VARIABLE-----NORMALIZED AUTOCORRELATION FUNCTION
VALUE = A*SCALE + B , A = 10** 0 B = -0.6000E 00.

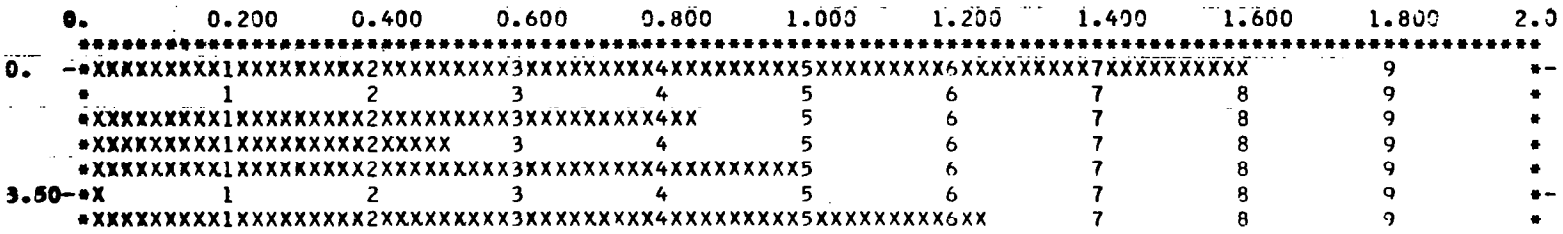

FIGURE 54

RUN CASE BP-33

AUTOCORRELATION OF O K G . TEST NUMBER 1-48 F. TAPE NUMBER BIO-08. NOV. 11,1964 PAGE

COMPUTATIONS FROM 10.(HOURS), 911.008(SECONDS) TO 10.(HOURS), 912.309(SECONDS) AT EVERY 10 FRAMES.
NUMBER OF FRAMES = 13. NUMBER OF LAGS = 6. DATA TIME RESOLUTION = 0.100098.
AUTOCORRELATION FUNCTION TIME RESOLUTION = 0.100. FROM 0. (SEC) TO 0.601(SEC).
ZERO-LAG AUTOCORRELATION = 0.14270367E 05

TAU	AUTOCOR	TAU	AUTOCOR	TAU	AUTOCOR	TAU	AUTOCOR	TAU	AUTOCOR
-0.	1.000000	0.1001	0.013506	0.2002	-0.316529	0.3003	0.418784	0.4004	0.283195
0.5005	-0.368746								

FIGURE 55

RUN CASE BP-33

INDEPENDENT VARIABLE---TAU (SECONDS)
VALUE = A*SCALE + B , A = 10** 0 B = 0.

DEPENDENT VARIABLE-----NORMALIZED AUTOCORRELATION FUNCTION
VALUE = A*SCALE + B , A = 10** 0 B = -0.4000E-00.

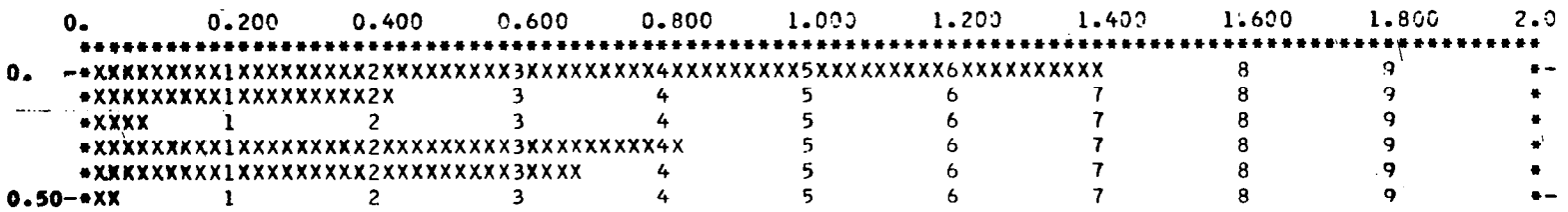

FIGURE 56

RUN CASE BP-34

AUTOCORRELATION OF O K G . TEST NUMBER 1-48 F. TAPE NUMBER BIO-C8. NOV. 11,1964 PAGE

COMPUTATIONS FROM 10.(HOURS), 911.008(SECONDS) TO 10.(HOURS), 912.000(SECONDS) AT EVERY 10 FRAMES.
NUMBER OF FRAMES = 10. NUMBER OF LAGS = 5. DATA TIME RESOLUTION = 0.100098.
AUTOCORRELATION FUNCTION TIME RESOLUTION = 0.100. FROM 0. (SEC) TO 0.500(SEC).
ZERO-LAG AUTOCORRELATION = 0.10755005E 05

TAU	AUTOCOR	TAU	AUTOCOR	TAU	AUTOCOR	TAU	AUTOCOR	TAU	AUTOCOR
-0.	1.000000	0.1001	-0.185501	0.2002	-0.590520	0.3003	0.278718	0.4004	0.288880

FIGURE 57

RUN CASE BP-34

INDEPENDENT VARIABLE---TAU (SECONDS)
VALUE = A*SCALE + B , A = 10** 0 B = 0.

DERENDENT VARIABLE-----NORMALIZED AUTOCORRELATION FUNCTION
VALUE = A*SCALE + B , A = 10** 0 B = -0.6000E 00.

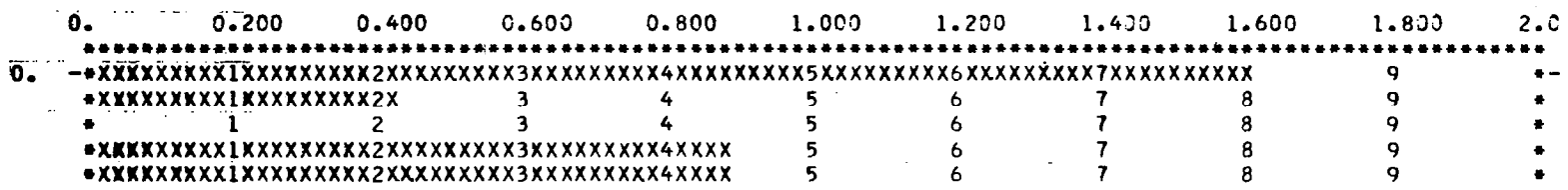

FIGURE 58

SYNTHETIC E C G - X-15 FLIGHT - RUN OCTOBER 23 , 1964 , TAPE BIO-02.

DESCRIPTORS FOR SIGNAL SEGMENT 13. SAMPLING RATE = 500.00 SAMPLES/SECOND.

NUMBER OF CYCLES = 66.
BASE HEART RATE = 120.0 BEATS/MINUTE.
LINEAR RATE VARIATION COEFFICIENT = 0. BEATS/MINUTE/SECOND.
SINUSOIDAL RATE VARIATION AMPLITUDE = 0. BEATS/MINUTE.
SINUSOIDAL RATE VARIATION FREQUENCY = 0. CYCLES/SECOND.

WAVE SEGMENT	BASE AMP. (MICROVOLTS)	LINEAR AMP. VARIATION COEFFICIENT (MICROVOLTS/SEC)	SINUSOIDAL AMP. VARIATION COEFFICIENT (MICROVOLTS)
1	0.	0.	0.
2	0.	0.	0.
3	150.000	0.	0.
4	0.	0.	0.
5	0.	0.	0.
6	-20.000	0.	0.
7	600.000	0.	0.
8	-125.000	0.	0.
9	0.	0.	0.
10	0.	0.	0.
11	200.000	0.	0.

SINUSOIDAL AMP. VARIATION FREQUENCY = 0. CYCLES/SECOND.
1 EXCEPTION CYCLES THIS SIGNAL SEGMENT...

FIGURE 82a (Page 1 of 2)

SYNTHETIC ECG - X-15 FLIGHT - RUN OCTOBER 23, 1964, TAPE B10-02

CYCLE	HR. BPM	TAU(MS)/ AMP(MV) 1	2	3	4	5	6	7	8	9	10	11	TIME (SEC.)
23	120.00	75.0	54.0	37.0	36.0	14.0	27.0	27.0	8.0	15.0	138.0	69.0	
		0.	0.	150.0	0.	0.	-20.0	600.0	-125.0	0.	0.	200.0	246.130
24	120.00	75.0	54.0	37.0	36.0	14.0	27.0	27.0	8.0	15.0	138.0	69.0	
		0.	0.	150.0	0.	0.	-20.0	600.0	-125.0	0.	0.	200.0	246.646
25	120.00	75.0	54.0	37.0	36.0	14.0	27.0	27.0	8.0	15.0	138.0	69.0	
		0.	0.	150.0	0.	0.	-20.0	600.0	-125.0	0.	0.	200.0	247.162
26	120.00	75.0	54.0	37.0	36.0	14.0	27.0	27.0	8.0	15.0	138.0	69.0	
		0.	0.	150.0	0.	0.	-20.0	600.0	-125.0	0.	0.	200.0	247.678
27	120.00	75.0	54.0	37.0	36.0	14.0	27.0	27.0	8.0	15.0	138.0	69.0	
		0.	0.	150.0	0.	0.	-20.0	600.0	-125.0	0.	0.	200.0	248.192
28	120.00	75.0	54.0	37.0	36.0	14.0	27.0	27.0	8.0	15.0	138.0	69.0	
		0.	0.	150.0	0.	0.	-20.0	600.0	-125.0	0.	0.	200.0	248.708
29	120.00	75.0	54.0	37.0	36.0	14.0	27.0	27.0	8.0	15.0	138.0	69.0	
		0.	0.	150.0	0.	0.	-20.0	600.0	-125.0	0.	0.	200.0	249.224
30	120.00	75.0	54.0	37.0	36.0	14.0	27.0	27.0	8.0	15.0	138.0	69.0	
		0.	0.	150.0	0.	0.	-20.0	600.0	-125.0	0.	0.	200.0	249.740
31	120.00	75.0	54.0	37.0	36.0	14.0	27.0	27.0	8.0	15.0	138.0	69.0	
		0.	0.	150.0	0.	0.	-20.0	600.0	-125.0	0.	0.	200.0	250.256
EXCEPTION		75.0	54.0	37.0	36.0	14.0	27.0	27.0	8.0	15.0	138.0	69.0	
		0.	0.	0.	0.	0.	-20.0	600.0	-125.0	0.	0.	200.0	
32	120.00	75.0	54.0	37.0	36.0	14.0	27.0	27.0	8.0	15.0	138.0	69.0	
		0.	0.	150.0	0.	0.	-20.0	600.0	-125.0	0.	0.	200.0	250.772
33	120.00	75.0	54.0	37.0	36.0	14.0	27.0	27.0	8.0	15.0	138.0	69.0	
		0.	0.	150.0	0.	0.	-20.0	600.0	-125.0	0.	0.	200.0	251.288
34	120.00	75.0	54.0	37.0	36.0	14.0	27.0	27.0	8.0	15.0	138.0	69.0	
		0.	0.	150.0	0.	0.	-20.0	600.0	-125.0	0.	0.	200.0	251.804
35	120.00	75.0	54.0	37.0	36.0	14.0	27.0	27.0	8.0	15.0	138.0	69.0	
		0.	0.	150.0	0.	0.	-20.0	600.0	-125.0	0.	0.	200.0	252.318

FIGURE 82b (Page 2 of 2)

STATISTICAL ANALYSIS OF NORMALLY DISTRIB , FROM 0.45005E 04 TO 0.85000E 04, TOTAL POINTS = 8000.

CLASS	CLASS LIMITS	OCCUPANCY	COMP. NORMAL	RELATIVE OCCUPANCY	RELATIVE NORMAL	LUMPED OCCUPANCY	LUMPED NORMAL	PROB. DENSITY	NORMAL DENSITY
BELOW		0	0.	0.	0.	0.	0.	0.	0.
1	-0.6000E 01	0	0.	0.	0.	0.	0.	0.	0.
2	-0.5480E 01	0	0.00	0.	0.0000004	0.	0.	0.	0.0000004
3	-0.4960E 01	0	0.04	0.	0.0000045	0.	0.	0.	0.0000049
4	-0.4440E 01	0	0.33	0.	0.0000418	0.	0.	0.	0.0000467
5	-0.3920E 01	0	2.43	0.	0.0003037	0.	0.	0.	0.0003504
6	-0.3400E 01	10	13.58	0.0012500	0.0016975	10.0	13.6	0.0012500	0.0020479
7	-0.2880E 01	61	58.31	0.0076250	0.0072884	61.0	58.3	0.0088750	0.0093362
8	-0.2360E 01	192	192.32	0.0240000	0.0240401	192.0	192.3	0.0328750	0.0333763
9	-0.1840E 01	503	487.48	0.0628750	0.0609344	503.0	487.5	0.0957500	0.0943107
10	-0.1320E 01	997	949.65	0.1246250	0.1187061	997.0	949.6	0.2203750	0.2130169
11	-0.8000E 00	1398	1421.98	0.1747500	0.1777474	1398.0	1422.0	0.3951250	0.3907643
12	-0.2800E-00	1532	1636.73	0.1915000	0.2045907	1532.0	1636.7	0.5866250	0.5953550
13	0.2400E-00	1485	1448.17	0.1856250	0.1810212	1485.0	1448.2	0.7722500	0.7763762
14	0.7600E 00	1000	984.96	0.1250000	0.1231194	1000.0	985.0	0.8972500	0.8994956
15	0.1280E 01	553	514.92	0.0691250	0.0643645	553.0	514.9	0.9663750	0.9638600
16	0.1800E 01	198	206.89	0.0247500	0.0258614	198.0	206.9	0.9911250	0.9897214
17	0.2320E 01	55	63.88	0.0068750	0.0079852	55.0	63.9	0.9980000	0.9977066
18	0.2840E 01	16	15.15	0.0020000	0.0018941	16.0	15.2	1.0000000	0.9996008
19	0.3360E 01	0	2.76	0.	0.0003451	0.	0.	1.0000000	0.9999459
20	0.3880E 01	0	0.39	0.	0.0000484	0.	0.	1.0000000	0.9999943
21	0.4400E 01	0	0.04	0.	0.0000052	0.	0.	1.0000000	0.9999995
22	0.4920E 01	0	0.00	0.	0.0000004	0.	0.	1.0000000	1.0000000
23	0.5440E 01	0	0.00	0.	0.0000000	0.	0.	1.0000000	1.0000000
24	0.5960E 01	0	0.	0.	0.	0.	0.	1.0000000	1.0000000
25	0.6480E 01	0	0.	0.	0.	0.	0.	1.0000000	1.0000000
ABOVE	0.7000E 01	0	0.	0.	0.	0.	0.	1.0000000	1.0000000

SAMPLE MEAN = -0.19609E-02 SAMPLE STAN DEV = 0.10026E 01 MINIMUM = -0.30690E 01
SAMPLE E(X**2) = 0.10050E 01 SAMPLE VARIANCE = 0.10051E 01 OCCURRED AT TIME = 0.56195000E 04
SAMPLE E(X**3) = -0.14127E-01 SAMPLE SKEWNESS = -0.81519E-02 MAXIMUM = 0.32035E 01
SAMPLE E(X**4) = 0.28486E 01 SAMPLE KURTOSIS = 0.28195E 01 OCCURRED AT TIME = 0.54135000E 04
TOTAL OF 0 BAD POINTS

FIGURE 84

STATISTICAL ANALYSIS OF NORMALLY DISTRIB , FROM 0.45005E 04 TO 0.85000E 04, TOTAL POINTS = 8000.

MISCELLANEOUS STATISTICAL TESTS

HYPOTHESIS THAT THIS DATA IS NORMALLY DISTRIBUTED IS ACCEPTED AT THE 95 PERCENT CONFIDENCE LEVEL,
EPSILON =0.081828, BANDWIDTH ASSUMED = 100.00 PERCENT, COMPUTED CHI-SQUARE = 16.68,
AND 10 DEGREES OF FREEDOM.

HYPOTHESIS THAT THIS DATA IS RANDOM BY RUN TEST METHOD IS ACCEPTED AT THE 95 PERCENT CONFIDENCE LEVEL,
WITH 3971 RUNS, LEVEL = 0.1000E-08, 4007 POINTS ABOVE LEVEL, 3993 POINTS BELOW, MU SUB-R = 0.4000E 04,
AND SIGMA SUB-R = 0.4472E 02.

FIGURE 85